12-2005

Interdisciplinary Approaches to New Chemical Analysis

David Lynn Rodman
University of Tennessee - Knoxville

To the Graduate Council:

I am submitting herewith a dissertation written by David Lynn Rodman entitled "Interdisciplinary Approaches to New Chemical Analysis." I have examined the final electronic copy of this dissertation for form and content and recommend that it be accepted in partial fulfillment of the requirements for the degree of Doctor of Philosophy, with a major in Chemistry.

Ziling (Ben) Xue, Major Professor

We have read this dissertation and recommend its acceptance:

Craig E. Barnes, Bin Zhao, Charles F. Moore

Accepted for the Council:
Carolyn R. Hodges

Vice Provost and Dean of the Graduate School

(Original signatures are on file with official student records.)

To the Graduate Council:

I am submitting herewith a dissertation written by David Lynn Rodman entitled “Interdisciplinary Approaches to New Chemical Analysis.” I have examined the final electronic copy of this dissertation for form and content and recommend that it be accepted in partial fulfillment of the requirements for the degree of Doctor of Philosophy, with a major in Chemistry.

Ziling (Ben) Xue
Major Professor

We have read this dissertation
and recommend its acceptance:

Craig E. Barnes

Bin Zhao

Charles F. Moore

Accepted for the Council:

Anne Mayhew
Vice Chancellor and Dean of the
Graduate School

(Original Signatures are on file with official student records)

INTERDISCIPLINARY APPROACHES TO NEW CHEMICAL ANALYSIS

A Dissertation

Presented for the

Doctor of Philosophy Degree

The University of Tennessee, Knoxville

David Lynn Rodman

December 2005

DEDICATION

This dissertation is dedicated to my wife,

parents, and family, from whom I draw

love, support, and encouragement.

ACKNOWLEDGEMENTS

There are many people that I would like to thank who have, in some way or another, had an impact on my life during my graduate studies. First and foremost, I owe a special thanks to my advisor, Dr. Ziling (Ben) Xue for his encouragement and guidance during my graduate studies at the University of Tennessee. Dr. Xue has been a great mentor to me, instilling a good work ethic and pushing me to succeed. I would also like to extend thanks to my committee members, Drs. Craig E. Barnes, Bin Zhao, and Charles F. Moore for their time and consideration of this dissertation.

The chemistry department faculty and support staff, including but not limited to Dr. Fred Schell, Dr. Mark Dadmun, Dr. Jeffery Kovac, Dr. James Chambers, Dr. Youngmi Lee, Dr. Peter Zhang, Dr. David Young, Dr. Bin Zhao, Dr. Jimmy Mays, Carol Moulton, Emily Jones, Marilyn Ownby, Art Pratt, John Nelson, Bill Gurley, Johnny Jones, Tiffany Manes, Rachelle Allen, Kelly Preston, Jan McGuire, Darrel Lay, Sharon Marshall, and Tray Allen have always been willing to help in any way needed, and I greatly appreciate their help. A special thanks goes to other people who have provided technical assistance with my experiments and projects: Dr. Hongjun Pan and Dr. Xiaobing Feng of the UTK department of mathematics for help with the diffusion model mathematics, Dr. Kish Goswami of Innosense LLC for help with the modified Fujiwara reaction studies, Dr. Gilbert Brown of Oak Ridge National Laboratory for help with various experiments, Jason Clark for help with solid state NMR experiments, Dr.

Kathleen Giesfeldt for help with IR and AAS experiments, Nathan Carrington for help with learning various other instrumental methods, and the organometallics portion of the Xue research group for help with inert atmosphere experiments. Funding for the research in this dissertation has been provided by the Measurement and Control Engineering Center, National Science Foundation, Environmental Protection Agency, Department of Energy, and National Institutes of Health.

During my stay at the University of Tennessee, I have been fortunate to work with a wonderful group of people, many of whom I consider to be good friends and will never forget. Some of these people include but are not limited to Jason Clark, Nathan Carrington, Lance Riddle, Dr. Ruitao (Ray) Wang, Jay Chocklett, Cheri Clavier, Dr. Jaime Blanton, Dr. Xianghua (Bruce) Yu, Dr. Laurie Morton, He (Steve) Qiu, Dr. Laura Pence, Dr. Li Yong, Dr. Tianniu (Rick) Chen, Dr. Hee-Jung Im, Dr. Hu (Frank) Cai. I will miss our lunch time conversations and other daily interactions. I would like to include a special thanks to Jason Clark, whom I have known since the beginning of my graduate school journey, I will never forget all of the never-ending workouts in the gym and hiking trips as well as casual conversations in the lab. Other special thanks go to Nathan Carrington, our daily discussions and debates in the lab have taught me to always be very careful of what I say. I would also like to thank Lance Riddle for introducing me to the game of golf and keeping us updated on the news in the world of sports.

My greatest debt is owed to my family, without whose love and support I could have never achieved this accomplishment. To my parents David and Mary Rodman and Pat and John Massengale, I appreciate all that you have taught me and done for me. You have all made me who I am today, and I will always remember that. Thanks to my sister Julie for always being there to provide encouragement and support. Last, but certainly not least, Nikki, I love you very much, and I am thankful to have someone who is always so understanding and supportive by my side each day.

ABSTRACT

The primary focus of this dissertation is the development of new chemical analyses for inorganic, organic, and organometallic compounds. Interdisciplinary approaches combining analytical, polymer, inorganic, organic, and materials chemistry have been used to develop new analytical methods. Topics discussed in this dissertation include the development of a sol-gel based metal ion sensor, photochemical oxidation of a biomimetic Cr(III) complex, photochemical oxidation of organic ligands and other interferences in model Pd catalyst complexes, modified Fujiwara reactions for the detection of halogenated hydrocarbons, and the development of a controlled-release polymer for delivery of reagents needed for chemical sensing applications.

TABLE OF CONTENTS

LIST OF TABLES

LIST OF FIGURES

NOMENCLATURE AND ABBREVIATIONS

A	absorbance
A_p	absorbance of the product(s)
Å	angstrom
AA	atomic absorption
AOP	Advanced Oxidation Process
APS	aminopropylsilane
BET	Brunauer-Emmett-Teller
°C	degrees Celcius
C	concentration
C_0	solution concentration
$C_{Cu(II)}$	Cu(II) concentration
cc	cubic centimeter
cm	centimeter
cm^{-1}	wavenumber
CRP	controlled-release polymer
D	diffusion coefficient
dm	decimeter
DRIFT	diffuse reflectance infrared Fourier transform
EDTA	ethylene diamine tetraacetate
FT-IR	Fourier transform infrared
g	gram

HHC	halogenated hydrocarbon
ICP	inductively coupled plasma
IR	infrared
ISE	ion selective electrode
J	flux
K	slope from A vs. $t^{1/2}$ plot
kHz	kilohertz
ℓ	length
L	liter
L_0	ligand concentration
mm	millimeter
mM	millimolar
M	molar
M^{n+}	metal ion
MAS	magic angle spinning
MeOH	methanol
mg	milligram
MHz	megahertz
min	minute
mL	milliliter
N_p	number of moles of product
nm	nanometer
NMR	nuclear magnetic resonance

PC	personal computer
ppm	parts per million
PVA	poly (vinyl)alcohol
R	correlation coefficient
R^2	square of correlation coefficient
s	seconds
SSNMR	solid-state nuclear magnetic resonance
t	time
$t^{1/2}$	square root of time
TMOS	tetramethyl orthosilicate
UV	ultraviolet radiation
w/w%	weight percent
W	watt
λ	wavelength
ε_p	molar absorptivity of products
ε_r	molar absorptivity of reagents
∂	partial derivative
ν	Frequency

Part 1

Introduction and Background

1.1. Foreword

New chemical analysis and chemical sensors have been of intense current interest.[1] Rapid advances in many areas of science, especially materials chemistry, have allowed the use of new materials and analytical methods. On the other hand, these advances also require the development of new and/or better methods in chemical analysis.

One key feature of our work in new chemical analysis and sensors is the diverse targets for analysis and approaches we have taken to analyze them. As this dissertation reveals, our targets for analysis include inorganic, organic, organometallic, and biomimetic compounds. Topics discussed in this dissertation range from the development of a Cu(II) sensor in a flowing solution, to the use of an oxidation process for the removal of ligands in metal complexes, and to the use of polymers for controlled-release of chemical reagents for sensing applications. The commonality between these projects that seem so diverse in nature is the overall goal of developing new chemical analyses using interdisciplinary approaches. These interdisciplinary approaches have combined and utilized several areas of chemistry including analytical, inorganic, organic, and polymer chemistry.

1.2. Summary of Dissertation Parts

1.2.1. Part Two

An optical copper ion sensor based on the diffusion-reaction process of copper ions within a functionalized sol-gel monolith is reported in Part 2. A discussion of the sol-gel chemistry and synthesis of the sensor monoliths is given, followed by characterization of the sol-gel monoliths. A mathematical model is reported that describes the diffusion and complexation reactions between Cu(II) ions in solution and the grafted amine groups within the pores of the monolith. The mathematical model was developed in order to correlate the change in absorbance associated with the Cu(II) diffusion/complexation in the sol-gel monolith to the copper ion concentration. The result of this project was the development of a reversible optical sensor capable of quantifying Cu(II) concentrations at levels as low as 20 mM with a high level of reproducibility. Two articles about the preparation of the sol-gel monoliths and Cu(II) sensing, respectively, have been published.[2-3]

1.2.2. Part Three

The application of the Advanced Oxidation Process (AOP) and photo Fenton process to a biomimetic Cr species is reported in Part 3. The primary goal of this project is to quantitatively oxidize Cr(III) to Cr(VI) and to remove ligands in the biomimetic Cr complex for subsequent electrochemical analysis. To our knowledge, this is the first known application of AOP for the treatment of a

metal complex. In addition to the oxidation of Cr(III) to Cr(VI) in the process, the organic ligands in the biomimetic Cr(III) complex were oxidized and removed. Thus Cr(VI) generated from the AOP treatment could be analyzed directly. A description of the Advanced Oxidation Process (AOP) and the photo Fenton process is given. Studies to optimize the conditions for the oxidation processes are reported.

1.2.3. Part Four

We have further explored the use of AOP to remove ligands in metal complexes for subsequent metal analysis. AOP treatment of catalytic palladium complexes was investigated in Part 4 of this dissertation. Unlike the biomimetic Cr complex discussed in Part 3, the Pd complexes are insoluble in water. Extensive effort was made to find methods to dissolve/disperse them in water-containing solution for subsequent AOP treatment. AOP was successfully used to remove organic ligands from palladium acetate $Pd(OAc)_2$ and palladium acetylacetonate $Pd(acac)_2$. Subsequent Pd analysis gave good, consistent results. Control samples that were *not* treated by *AOP* showed large errors in Pd(II) analysis.

1.2.4. Part Five

New alternative approaches to the Fujiwara reaction for detection of chloroform and carbon tetrachloride are reported in Part 5. The Fujiwara reaction is the only known reaction for detecting halocarbons spectrophotometrically in

the visible region, and it has been conducted with toxic, offensive-smelling pyridine and a strong base such as NaOH. New alternative approaches to conducting the Fujiwara reactions have been developed using solid pyridine derivatives and new bases for the detection of chloroform and carbon tetrachloride. The reactions of these halocarbons with 2,2′-dipyridyl (or 4,4′-dipyridyl) and tetra-*n*-butylammonium hydroxide (*n*-Bu_4NOH) or potassium *tert*-butoxide (KO-*t*-Bu) were found to yield colored species with detection limits of 0.17 mg/L for chloroform and 0.50 mg/L for CCl_4. The use of potassium *tert*-butoxide as the base in the Fujiwara reactions allows for the detection of the halocarbons in systems sensitive to water. The results here have been published.[4]

1.2.5. Part Six

Attempts to develop controlled-release polymers for delivery of reagents for modified Fujiwara reactions are reported in Part 6. As discussed in Part 5, the reaction of the analyte species and the reagents used in the modified Fujiwara reactions is irreversible. For continuous monitoring of halocarbons using the modified Fujiwara reaction, the reagents including 2,2′- or 4,4′-dipyridyl and tetra-*n*-butylammonium hydroxide need to be replenished for each sample analysis. A method to incorporate these reagents into poly(vinyl alcohol) (PVA) monoliths is reported. Controlled-release studies of the reagents from the PVA monolith were conducted and those results are reported as well. The release of reagent from the PVA monoliths was found to proceed in a controlled manner,

yielding consistent results among different reagent-loaded PVA monoliths. Although the new controlled-release process worked well, the presence of a large amount of water in the system was found to be detrimental to the Fujiwara reaction.

References

1. A Scifinder (Chemical Abstracts) search in August 2005 using the term "chemical analysis" and refined by the year "2004" yielded 75,405 hits.
2. Rodman, D. L.; Pan, H.; Clavier, C. W.; Feng, X.; Xue, Z. *Anal. Chem.* **2005**, *77*, 3231.
3. Clavier, C. W.; Rodman, D. L.; Sinski, J. F.; Allain, L. R.; Im, H. J.; Yang, Y.; Clark, J. C.; Xue, Z. *J. Mater. Chem.* **2005**, *15*, 2356.
4. Rodman, D. L.; Carrington, N. A.; Qiu, H.; Goswami, K.; Xue, Z.; *Anal. Chim. Acta* **2005**, *548*, 143.

Part 2

An Optical Metal Ion Sensor Based on Diffusion Followed by an Immobilizing Reaction. Quantitative Analysis by a Mesoporous Monolith Containing Functional Groups

2.1. Introduction

Optical sensors for metal ions are of intense current interest.[1] Metal-ligand complexes are a major class of chemical compounds and are the basis of many methods of metal analysis. The overall equilibria of complex formation as shown in Equation 2.1

$$M + nL \rightleftharpoons ML_n \qquad \text{(Eq. 2.1)}$$

are usually shifted exclusively to the complexes, and their equilibrium/stability constants are thus exceedingly large, as shown in Equation 2.2 for a Cu^{2+}-amine complex.[2] As a result, ligands are normally quickly saturated, especially when thin test strips with a small amount of ligands are used. It is thus difficult to make the quantitative analyses based on metal-ligand complexation except in cases when the amount of M is too small to saturate the ligands. This has limited the approaches for quantitative metal ion sensing.[1a] Wolfbeis and coworkers have recently developed a novel approach based on pattern recognition algorithms using signals of unselective metal sensor probes.[3] Metal-complexing reagent Eriochrome Cyanine R (ECR) encapsulated in sol-gel silica has been used as a Cu(II) sensor in which slopes of absorbance A vs. $t^{1/2}$ plots were plotted vs. log $C_{Cu(II)}$ to give a correlation with the Cu^{2+} concentration.[4] Another empirical approach using the early slopes of nonlinear A vs. t plots to obtain M^{n+} concentrations has been reported.[1i-j]

$$Cu^{2+} + 4\ NH_2Et \rightleftharpoons Cu(NH_2Et)_4^{2+} \quad K = 3.2 \times 10^{10} \qquad \text{(Eq. 2.2)}$$

Porous polymeric and inorganic solids containing functional groups/molecules have been widely studied in recent years[5,6] as new materials for, e.g., sensors.[5] In particular, sol-gel reactions to yield the inorganic solids at relatively low temperatures allow encapsulation or grafting of organic functional groups/molecules into porous inorganic solids. The encapsulated or grafted functional groups/molecules that retain their chemical, biological and physical properties in the hybrid solids are attractive, as they combine mechanical and thermal stabilities of inorganic backbones with specific chemical reactivities of the functional groups/molecules. In addition, these hybrid sol-gel materials are transparent well into the UV region, and thus allow for their application in spectroscopic characterizations. Many such inorganic-organic hybrid materials have been developed as, e.g., novel chemical and biological sensors.[5,6]

We have reasoned that novel sensors for quantitative metal ion analysis may be developed based on two fundamental processes that metal ions in a solution undergo when exposed to a porous monolith grafted with ligands selective for the metal ions: (a) diffusion of metal ions to the binding sites – The higher the concentration of the metal ions (C_0), the faster the metal ions reach the ligands inside the monolith; (b) metal-ligand (ML_n) complexation. *Although it is difficult to use either alone for quantitative analysis of the metal ions,*[7] *a model unifying both processes might provide a unique approach to determine the concentration of the metal ions* C_0*.* Our work to develop this novel mathematical

model is reported here. The use of the model in a mesoporous sol-gel monolith containing grafted amine ligands for quantitative Cu^{2+} sensing is demonstrated as a part of our studies to develop new optical sensors.[8]

2.2. Experimental

2.2.1. Reagents

The chemicals used in this study, including $H_2N(CH_2)_3Si(OMe)_3$ (3-aminopropyltrimethoxysilane, Aldrich), $Si(OMe)_4$ (TMOS, Aldrich, 99%), methanol (MeOH) (Aldrich, HPLC grade), ethylene glycol (Fisher, certified) were used as received. Deionized water was used in the preparation of sol-gel monoliths and aqueous $CuCl_2$ solutions.

2.2.2. Instrumentation

Brunauer-Emmett-Teller (BET) measurements were performed on a Nova 1000 High Speed Surface Area and Pore Size Analyzer by Quantachrome Corp using N_2 gas adsorption. A blank monolith was ground into a powder and dried at 100 °C for at least 24 hours before BET measurements. The adsorption portion of the N_2 adsorption/desorption isotherms was used to calculate the pore size distribution of the monolith.

Blank and amine-grafted monoliths were each dried at 100 °C and ground to powders before their diffuse reflectance infrared Fourier transform (DRIFT) spectra were taken on a Bio-Rad FTS 60A FT-IR spectrometer. Spectra in the

range of 400-4000 cm^{-1} were collected using 256 scans. The difference spectrum between that of the sample and a control blank was used in the studies.

^{29}Si magic-angle-spinning (MAS) solid-state NMR experiments were performed on a Varian-Inova 400 MHz spectrometer operating at the frequency of 79.43 MHz. The samples of blank and amine-grafted gels were ground into powders, and the NMR spectra were recorded with a 5.5 KHz spin rate and 1800-5300 scans. ^{29}Si chemical shifts were externally referenced to tetramethylsilane. All spectra were collected under ambient conditions.

Visible spectrometry was performed on an Ocean Optics S2000 miniature fiber optic spectrophotometer equipped with a tungsten halogen source lamp. The spectrometer was interfaced to a PC for data collection using Ocean Optics OOIBase32 operating software. A flow cell was designed to support two fiber optic cables and to hold the sol-gel monolith in $CuCl_2$ solution that was pumped into the cell at ca. 13.8 mL min^{-1}.

2.2.3. Sol-gel Monolith Synthesis

Sol-gel monoliths were prepared from $Si(OMe)_4$, MeOH, ethylene glycol (porogen), and 50 mM NaOH aqueous solution (catalyst) in a small glass vial.[9] The monolith that developed was covered with a layer of MeOH before allowing to stand overnight. The MeOH solution was decanted and replaced stepwise with 75% MeOH, 50% MeOH, 25% MeOH, and finally pure water.[9] The water above the gel was changed several times before use to give the blank monolith.

It is assumed that ethylene glycol (porogen), MeOH and catalyst NaOH had thus been removed from the monolith during this process.

The monolith (thickness: 0.387 cm; diameter: 1.095 cm; volume: 3.64×10^{-4} dm^3) was then immersed in a blue solution of $Cu[H_2N\text{-}(CH_2)_3\text{-}Si(OMe)_3]_4^{2+}$ in MeOH (amine ligand: 0.1112 M; $[Cu^{2+}]$: 0.02575 M; volume: 1.660 mL) until the supernatant solution was colorless (ca. 12 hours). A subsequent visible spectrum of the supernatant solution showed no absorption of $Cu[H_2N\text{-}(CH_2)_3\text{-}Si(OMe)_3]_4^{2+}$ at 730 nm. This observation suggested that the Cu(II) complex had grafted onto the monolith. The amount of the ligands grafted on the monolith is thus 1.84×10^{-4} mol, and the concentration of the ligands in the monolith of 3.64×10^{-4} dm^3 is 0.507 M.[11] Assuming that 4 equiv of the ligand reacts with 1 equiv of Cu^{2+} to give $Cu[H_2N\text{-}(CH_2)_3\text{-}Si(O\text{–})_3]_4^{2+}$ grafted in the solid, $L_0 = 0.507/4 = 0.127$ M in the current case.

The blue, transparent monolith was found to have a band at 730 nm in the visible spectrum with molar extinction coefficient $\varepsilon_p = 32.2$ M^{-1} cm^{-1}. Aqueous EDTA solution was then used to remove the imprinted Cu^{2+} ions from the monolith to yield an amine-grafted, Cu^{2+}-free monolith, as EDTA has a higher binding affinity for Cu^{2+} ions than the amine ligands in the monolith.[10] After washing the monolith with water, the monolith was found to uptake Cu^{2+} ions from aqueous solution. The new complex was found to have a band at 730 nm, suggesting that the original imprinted $Cu^{2+}/4NH_2\text{-}(CH_2)_4\text{-}Si(O\text{–})_3$ complex was likely formed. The ligands are chemically grafted on silica. Loss of silica (and

thus ligands) from the monolith may occur during the EDTA wash. Such a loss was not observed, and is expected to be small.

2.2.4. Measurements of Visible Spectra

A blank, amine-*free* monolith was placed into the compartment of a flow cell.[8] A $CuCl_2$ solution was then pumped through the system at a flow rate of 13.8 mL min^{-1}. After 2 min, a reference spectrum was recorded. An amine-grafted monolith was then placed into the cell. Upon initiation of the flow of the $CuCl_2$ solution, a complete spectrum over the range of 400-850 nm was recorded every 10 s for 15 min to give the A_p (730 nm) vs. $t^{1/2}$ plots. For each Cu^{2+} concentration, at least three monoliths from the same batch were used to conduct the test, and the average slopes (K) of their A_p vs. $t^{1/2}$ plots are discussed later.

2.3. Results and Discussion

Rate of access to the binding sites in the inorganic-organic hybrid solids and kinetics of the uptake of external reagents by silica gels have attracted much recent interest,[12-13] as these are often critical to fast sensor response and rapid separation. Walcarius and coworkers have studied the diffusion of H^+ and metal ions inside spherical amorphous silica.[12]

One key feature of the hybrid solids is that, in many cases, the diffusing external reagents react with, and are immobilized by the functional groups/molecules inside the solids. In other words, the diffusing external

reagents are prevented from further diffusion.[14] In many such cases, a limited number of functional groups/molecules in the solids react with a large excess or a constant supply of external reagents in, e.g., online or miniature sensing. In other words, there is an "*unlimited*" supply of external reagents. Earlier studies of chemical diffusion followed by immobilization usually either involved a *limited* supply of external reagents[14c] or led to mathematical models in the form of infinite series solutions that require numerical solutions.[14b] Although numerical methods are now widely used with modern computers and software, mathematical models using analytical methods are known to reveal physics and chemistry behind observed data and phenomena, and are needed for benchmarking and validating numerical solutions and methods.[15] A new model is desired for diffusion of an *unlimited* supply of external reagents and their subsequent immobilization in the sensor solid. The model developed below addresses this need, and, as demonstrated in the quantitative Cu(II) analysis discussed below, the model is straightforward to use.

2.3.1. Mathematical Model

In the following work to derive the model, metal ions and ligands grafted in a silica monolith are used to represent the external reagent and grafted/encapsulated functional groups/molecules, respectively. This model was developed for a plane sheet occupying the region $0 \le x \le 2\ell$ with symmetry about $x = \ell$. The diffusion of the metal ions with concentration C_0 is linear, that is, one

dimensional in the direction perpendicular to the vertical sides of the plane of the sheet, and there is no diffusion across the central plane of the sheet as shown in Figure 2.1. The boundary conditions may be written as:

$$C = C_{0,} \qquad x = 0, \qquad t \geq 0 \qquad \text{(Eq. 2.3)}$$

$$\partial C/\partial x = 0 \qquad x = \ell, \qquad t \geq 0 \qquad \text{(Eq. 2.4)}$$

It is more convenient to consider only a half of the sheet, $0 \leq x \leq \ell$, instead of using the conditions $C = C_0$, $x = 2\ell$.

The (immobilization) reaction between the metal ions and ligands is usually fast, and, after the reaction, metal ions in the complex are prevented from taking further part in the diffusion process. In other words, metal ions of the diffusion front are used to bind to the ligands. Only after the latter are saturated will the newly arrived metal ions diffuse forward into the next region.[14a,e] If the metal ion front has just reached $x = u(t)$ (Figure 2.1) at time t, the ligands in the region behind $[0 \leq x \leq u(t)]$ are all saturated. In other words, diffusing metal ions reaching the point x will all diffuse further into the monolith. These assumptions are essentially the same as those with moving boundaries.[14a,e] We thus have the following conditions:

$$C = C_0, \qquad x = 0, \qquad \text{(Eq. 2.5)}$$

$$C = 0, \qquad x = u(t) \qquad \text{(Eq. 2.6)}$$

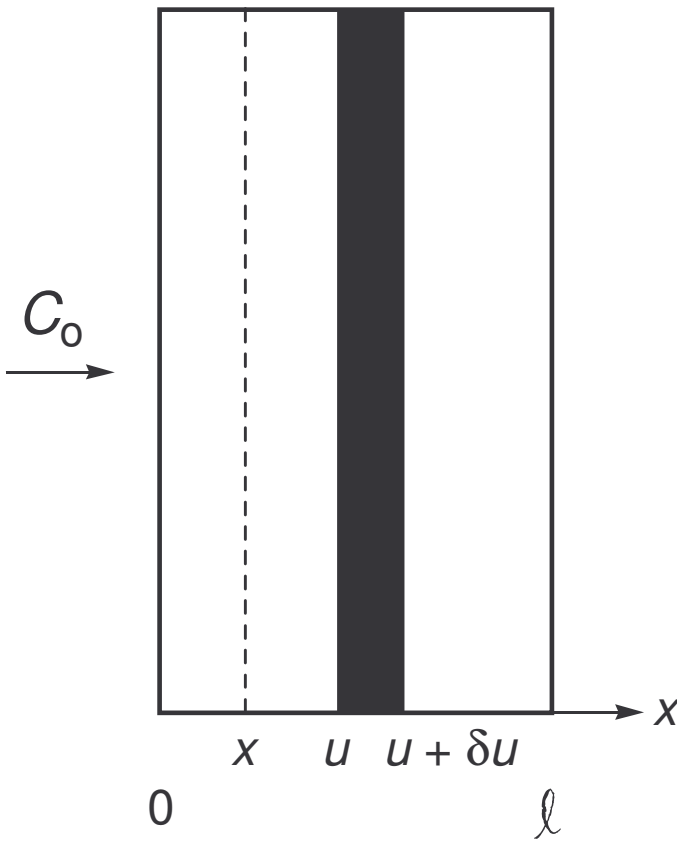

Figure 2.1. Schematic depicting the progression of the diffusion front within a sol-gel monolith.

The diffusion inside the region $0 \le x \le u(t)$, which is free of the immobilizing reaction, has reached the steady state, and there is a linear decrease of the concentration of the metal ions (Equation 2.7) in this region:

$$C(x) = C_0\left(1 - \frac{x}{u(t)}\right) \quad \text{or} \quad \frac{dC(x)}{dx} = -\frac{C_0}{u(t)} \qquad \text{(Eq. 2.7)}$$

where $C(x)$ is the concentration of the diffusing metal ions at x. Equation 2.7 may also be derived from Laplace's equation:

$$\frac{d^2C(x)}{d^2x} = \nabla^2 C(x) = 0 \qquad \text{(Eq. 2.8)}$$

Equations 2.7 and 2.8 are similar to the steady-state heat equation,[16] and has also been used in chemical diffusion processes.[14c] From Equation 2.7, the concentration gradient of the diffusing metal ions at $u(t)$ is:

$$\left.\frac{dC(x)}{dx}\right|_{x = u(t)} = -\frac{C_0}{u(t)} \qquad \text{(Eq. 2.9)}$$

The flux of the diffusing metal ions (J) through a unit area at $u(t)$ is:

$$\frac{dN}{dt} = J = -D\left.\frac{dC}{dx}\right|_{x = u(t)} = D\frac{C_0}{u(t)} \qquad \text{(Eq. 2.10)}$$

where N is the number of moles of the metal ions diffusing per unit area through the plane at $u(t)$.

Let L_0 equal the concentration (M = mol L^{-1} = mol dm^{-3}; i.e., moles per unit area on the plane and per unit length along the direction of the diffusion x) of the ligands inside the solid. When the diffusion front reaches $u + \delta u$, the ligands in the region δu will immobilize the metal ions in the time period of δt. In other words, the ligands in this region are saturated within the time δt. Thus the moles of the ligands in this region $L_0 \delta u$ equals the moles of metal ions diffused into this region during the time δt to give Equation 2.11.

$$L_0 \delta u = \frac{dN}{dt} \delta t = D \frac{C_0}{u} \delta t \qquad \text{or} \qquad \frac{DC_0}{L_0} dt = u du \qquad \text{(Eq. 2.11)}$$

with the following conditions:

$$t = 0, \qquad u = 0 \qquad \text{(Eq. 2.12)}$$

Integration of Equation 2.11 using the conditions in Equation 2.12 yields:

$$u(t) = \left(\frac{2C_0 Dt}{L_0} \right)^{1/2} \qquad \text{(Eq. 2.13)}$$

Clearly, Equation 2.13 is valid *before* the front of the diffusion reaches the central plane of the sheet at $x = \ell$. During this stage of the diffusion, there are still *free* ligands in the porous solid that have not reacted with the diffusing metal ions. Since, at time t, the ligands in the region $0 \le x \le u(t)$ have been saturated (Figure 2.1), *the moles of the product* (N_p) between the ligands and the diffusing metal ions for a half of the plane sheet is:

$$N_p = L_0 u(t) = (2L_0 C_0 Dt)^{1/2} \qquad \text{(Eq. 2.14)}$$

Equations 2.13 and 2.14 indicate that the distance $u(t)$, which the front of the diffusing metal ions has traveled through diffusion, as well as the moles of the product (N_p) formed in the solid are each a linear function of *square roots* of both the time t and the concentration C_0 of the metal ions in the external solution. These relationships are used in the design of optical sensors to be discussed below.

2.3.2. Spectroscopic Characterization of the Diffusion Process

If the product between the ligands and the diffusing metal ions in the region $0 \le x \le u(t)$ could be observed spectroscopically, and the spectrum follows Beer's law, we have, for *both halves* of the plane sheet,[11]

$$A_p = 2\varepsilon_p L_0 u(t) = 2\sqrt{2}\varepsilon_p (L_0 C_0 Dt)^{1/2} = Kt^{1/2} \qquad \text{(Eq. 2.15)}$$

$$K = 2\sqrt{2}\varepsilon_p (L_0 C_0 D)^{1/2} \ (s^{-1/2}) \qquad \text{(Eq. 2.16)}$$

where is ε_p = molar extinction coefficient of the product; A_p = absorbance of the product.

Equations 2.15 and 2.16 indicate that, if the absorbance of the product (A_p) is monitored with time of diffusion (t), the slopes (K) from the A_p vs. $t^{1/2}$ plots with different concentrations of the metal ions (C_0) in the external solution are a linear function of the square root of C_0. With higher concentrations of C_0 in the external solution, faster diffusion of the metal ions into the solid is expected, leading to larger values for slopes K in the A_p vs. $t^{1/2}$ plots. The slope K should increase linearly with $C_0^{1/2}$, as suggested by Equation 2.16. In addition, if the concentration of the ligands (L_0) in the solid and molar extinction coefficient of the product (ε_p) are known, the diffusion coefficient (D) may be obtained from the K vs. $C_0^{1/2}$ plot (Equation 2.16). If the diffusing metal ions absorb at the wavelength of observation, the use of a reference containing the diffusing metal ions would remove this absorbance as a source of error.[17]

2.3.3. Quantitative Cu(II) Analysis – A Demonstration of the New Model

The mathematical model and organically modified mesoporous monoliths in the current work could be used as a new approach to chemical sensing. Copper(II) was chosen here due to its common occurrence in a variety of industrial applications. Copper electroplating is employed in many industrial

processes, including the manufacture of next-generation microelectronic devices in the semiconductor industry.[18] Copper plating onto silicon wafers in very low acid or neutral solutions was recently developed.[18b] Copper(II) is also recognized by the U.S. Environmental Protection Agency (EPA) as a toxic pollutant and is RCRA (Resource Conservation and Recovery Act) regulated.[18c] Heavy metal ion sensors including those for Cu(II) have been actively studied.[1] As discussed below, the current work using the amine-grafted monoliths and the mathematical model provides a unique optical sensor for quantitative Cu(II) analysis.

Porous, cylindrical silica sol-gel monoliths (thickness: 0.387 cm; diameter: 1.095 cm; volume: 3.64×10^{-4} dm^3; Figure 2.2)[11] were used in the current studies. These monoliths are not ideal plane sheets. Their diameter is however significantly larger than their width, and the Cu^{2+} diffusion is monitored with optical fibers mounted at the monolith center. Fewer Cu^{2+} ions that diffuse radially reach the center (of the monoliths) than those diffusing from the two faces. If, as the first approximation, the radial contribution is ignored, the Cu^{2+} diffusion to these monoliths grafted with amine ligands may be treated by the model developed in the current work. In other words, an approximation was made when using this model for the amine-grafted monoliths in the current work.

The sensor monoliths were prepared by a procedure shown in Figure 2.3.[9] Blank monoliths were first synthesized through the hydrolysis of $Si(OMe)_4$ in the presence of a porogen. The monoliths were then washed with $MeOH/H_2O$ and then H_2O to remove the porogen and catalyst NaOH. Amine $H_2N\text{-}(CH_2)_3\text{-}Si(O–)_3$

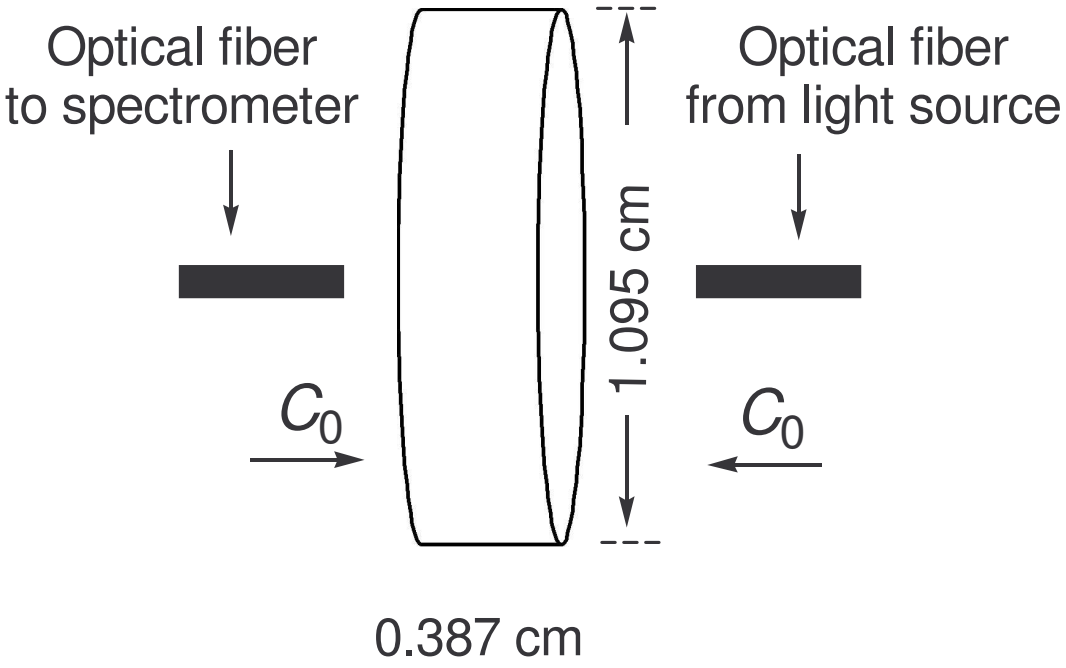

Figure 2.2. Schematic depicting the dimensions of the monolith and the fiber-optic cables as used during UV-vis spectroscopic analysis of the diffusion process.

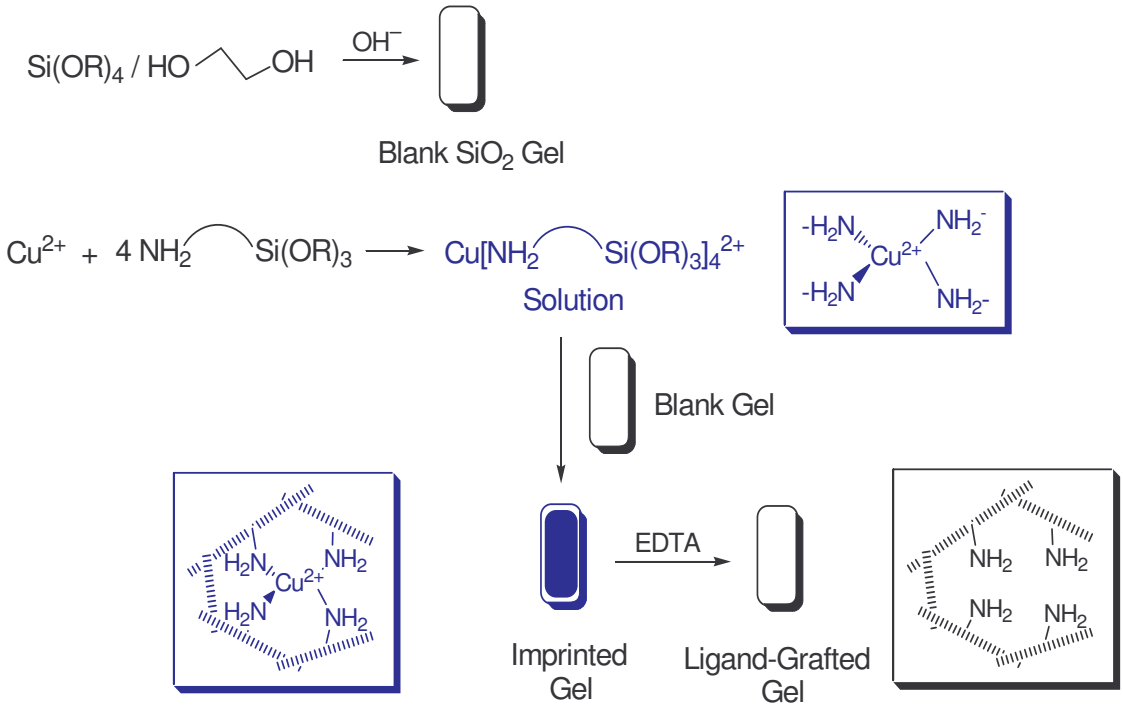

Figure 2.3. Preparation of the blank and amine-grafted sol-gel monolith.

was imprint-grafted[19] by immersing the monoliths in solutions of $Cu[H_2N\text{-}(CH_2)_3\text{-}Si(OMe)_3]_4^{2+}$ complex, and the latter diffused into and grafted onto the monoliths. After the grafting, the monoliths turned blue, and visible spectra of the monoliths showed a band at 730 nm.

BET gas adsorption experiments indicate that these monoliths are mesoporous with an average pore diameter of ca. 47 Å. A plot of pore volume as a function of pore diameter (Figure 2.4) indicates that the monoliths have a pore size distribution that is consistent throughout the bulk of the material. The peak of this plot near 47 Å represents the size of pores that contribute most to the pore volume. Figure 2.5 shows the N_2 adsorption isotherm plot with a Z-shaped hysteresis loop. This hysteresis loop is common in mesoporous materials including inorganic oxides and glasses.[20] The specific surface area is 232 m^2/g, and the total pore volume is 0.24 cc/g for all pores of the monolith less than 174 Å.

A diffuse reflectance infrared Fourier transform spectrum (DRIFT) of powders from such a monolith (Figure 2.6) shows the C-C and C-N stretching frequencies at 1200–800 cm^{-1} and 1200–1020 cm^{-1}, respectively and C-H twisting and wagging frequencies at 1350–1150 cm^{-1}, although they are not distinguishable from each other in the 1300–1150 cm^{-1} region.[21a] These observations support the grafting of the amine $H_2N\text{-}(CH_2)_3\text{-}Si(O\text{–})_3$ ligand onto our sol-gel monolith. The Si-OH bands (isolated and bridged silanols at 3740 and 3550-3670 cm^{-1}, respectively) in the samples may overlap with the N-H

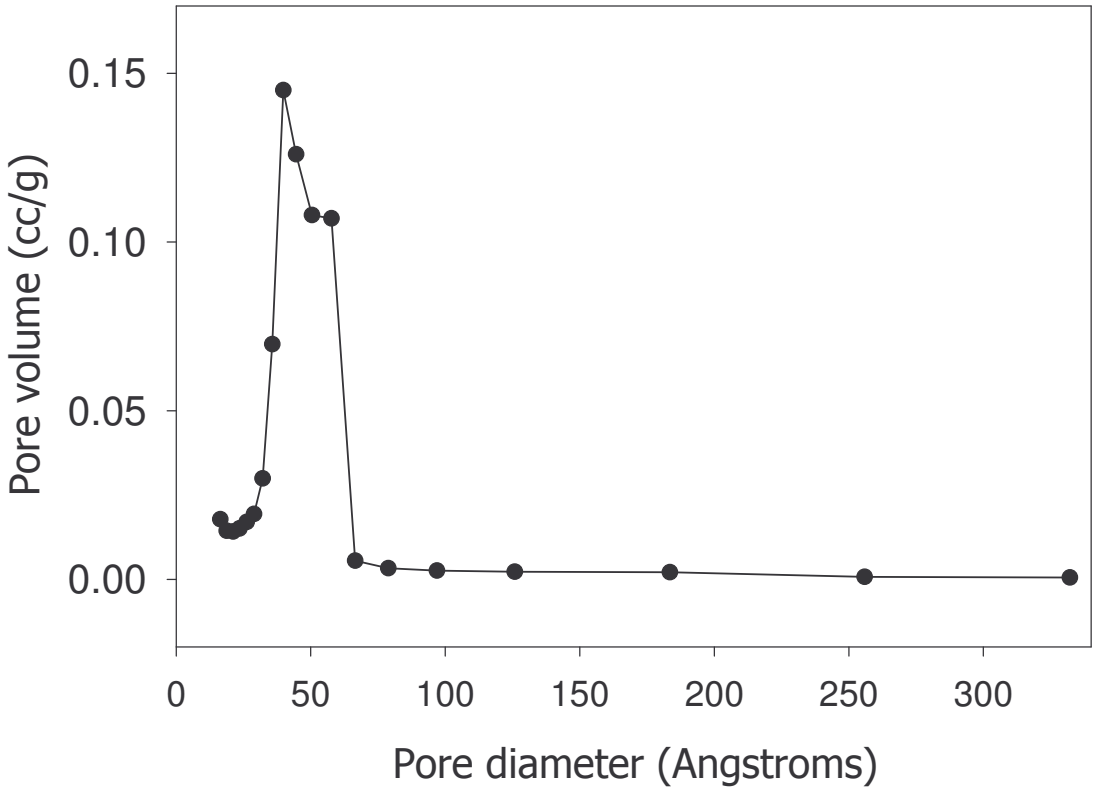

Figure 2.4. BET pore size distribution plot for an amine-grafted sol-gel monolith. Average pore size is shown to be ~47 Å.

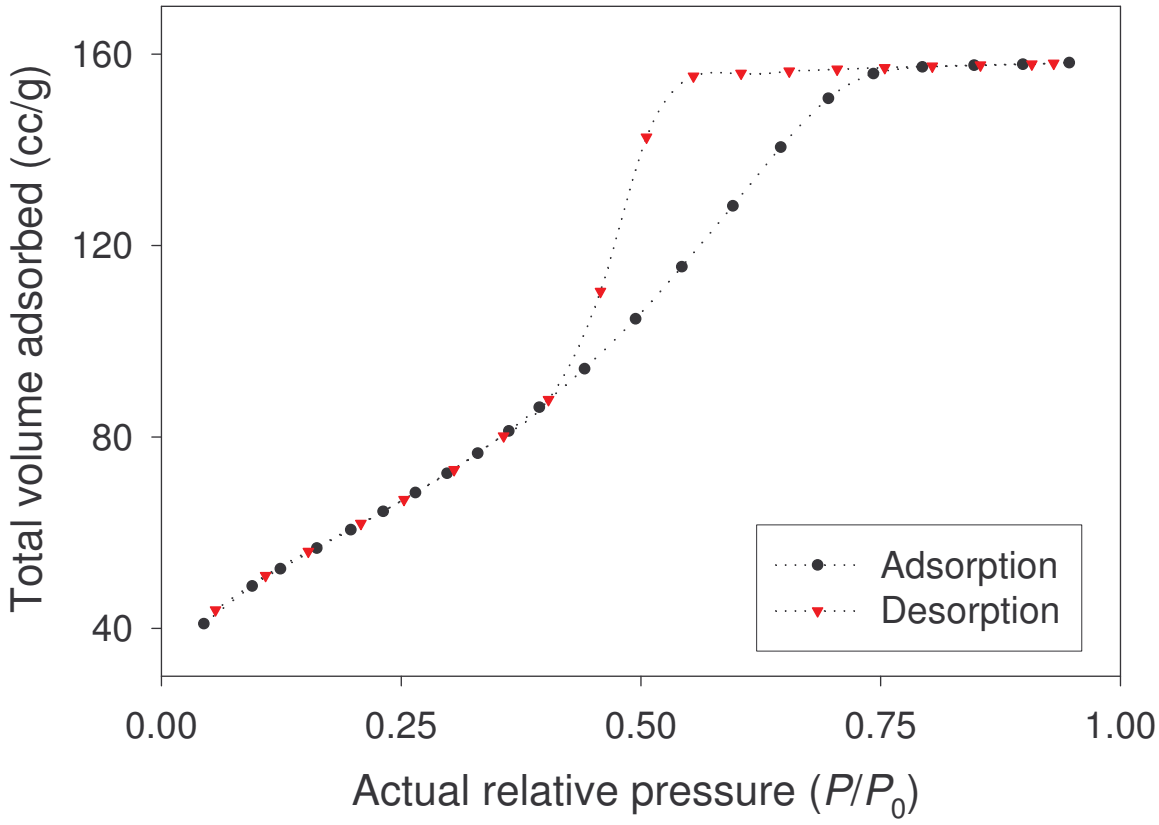

Figure 2.5. N_2 gas adsorption/desorption isotherm for the sol-gel monolith: adsorption (●); desorption (▼).

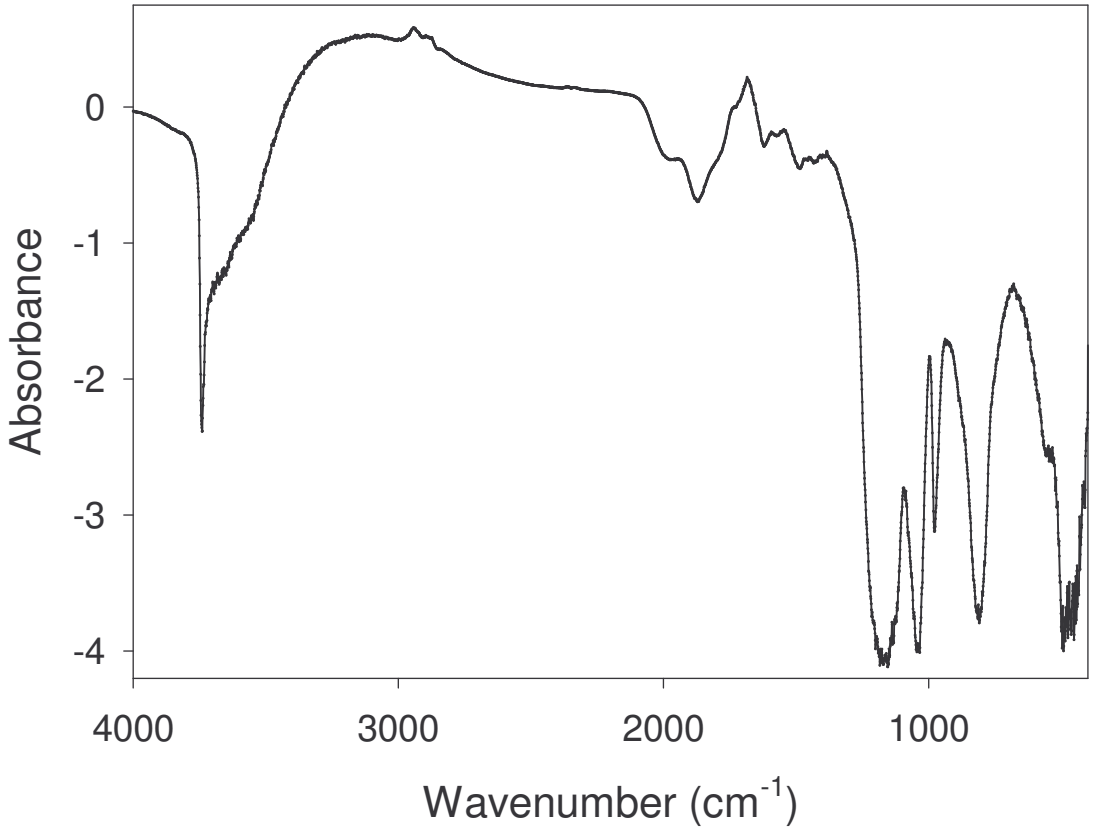

Figure 2.6. A difference DRIFT spectrum between the powders of an amine H_2N-$(CH_2)_3$-$Si(O–)_3$ grafted monolith and a blank sol-gel control.

stretching frequencies at 3800-2700 cm^{-1} (ν_{as} = 3358 and ν_s = 3279 cm^{-1} for a $-NH_2$ group[21b]).

^{29}Si solid-state NMR spectroscopy has been used extensively to elucidate the molecular environment in silicate materials.[22] ^{29}Si solid-state NMR spectra of the sol-gel solids show signals representative of various substructures of the T^n and Q^n silane moities. Spectra displaying Q^n ($n \leq 4$) peaks indicate that the condensation of the silicon alkoxide precursor is incomplete.[22e] As the degree of condensation increases, the T^n and Q^n peaks are shifted to higher field in the NMR spectrum. Characteristic NMR signals of unmodified silica gel are silanediol groups (Q^2), silanol groups (Q^3), and siloxane groups (Q^4), which appear at –92, –101, and –110 ppm, respectively.[22a] Q^n peaks, which are representative of the silica support, are the only peaks expected for the blank sol-gel monolith in the current studies. T^n peaks are representative of silicon atoms in the sol-gel matrix directly bonded to an organic species. As n increases in the T^n species, the number of organic species bonded to a silicon atom decreases. Since the APS ligand has only one organic group attached directly to the silicon atom, only T^3, Q^2, Q^3, and Q^4 peaks are expected in the NMR spectrum of the APS-grafted monolith. The ^{29}Si NMR spectra of a blank and APS-grafted monolith are shown in Figure 2.7. As expected, the blank shows only Q^2, Q^3, and Q^4 peaks in the NMR spectrum which are representative of a siloxane matrix with no organic groups directly bound to silicon. The APS-grafted monolith shows only a T^3 peak in addition to the expected Q peaks, which indicates that the APS ligand is in fact, bound to the sol-gel monolith as proposed.

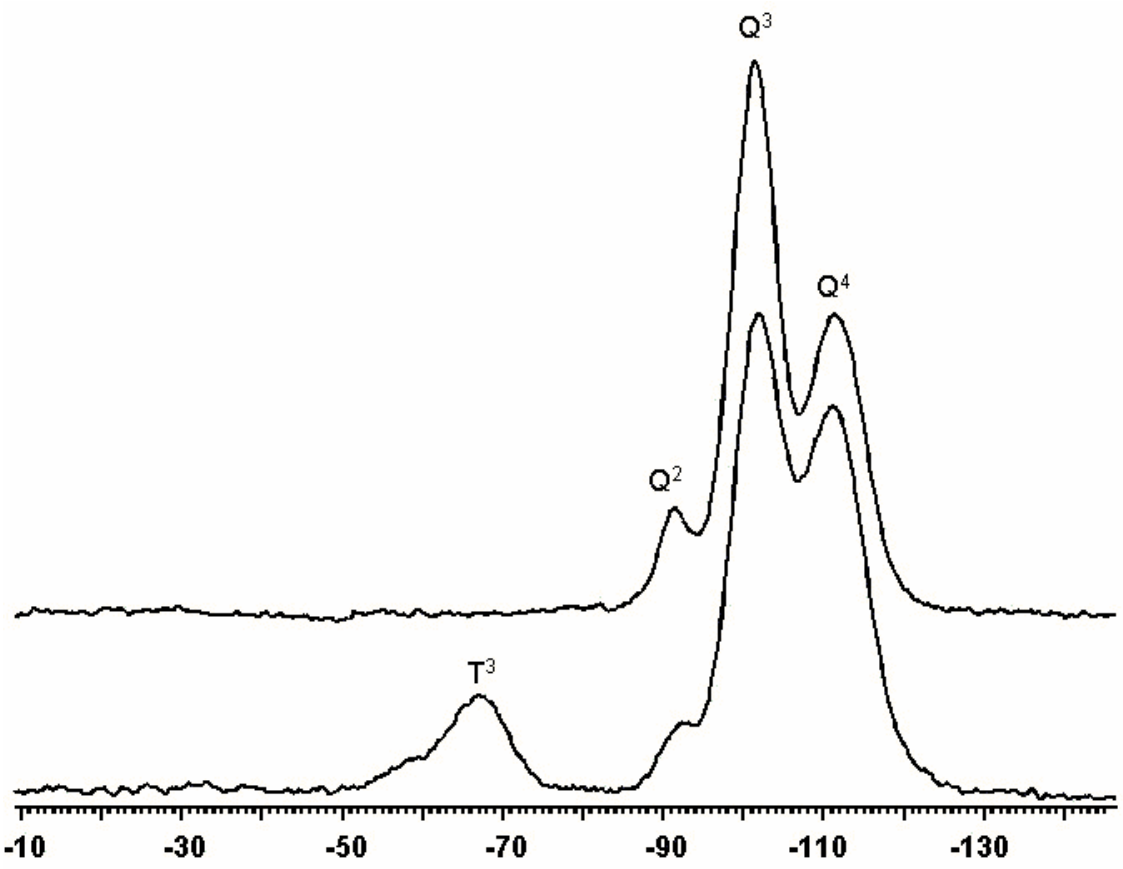

Figure 2.7. ^{29}Si MAS solid-state NMR spectra of a blank (top) and APS imprint-grafted sol-gel monolith (bottom).

The reactions between Cu^{2+} and amines to give their complexes are known to be fast. For example, the rate constants of reactions of tetraamine $H_2N(CH_2)_2NH(CH_2)_2NH(CH_2)_2NH_2$ with $Cu(OH)_4^{2-}$ and $Cu(OH)_3^-$ are $1.0(0.7) \times 10^7$ and $4.3(0.2) \times 10^6$ M^{-1} s^{-1}, respectively.[23] A separate test of such a $Cu[H_2N\text{-}(CH_2)_3\text{-}Si(O-)_3]_4^{2+}$ grafted monolith showed a visible band at 730 nm for this complex in the silica gel with the molar extinction coefficient ε_p = 32.2 M^{-1} cm^{-1}.[11,24] The amine was chosen in part because of the high affinities of alkyl amines for Cu^{2+} ions (Equation 2.2).[2] After the grafting of the Cu^{2+} complex, Cu^{2+} ions were then removed by immersing the monoliths in solutions of ethylenediaminetetraacetate (EDTA).

Such a monolith containing the amine ligands was then placed in the path of optical fibers connected to a UV-visible spectrometer. The monolith and optical fibers were housed in a Teflon cell, and an aqueous $CuCl_2$ solution (ca. 300 mL) was pumped through the chamber at a rate of 13.8 mL/min. Cu^{2+} ions diffused into the monolith and were immobilized by the amine ligands. During the Cu^{2+} uptake process, a peak at 730 nm was observed for the Cu^{2+}-amine complex. This peak is at the same wavelength as that of the original, imprint-grafted tetra-amine complex $Cu[H_2N\text{-}(CH_2)_3\text{-}Si(O-)_3]_4^{2+}$, suggesting that the newly formed complex is a Cu^{2+} tetra-amine complex as well. The Cu^{2+} uptake process was monitored spectroscopically at 730 nm, and the visible spectra of the monolith were recorded. A blank monolith *without* the ligands was used as the reference, and was placed in the chamber. The same aqueous $CuCl_2$

solution (ca. 300 mL) was pumped through the chamber at a rate of 13.8 mL/min before the spectra were recorded as reference. Although Cu^{2+} ions have an absorbance at 730 nm (ε_r = 9.55 M^{-1} cm^{-1}), it is reasonable to assume that the use of the blank monolith as reference eliminates the absorbance of free Cu^{2+} ions inside the sample monolith as a source of error.[17]

Absorbance (A_p) vs. $t^{1/2}$ plots by Equation 2.15 for Cu^{2+} diffusion and immobilization in the amine-grafted monoliths are shown in Figure 2.8. For Cu^{2+} concentrations (C_0) between 0.0200 to 0.0800 M, these plots are linear with correlation coefficients $R^2 \geq 0.998$, as expected from Equation 2.15. These observations support the new mathematical model in the current work. It should be noted that the current model is limited to the cases with a constant Cu(II) concentration (C_0) during the diffusion of Cu(II) ions into the monolith.

The average slopes (K_{av}) of these A_p vs. $t^{1/2}$ plots, from at least three measurements for each C_0 concentration from the same batch of monoliths, as well as the values of $2\varepsilon_p C_0^{1/2}$ according to Equation 2.16 are given in Table 2.1. Small errors (< 2%) in the K_{av} values were observed for the measurements at each Cu^{2+} concentration, indicating that these measurements are highly reproducible for each batch of monoliths.

The K vs. $2\varepsilon_p C_0^{1/2}$ plot is given in Figure 2.9. A linear fit of the data points gives a correlation coefficient, R^2 = 0.988, suggesting a linear correlation. The slope in Figure 2.9 and Equation 2.16 give $(2L_0D)^{1/2} = 1.56 \times 10^{-3}$ $s^{-1/2}$ $M^{1/2}$ cm and $D_{Cu(II)} = 9.6 \times 10^{-6}$ cm^2 s^{-1} as the diffusion coefficient for *free* Cu^{2+} ions inside

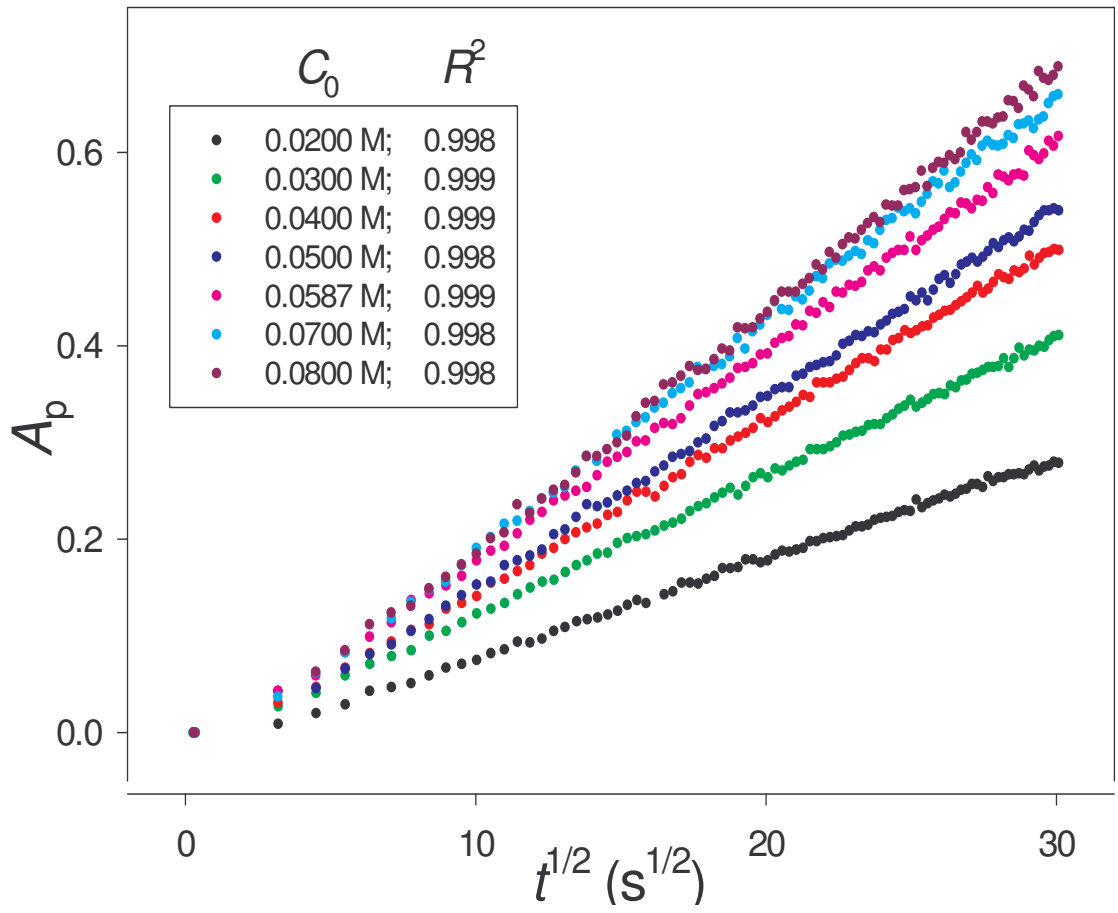

Figure 2.8. A_p vs. $t^{1/2}$ plots for Cu^{2+} diffusion and immobilization in the amine-grafted monoliths.

Table 2.1. Slopes (K_{av}) of the A_p vs. $t^{1/2}$ plots.

C_0 (M)	K_{av} ($s^{-1/2}$)	$2\varepsilon_p C_0^{1/2}$ ($M^{-1/2}$ cm^{-1})
0.0200	0.0103 ± 0.0002	9.1075
0.0300	0.0143 ± 0.0001	11.1544
0.0400	0.0176 ± 0.0002	12.8800
0.0500	0.0195 ± 0.0002	14.4003
0.0587	0.0217 ± 0.0002	15.6029
0.0700	0.0228 ± 0.0003	17.0386
0.0800	0.0248 ± 0.0002	18.2151

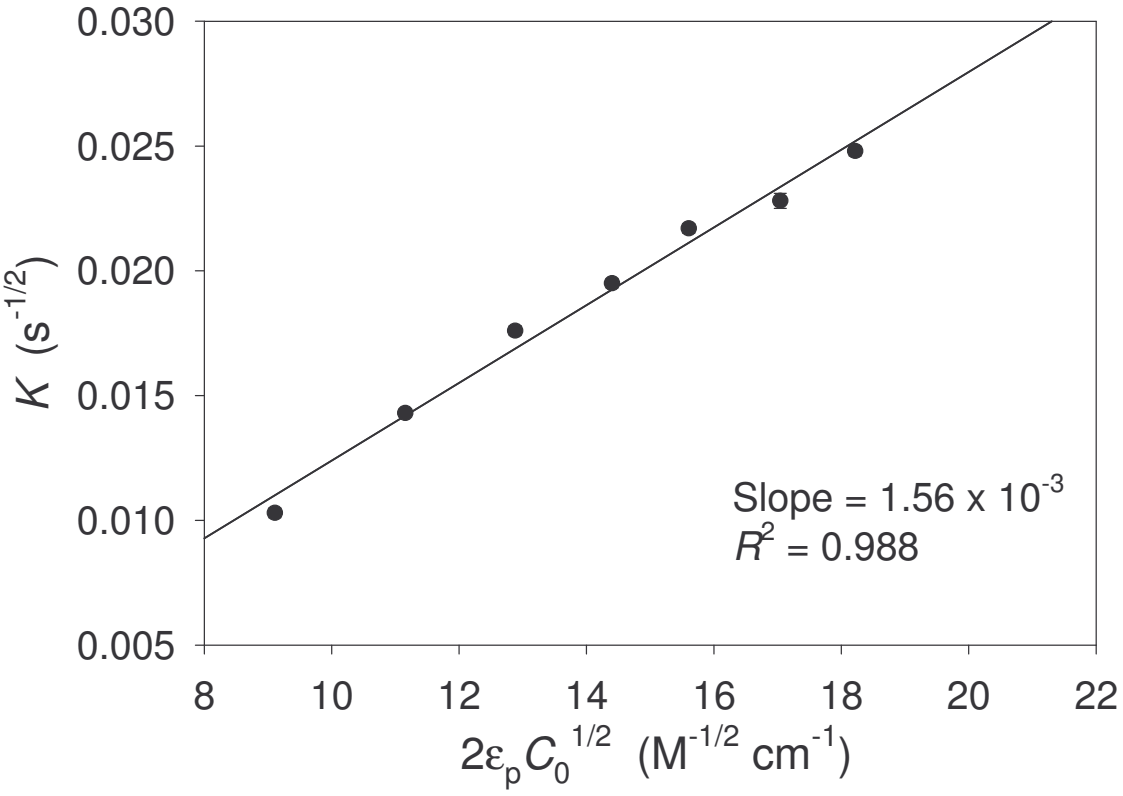

Figure 2.9. Plot of K_{av} vs. $2\varepsilon_p C_0^{1/2}$ according to Equation 2.16.

the mesoporous, amine-grafted monoliths. It should be pointed out that the Cl^- anions diffuse along with Cu^{2+} cations in the current process to balance the charge. It is interesting to compare the diffusion coefficient obtained here with a reported coefficient for Cu^{2+} diffusion inside silica gels that did not contain ligands.[25] Eversole and Doughty have measured by a photometric method the diffusion of Cu^{2+} ions in such silica gels, and estimated the diffusion coefficient to be $D_{Cu(II)} \approx 4.6 \times 10^{-6}$ cm^2 s^{-1}.[25] The two $D_{Cu(II)}$ values are comparable, supporting the validity of the new model in the current work. In our current model, the immobilization of Cu^{2+} ions by the grafted amine in the monoliths is accounted for to give the $D_{Cu(II)}$ value for *free* Cu^{2+} ions. The relatively large pore sizes of 47 Å perhaps make the diffusion of small Cu^{2+} ions relatively unhindered in the mesoporous solids.

The monoliths in the current work were prepared in batches, each containing at least 30 individual monoliths. The errors in K in Table 2.1 show that the monoliths in the same batch gave highly reproducible results. In addition, reproducibility among different batches was tested. Monoliths from six different batches were tested in 0.0500 M $CuCl_2$ solutions to give uncertainties of $\delta K/K$ = 0-3.9%. Thus a few monoliths may be used to establish, e.g., the K_{av} vs. $2\varepsilon_p C_0^{1/2}$ calibration plot (Figure 2.9), and other monoliths could then be used as sensors for unknown Cu^{2+} solutions to determine their concentrations. With a good quality control in the monolith preparation, an even higher reproducibility among different batches may be achieved.

2.3.4. Comparison of the Current Model With Earlier Models for Chemical Diffusion

There have been many excellent models describing different chemical diffusion processes. It is thus important to note the uniqueness of the current model.

As in other diffusion processes involving moving boundaries that Crank has summarized in his classic book on the mathematics of diffusion,[14c] the current model is based on the assumption of the presence of two regions (Figure 2.1) separated by the moving boundary. In the region behind the boundary, all sites of ligands in the solid are occupied and immobilization is complete. In the region before the boundary, the concentration of the freely diffusing metal ions is zero, and none of the sites are occupied. This model thus applies to cases where the binding constants between the ligands and the metal ions are large. Many complexes between ligands and metal ions have large stability constants[10] including thiol (–SH) with Hg^{2+},[26] crown ethers with alkali metals,[10] and the current Cu^{2+}-amine complex.[2]

The current model is thus for processes different from diffusion followed by a chemical reaction with the external reagents[14e] or sorption of dye molecules for example in microporous materials such as silica beads and zeolites.[27] In diffusion followed by a chemical reaction, it is assumed that some unoccupied sites are always available,[14e] and the processes may depend on the kinetics of the reactions as well. Crank has summarized the earlier work in this area.[14e] The sorption is a non-steady state process, and relies on the Langmuir isotherm

with the equilibrium for the immobilization.[27]

In the current model the immobilized external reagents such as Cu^{2+}-amine complexes do not undergo additional reactions. This is different from those that involve the consumption of the external reagents by the reactive sites such as diffusion of O_2 to biological tissues[28] and diffusion of reactants/substrates to chemical or enzymatic catalytic sites inside the solid support followed by their reactions. However the current model applies to cases where the products between external reagents and the functional groups/molecules inside the solid undergo reactions such as quenching or activation of photoluminescence, and the functional groups/molecules are subsequently not available for binding.

Crank has developed a model for *steady state* diffusion followed by immobilization for processes with *limited* supplies of the external reagents.[14c] In those cases, the surface concentrations of the external reagents in Figure 2.1 are a function of time. He also developed another model for *unlimited* supplies of the external reagents and *non-steady state* diffusion.[14b] In this case, the model is in the form of infinite series solutions, and requires numerical and/or graphical solutions.[14b] In comparison, the current model is designed for the *steady state* diffusion processes and is in the form of analytical solutions.

2.4. Concluding Remarks

In summary, the current model for chemical sensors combine both diffusion and a subsequent immobilizing reaction, the two fundamental processes

that metal ions often undergo in a monolith grafted with ligands, to provide a unique approach for quantitative metal ion analysis. The model (Equations 2.15 and 2.16) is straightforward and may be used for sensors of other analytes that undergo both diffusion and immobilizing reactions with functional groups/molecules grafted/encapsulated in porous monoliths.

References

1. See, e.g., the following papers on sensors for heavy metals: (a) Oheme, I.; Wolfbeis, O. S. *Mikrochim. Acta* **1997**, *126*, 177. (b) Seitz, W. R. in *Fiber Optic Chemical Sensors and Biosensors*, Wolfbeis Ed., Vol. 2., CRC, Boca Raton, **1991**, pp. 1-17. (c) Saito, T. *Talanta* **1994**, *41*, 811. (d) Preininger, C.; Wolfbeis, O. S. *Biosens. Bioelectron.* **1996**, *11*, 981. (e) Saari, L. A.; Seitz, W. R. *Anal. Chem.* **1984**, *56*, 810. (f) Oheme, I.; Prokes, B.; Murkovic, I.; Werner, T.; Klimant, I.; Wolfbeis, O. S.; *Fresen J. Anal. Chem.* **1994**, *350*, 563. (g) Lin, J.; Brown, C. W. *Trends Anal. Chem.* **1997**, *16*, 200. (h) Freeman, J. E.; Childers, A. G.; Steele, A. W.; Hieftje, G. M*. Anal. Chim. Acta* **1985**, *177*, 121. (i) Lu, J.-Z.; Zhang, Z.-J. *Analyst* **1995**, *120*, 453. (j) Lu, J.; Zhang, Z. *Anal. Lett.* **1994**, *27*, 2431. (k) Bright, F. V.; Poirier, G. E.; Hieftje, G. M. *Talanta* **1988**, *35*, 113. (l) Qin, W.; Zhang, Z.; Liu, H. *Anal. Chem*. **1998**, *70*, 3579. (m) Jerónimo, P. C. A.; Araújo, A. N.; Montenegro, M. C. B. S. M.; Pasquini, C.; Raimundo, I. M. Jr. *Anal. Bioanal. Chem.* **2004**, *380*, 108. (n) Shakhsher, Z. M.; Odeh, I.; Jabr, S.; Seitz, W. R. *Microchim. Acta* **2004**, *144*, 147. (o)

Steinberg, I. M.; Lobnik, A.; Wolfbeis, O. S. *Sens. Actuators, B* **2003**, *90*, 230. (p) Mahendra, N.; Gangaiya, P.; Sotheeswaran, S.; Narayanaswamy, R. *Sens. Actuators, B* **2003**, *90*, 118. (q) Zheng, Y.; Orbulescu, J.; Ji, X.; Andreopoulos, F. M.; Pham, S. M.; Leblanc, R. M. *J. Am. Chem. Soc.* **2003**, *125*, 2680. (r) Tunoglu, N.; Caglar, P.; Wnek, G. E. *J. Macromole. Sci. Pure Appl. Chem.* **1998**, *A35*, 637.

2. (a) Fisher, J. F.; Hall, J. L. *Anal. Chem.* **1967**, *39*, 1550. (b) Equation 1 gives the overall equilibrium constant for the $Cu(NH_2Et)_4^{2+}$ complex. There are four steps in the formation of such a 4-coordinated complex, and there is a usually smaller equilibrium constant for each step. See, e.g., Shriver, D. F.; Atkins, P.; Langford, C. H. *Inorganic Chemistry*, 2nd Ed., Freeman, New York, p. 262.

3. Mayr, T.; Igel, C.; Liebsch, G.; Klimant, I.; Wolfbeis, O. S. *Anal. Chem.* **2003**, *75*, 4389.

4. (a) Wallington, S.-A.; Labayen, T.; Poppe, A.; Sommerdijk, N. A. J. M.; Wright, J. D. *Sens. Actuators, B* **1997**, *38*, 48. (b) Sommerdijk, N. A. J. M.; Poppe, A.; Gibson, C. A.; Wright, J. D. *J. Mater. Chem.* **1998**, *8*, 565. (c) Sommerdijk, N. A. J. M.; Wright, J. D. *J. Sol-Gel Sci. Technol.* **1998**, *13*, 565.

5. See, e.g., (a) Avnir, D. *Acc. Chem. Res.* **1995**, *28*, 328. (b) Dave, B. C.; Dunn. B.; Valentine, J. S.; Zink, J. I. *Anal. Chem.* **1994**, *66*, 1120A. (c) Lev, O.; Tsionsky, M.; Rabinovich, L.; Glezer, V.; Sampath, S.; Pankratov, I.; Gun, J. *Anal. Chem.* **1995**, *67*, 22A. (d) Bescher, E.; Mackenzie, J. D.

Mater. Sci. Eng. C **1998**, *6*, 145. (e) Ingersoll, C. M.; Bright, F. V. *Chemtech* **1997** (January), 26. (f) Prasad, P. N.; Bright, F. V.; Narang, U.; Wang, R.; Dunbar, R. A.; Jordan, J. D.; Gvishi, R. *ACS Symp. Series* **1995**, *585*, 317. (g) Janata, J. *Anal. Chem.* **2001**, *73*, 150A. (h) Ellis, A. B.; Walt, D. R. *Chem. Rev.* **2000**, *100*, Issue 7. (i) Wolfbeis, O. S. *Anal. Chem.* **2002**, *74*, 2663.

6. See, e.g., (a) Schubert, U.; Hüsing, N.; Lorenz, A. *Chem. Mater.* **1995**, *11*, 2010. (b) Clark, J. H.; Macquarrie, D. J. *Chem. Soc. Rev.* **1996**, *25*, 303. (c) Corma, A. *Chem. Rev.* **1997**, *97*, 2373. (d) Maschmeyer, T.; Oldroyd, R. D.; Sankar, G.; Thomas, J. M.; Shannon, I. J.; Klepetko, J. A.; Masters, A. F.; Beattie, J. K.; Catlow, C. R. A. *Angew. Chem., Int. Ed.* **1997**, *36*, 1639. (e) Gelman, F.; Blum, J.; Avnir, D. *J. Am. Chem. Soc.* **2002**, *124*, 14460.

7. The technique of diffusive gradients in thin films (DGT) has developed recently as an effective way to determine in situ labile trace metal concentrations in aqueous solutions and sediments. After the analytes diffuse into the diffusive gel used in the DGT device, inductively coupled plasma mass spectrometry (ICP-MS), proton induced X-ray emission (PIXE) or X-ray fluorescence spectroscopy (XRF) is used to analyze the metal ions in the diffusive gel. See, e.g., (a) Zhang, H.; Davison, W. *Anal. Chem.* **1995**, *67*, 3391. (b) Warnken, K. W.; Zhang, H.; Davison, W. *Anal. Chim. Acta* **2004**, *508*, 41. (c) Garmo, O. A.; Royset, O.; Steinnes, E.; Flaten, T.P. *Anal. Chem.* **2003**, *75*, 3573.

8. (a) Allain, L. R.; Sorasaenee, K.; Xue, Z.-L. *Anal. Chem.* **1997**, *69*, 3076. (b) Allain, L. R.; Xue, Z.-L. *Anal. Chem.* **2000**, *72*, 1078. (c) Allain, L. R.; Xue, Z.-L. *Anal. Chim. Acta* **2001**, *433*, 97. (d) Allain, L. R.; Canada, T. A.; Xue, Z.-L. *Anal. Chem.* **2001**, *73*, 4592. (e) Canada, T. A.; Allain, L. R.; Beach, D. B.; Xue, Z.-L. *Anal. Chem.* **2002**, *74*, 2535. (f) Canada, T. A.; Xue, Z.-L. *Anal. Chem.* **2002**, *74*, 6073.

9. Clavier, C. W. MS Thesis, The University of Tennessee, **2001**, Ch. 3.

10. *NIST Standard Reference Database 46: NIST Critically Selected Stability Constants of Metal Complexes: Ver. 7.0.* National Institute of Standards and Technology, Gaithersburg, MD, 2003.

11. In Equation 2.15, units of C_0 and L_0, ε_p, and D are M, M^{-1} cm^{-1} and cm^2 s^{-1}, respectively. Although M = mol L^{-1} = mol dm^{-3} is based on dm rather than cm, the unit of M is cancelled in Equation 2.15, and thus does not affect the use of cm^2 s^{-1} as the unit for the diffusion coefficient. This is similar to the units in Beer's law where ε adopts the unit of M^{-1} cm^{-1}. The unit of volume in dm^3 is used to calculate L_0, the concentration of ligands in the monoliths.

12. (a) Walcarius, A.; Etienne, M.; Bessiere, J. *Chem. Mater.* **2002**, *14*, 2757. (b) Walcarius, A.; Etienne, M.; Lebeau, B. *Chem. Mater.* **2003**, *15*, 2161. (c) Walcarius, A.; Delacote, C. *Chem. Mater.* **2003**, *15*, 4181.

13. (a) El-Nahhal, I. M.; Zaggout, F. R.; El-Ashgar, N. M. *Anal. Lett.* **2000**, *33*, 2031. (b) Ma, W. X.; Liu, F.; Li, K. A.; Chen, W.; Tong, S. Y. *Anal. Chim.*

Acta **2000**, *416*, 191. (c) Im, H.-J.; Yang, Y.; Allain, L. R.; Barnes, C. E.; Dai, S.; Xue, Z. *Environ. Sci. Technol.* **2000**, *34*, 2209.

14. Crank, J. *The Mathematics of Diffusion*; 2nd Ed., Oxford University Press: London, 1975. (a) p. 286 (Section 13.1). (b) p. 298 (Section 13.3). (c) p. 44 (Section 4.2) and p. 310 (Section 13.6.1). (d) p. 312 (Section 13.6.2). (e) p. 326 (Section 14.1).

15. Eriksson, K.; Estep, D.; Hansbo, P.; Johnson, C. *Computational Differential Equations*, Cambridge University Press: Cambridge, Great Britain, 1996, p. 7.

16. Stefan, J. *Sitzungsber. Akad. Wiss. Wien, Math.-Naturwiss. Kl., Abt. 2A.* **1890**, *98*, 965.

17. A more comprehensive formula is given in Appendix A for the scenario in which the diffusing reagent itself such as Cu^{2+} has absorbance at the wavelength of observation, and this absorbance is *not* corrected as a part of reference during the acquisition of spectra.

18. (a) Andricacos, P. C.; Uzoh, C.; Dukovic, J. O.; Horkans, J.; Deligianni, H. *IBM J. Res. Dev.* **1998**, *42*, 567. (b) Landau, U.; D'Urso, J.; Lipin, A.; Dordi, Y.; Malik, A.; Chen, M.; Hey, P. In *Electrochemical Processing in ULSI Fabrication and Semiconductor/Metal Deposition II*; Andricaos, P. C.; Searson, P. C.; Reidsema-Simpson, C.; Allongue, P.; Stickney, J. L.; Oleszek, G. M. Eds.; The Electrochemical Society, **1999**; Vol. 99-9, pp. 25-39. (c) Alkhatib, E.; O'Connor, T. *Am. Environ. Lab.* **1998**, *10*, 6.

19. (a) Dai, S.; Burleigh, M. C.; Shin, Y.; Morrow, C. C.; Barnes, C. E.; Xue, Z.

Angew. Chem., Int. Ed. **1999**, *38*, 1235. (b) Dai, S.; Shin, Y. S.; Ju, Y. H.; Burleigh, M. C.; Lin, J. S.; Barnes, C. E.; Xue, Z.-L. *Adv. Mater.* **1999**, *11*, 1226. (c) Dai, S.; Burleigh, M. C.; Ju, Y. H.; Gao, H. J.; Lin, J. S.; Pennycook, S. J.; Barnes, C. E.; Xue, Z.-L. *J. Am. Chem. Soc.* **2000**, *122*, 992. (d) Burleigh, M. C.; Dai, S.; Hagaman, E. W.; Lin, J. S. *Chem. Mater.* **2001**, *13*, 2537.

20. (a) Kruk, M.; Jaroniec, M. *Chem Mater*. **2000**, *12*, 222. (b) Kruk, M., Jaroniec, M. *Chem. Mater*. **2001**, *13*, 3169.

21. (a) Mansur, H. S.; Vasconcelos, W. L.; Lenza, R. S.; Oréfice, R. L.; Reis, E. F.; Lobato, Z. P. *J. Non-Crystal. Solids* **2000**, *273*, 109. (b) Etienne, M.; Walcarius, A. *Talanta* **2003**, *59*, 1173.

22. (a) Engelhardt, G.; Michel, D. *High-Resolution Solid-State NMR of Silicates and Zeolites*, Wiley, New York, 1987. (b) Fyfe, C. A. *Solid-State NMR for Chemists*, CFC Press, Ontario, 1983. (c) Magi, M. Lippmaa, E.; Samoson, A.; Engelhardt, G.; Grimmer, A. R. *J. Phys. Chem*. **1984**, *88*, 1518. (d) Maher, J. M.; Cooper, N. J. *J. Am. Chem. Soc*. **1980**, *102*, 7606. (e) Gorlach, B.; Hellriegel, S. S.; Yiksel, H.; Albert, K.; Plies, E.; Hanack, M. *J. Mater. Chem*. **2001**, *11*, 3317.

23. (a) Drumhiller, J. A.; Montavon, F.; Lehn, J. M.; Taylor, R. W. *Inorg. Chem.* **1986**, *25,* 3751. (b) Wilkins, R. G. *Kinetics and Mechanism of Reactions of Transition Metal Complexes*, 2nd Ed., VCH: New York, p. 224. The four imprinted amine ligands in the cavities of the solids are similar to the tetraamine ligands quoted here.

24. Klonkowski and coworkers have studied spectroscopically the $Cu[NH_2(CH_2)_3(SiO–)_3]_n$ complexes grafted in silica sol gels. See, e.g., Klonkowski, A. M.; Grobelna, B.; Widernik, T.; Jankowska-Frydel, A.; Mozgawa, W. *Langmuir* **1999**, *15*, 5814.

25. Eversole, W. G.; Doughty, E. W. *J. Phys. Chem.* **1936**, *40*, 55.

26. Chen, X.; Feng X.; Liu, J.; Fryxell, G. E.; Gong, M. *Sep. Sci. Technol.* **1999**, *34*, 1121.

27. (a) Weisz, P. B. *Ind. Eng. Chem. Res.* **1995**, *34*, 2692. (b) Kocirik, M.; Micke, A. *Langmuir* **1995**, *11*, 3042.

28. Hill, A. V. *Proc. Royal Soc. London Ser. B.* **1928**, *104*, 39.

Part 3

Conversion of Chromium(III) Propionate to Chromate(VI) by the Advanced Oxidation Process and the Photo Fenton Process. Pre-Treatment of a Biomimetic Complex for Chromium Analysis

3.1. Introduction

Over forty years ago Mertz and coworkers discovered that chromium is an essential trace element for mammals,[1] a conclusion that has been supported by recent studies.[2] Two biologically occurring chromium-containing biomolecules have been described by Vincent and coworkers:[3] (1) iron transport protein transferrin which doubles as a Cr(III) transport agent; and (2) oligopeptide chromodulin (also known as the low-molecular-weight chromium-binding substance, LMWCr). Biological sample matrixes containing the chromium(III) species are usually complex, containing proteins, amino acids and various other organic species.[4a-h]

Chromium(III) has been used as a low-cost dietary supplement for the treatment of diabetes and its complications.[5] Chromium supplements as an adjuvant therapy hold the prospect of helping achieve euglycemia, or a normal level of glucose in the blood. Chromium levels in biological systems therefore need to be monitored periodically. Detection of chromium in biological fluids has been conducted by standard methods such as graphite furnace atomic absorption spectroscopy.[6] The organic ligands in chromium species as well as other organic species contained in biological samples often interfere with the chromium detection and quantification. There is currently a need to develop new reliable methods for the analysis of chromium in biological fluids to assess chromium deficiency and the effect of chromium as adjuvant therapy for type 2 diabetes.[3a,4]

Metal complexes are a class of compounds composed of metals and ligands. In many cases, the ligands are organic compounds or ions. Standard analyses of metals by instruments such as ion selective electrodes (ISEs) are, however, for metal ions free of ligands (other than water or oxo). For the detection and quantification of metals in complexes by methods other than high-temperature processes such as inductively coupled plasma (ICP)[4e,4g] and graphite furnace atomic absorption spectroscopy,[4a,4b,4h] the organic ligands usually need to be decomposed or removed to free the metals prior to the qualitative and quantitative analysis of the metals.

Wet ashing using strong acids and dry ashing in a high-temperature, O_2-rich environment have been used to remove organic interferents prior to the analysis of Cr and other trace metals contained in biological matrixes.[7] Errors associated with both ashing procedures have been shown to be minimal in most cases. The hazards associated with the use of strong acids in the wet ashing procedure make it less desirable for routine analysis of samples. While dry ashing has also been shown to be effective for the oxidation of biological matrix components, the time requirements for complete oxidation of organic materials by this procedure is often several hours, thus making it a less desirable method. Although these methods have been proven effective for oxidation of metals as well as organic matrix components, safer, environmentally benign, and cost-effective methods are desirable.

We have explored the removal of organic ligands and oxidation of Cr(III) in chromium(III) propionate (Figure 3.1), a biomimetic chromium compound, to

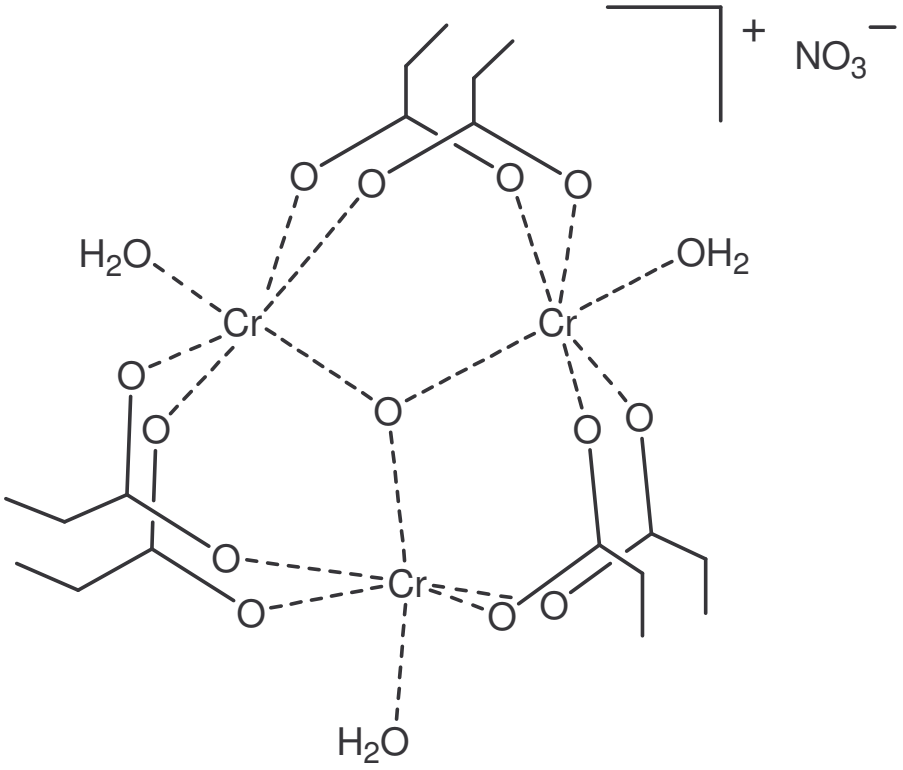

Figure 3.1. Oxohexakis(propionato)triaquotrichromium nitrate or chromium(III) propionate, a biomimetic compound used in the current studies.

chromate/dichromate (CrO_4^{2-} or $Cr_2O_7^{2-}$) by the Advanced Oxidation Process (AOP). AOP is a process that uses •OH radicals generated from, e.g., H_2O_2 and UV, as oxidant. It has been widely used in the decomposition of organic compounds.[8-10] During AOP, organic ligands are converted to CO_2 and removed, thus eliminating the potential interference from organic ligands. In addition to the removal of ligands in the current case, AOP converts Cr(III) in chromium propionate to Cr(VI). Established procedures for chromate/dichromate analysis may then be used to determine the total amount of Cr present. To our knowledge, this is the first AOP study for the removal of ligands in a complex and conversion of metals to their high oxidation states.

The studies here may lead to the development of a two-stage analyzer for the detection and quantification of total chromium in biological fluid samples. In the first stage, the sample is treated by AOP to remove all organic interferents and oxidize all chromium species to Cr(VI) or chromate/dichromate. The second stage of the analyzer consists of a detector that is selective for Cr(VI).

This dissertation part focuses on the use of AOP including the photo Fenton process in the treatment of chromium(III) propionate, a water soluble biomimetic for chromium in oligopeptide chromodulin,[5a,11] and the formation of chromate/dichromate [Cr(VI)] for subsequent electrochemical detection. Several experimental parameters in the oxidation processes have been investigated including H_2O_2 concentration, sample pH, catalyst addition, UV irradiation length, reactor size, and lamp wattage. A summary of our studies is presented here.

3.2. Experimental

3.2.1. Reagents

The chemicals used in this study, including H_2O_2 (Fisher, 30%; Kroger brand, 3%); 1,5-diphenylcarbazide (Aldrich, ACS reagent); ferric sulfate (Mallinckrodt, analytical reagent); and chromium(VI) atomic absorption (AA) standard (Aldrich, 1017 ppm Cr), were used as received. The biomimetic chromium complex, oxohexakis(propionato)triaquotrichromium nitrate [or chromium(III) propionate] was prepared by a literature procedure.[12a-b] Deionized water (18 MΩ) was used in the preparation of all solutions and standards.

3.2.2. Analytical Instrumentation

All UV-visible spectra were collected using a Hewlett-Packard 8452 photodiode array UV-visible spectrophotometer or an Ocean Optics S-2000 spectrometer and a standard 1.0 cm quartz cuvette. Blank spectra of solutions containing all matrix components other than the analyte were recorded and subtracted from all subsequent spectra.

AA analyses were performed using a Perkin-Elmer 5100 atomic absorption spectrophotometer using an air/acetylene flame under standard conditions[13] unless otherwise noted.

3.2.3. Photochemical Reactors and UV Lamps

Three different photochemical reactor designs were used in the current studies. These photoreactors consist of an outer vessel containing the sample, into which a quartz immersion well/water jacket housing the UV lamp is immersed (Figure 3.2). Three different reactors with volumes of 500 mL, 100 mL, or 15 mL, respectively, were used in the current studies. These reactors were designed and built in house, except for quartz immersion wells, which were purchased from Ace Glass. UV lamps used in the current studies were either a 450-W quartz medium-pressure mercury-vapor immersion lamp with a 5-in. arc length (Ace Glass 7825-34), or a 5.5-W quartz low-pressure cold cathode mercury gaseous discharge lamp (Ace Glass 12132-08).

3.2.4. Procedures for Chromium(III) Propionate Sample Preparation and Treatment

3.2.4.1. A Cr(III) Propionate Sample Used for Preliminary AOP Testing

An aqueous Cr(III) propionate sample was made by dissolving 0.1352 g of Cr(III) propionate crystals (21.5% Cr by mass) in 300 mL of deionized water in the photoreactor. A Teflon-coated magnetic stir bar was then inserted into the 500-mL photoreactor. H_2O_2 (30%, 5.0 mL) was next added to the solution in the photoreactor. After shielding of the photoreactor with aluminum foil, this sample was irradiated using the 450-W UV lamp for 3.5 hours. At the conclusion of the

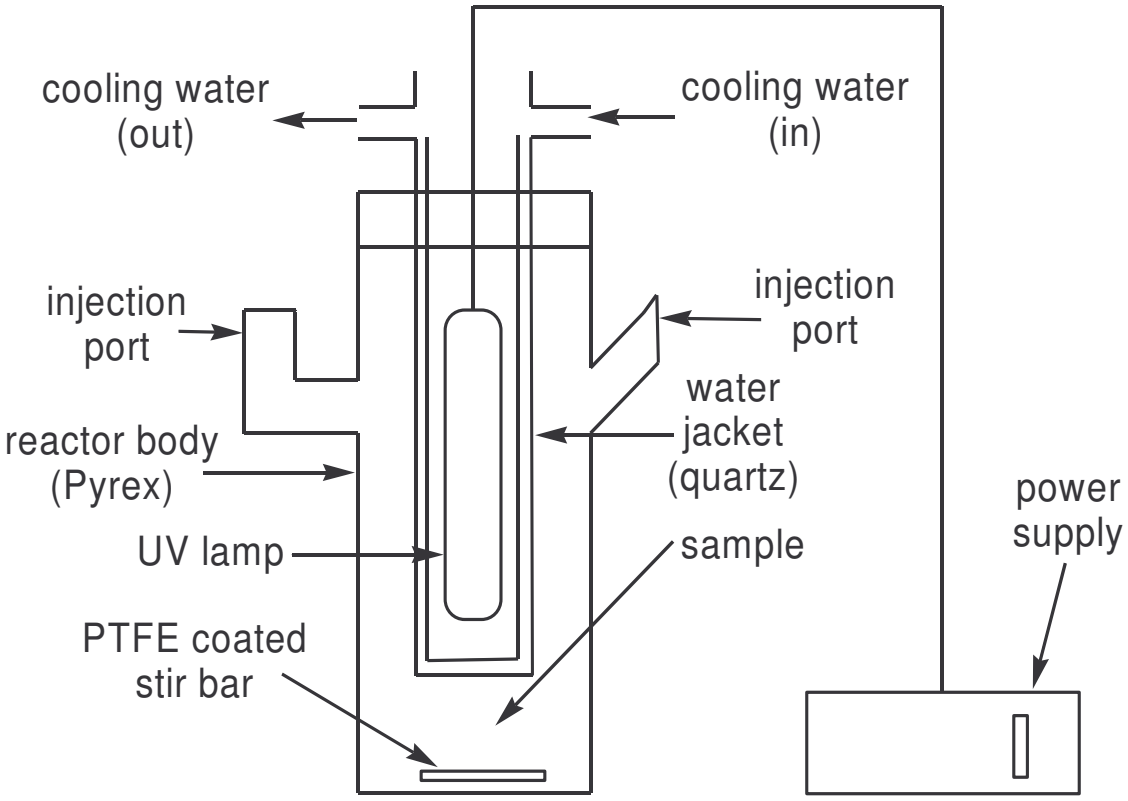

Figure 3.2. Schematic of the photochemical reactor used in the current studies.

AOP treatment, 10 mL of the sample was removed for qualitative UV-vis analysis.

3.2.4.2. A Cr(III) Propionate Sample Used for a Control Study

An aqueous Cr(III) propionate sample was prepared by adding 0.1144 g of a 1679.8 ppm Cr(III) stock solution [from Cr(III) propionate crystals] to deionized water (10.0 mL) in a 15-mL photoreactor containing a Teflon-coated magnetic stir bar. $Fe_2(SO_4)_3$ (1.0 mg) was then added to the photoreactor. Next, NaOH (1.05 M, 16 µL) was added to the sample, bringing the pH of the solution to 9.1. There is *no* H_2O_2 in this sample, and the sample was *not* exposed to UV radiation. After 3 hours, this control sample was quantitatively transferred and diluted to 25 mL in a volumetric flask. It was later analyzed for total Cr content by AA and for Cr(VI) by the 1,5-diphenylcarbazide method.[14]

3.2.4.3. Studies of the Length of UV Irradiation in the AOP Treatment

Aqueous Cr(III) propionate samples were prepared by adding 100 µL of a 147.9 ppm Cr(III) stock solution [from Cr(III) propionate crystals] to 10.0 mL of deionized water in a 15 mL-photoreactor containing a Teflon-coated magnetic stir bar. NaOH (0.110 M, 15 µL) was then added to each sample, bringing its pH to 9.9. One minute before the UV irradiation process started, H_2O_2 (30%, 170 µL) was added to each sample. After shielding the photoreactor with aluminum foil, each sample was UV-irradiated in the 15-mL photoreactor using a 5.5-W UV lamp for varied lengths of time between 0 and 60 min. At the conclusion of the

AOP treatment, each sample was quantitatively transferred and diluted to 25 mL in a volumetric flask. All samples were later analyzed for total Cr content by AA and for Cr(VI) by the 1,5-diphenylcarbazide method.[14]

3.2.4.4. Studies of the Length of UV Irradiation in the Photo Fenton Process

Aqueous Cr(III) propionate samples were prepared by adding 100 µL of a 147.9 ppm Cr(III) stock solution [from Cr(III) propionate crystals] to deionized water (10.0 mL) in the 15 mL-photoreactor containing a Teflon-coated magnetic stir bar. $Fe_2(SO_4)_3$ (1.1 mg) was added to the sample as a catalyst for the photo Fenton process. NaOH (1.05 M, 16 µL) was added to each sample, bringing its pH to 9.6. One minute before the UV irradiation process started, H_2O_2 (3%, 100 µL) was added to each sample. After shielding the photoreactor with aluminum foil, each sample was UV-irradiated in the 15-mL photoreactor using a 5.5-W UV lamp for varied lengths of time (0-60 min). At the conclusion of the photo Fenton process treatment, each sample was quantitatively transferred and diluted to 25 mL in a volumetric flask. All samples were later analyzed for total Cr content by AA and for Cr(VI) by the 1,5-diphenylcarbazide method.[14]

3.2.4.5. Studies of the Optimum H_2O_2 Concentration in the Photo Fenton Process

Aqueous Cr(III) propionate samples were made by adding 100 µL of a 147.9 ppm Cr(III) stock solution [from Cr(III) propionate crystals] to deionized

water (10.0 mL) in the 15-mL photoreactor containing a Teflon-coated magnetic stir bar. $Fe_2(SO_4)_3$ (1.1 mg) was added as a catalyst for the photo Fenton process. NaOH (1.05 M, 16 µL) was then added to each sample, bringing its pH to 9.6. One minute before the UV irradiation process started, a measured volume of 3% H_2O_2 (varied from sample to sample) was added to each sample. After shielding the photoreactor by aluminum foil, each sample was UV-irradiated in the 15-mL photoreactor using a 5.5-W UV lamp for 30 min. At the conclusion of each AOP treatment, each sample was quantitatively transferred and diluted to 25 mL in a volumetric flask. All samples were later analyzed for total Cr content by AA and for Cr(VI) by the 1,5-diphenylcarbazide method.[14]

3.2.4.6. Studies of the Optimum pH in the Advanced Oxidation Process

Aqueous Cr(III) propionate samples were prepared by adding 1.0 mL of a 2230.6 ppm Cr(III) stock solution [from Cr(III) propionate crystals] to deionized water (100 mL) in the 100-mL photoreactor. Sample pH values were adjusted from 0.23 to 9.97 by addition of H_2SO_4 or NaOH. One minute before the UV irradiation process started, H_2O_2 (30%, 1.680 mL) was added to each sample. A stir bar was not needed in these studies since the design of this photoreactor allows the sample to continuously reside directly in the UV path. After shielding the photoreactor by aluminum foil, each sample was UV-irradiated in the 100-mL photoreactor using a 450-W UV lamp for 30 min. At the conclusion of the AOP treatment, each sample was quantitatively transferred and diluted to 250 mL in a

volumetric flask. All samples were later analyzed for total Cr content by AA and for Cr(VI) by the 1,5-diphenylcarbazide method.[14]

3.2.5. Analysis of Total Chromium Content and Cr(VI) Species

Calibration standards were prepared gravimetrically using standard analytical techniques. At the conclusion of the UV-irradiation step, samples were quantitatively transferred and diluted in volumetric flasks. After dilution, samples were analyzed for total chromium content by AA and Cr(VI) content by UV-vis.

A UV-vis analysis of Cr(VI) utilizing 1,5-diphenylcarbazide, a ligand selective for chromate/dichromate,[14] was then used to measure total oxidized Cr(VI) content in each sample. Upon addition of the ligand to a Cr(VI) solution, a colored complex is formed. Cr(VI) content in the standards and samples was determined by monitoring the absorbance at 544 nm in the UV-vis spectrum.

Total chromium content in each sample was analyzed by atomic absorption (AA) spectrometry using an air-acetylene flame. Standard solutions were prepared by serial dilution of a 1017 ppm Cr(VI) AA standard solution and addition of sample matrix components such as Fe^{3+} or NaOH, depending on the contents of each sample. The sample was then diluted to the proper volume. The standard curves were made by measuring the absorbance at 357.9 nm using a slit width of 0.70 nm with a lamp current of 15 mA[13] during analysis of the standards and samples for total chromium.

Cr(III) to Cr(VI) conversion was calculated by dividing the Cr(VI) concentration from the UV-vis analysis by the total Cr concentration from the AA

analysis. Detailed procedures and errors in the determination of total Cr and Cr(VI) are given in Appendix B.

3.3. Results and Discussion

3.3.1. The Advanced Oxidation Process

The Advanced Oxidation Process utilizes a combination of hydrogen peroxide (H_2O_2), a common household reagent, and ozone (O_3) or ultraviolet (UV) radiation to generate strongly oxidizing hydroxyl radicals OH•.[8a,b] When H_2O_2 is irradiated with UV light at wavelengths $\lambda < 300$ nm, homolytic splitting of the oxygen-oxygen bonds occurs thus yielding hydroxyl radicals (Equation 3.1).

$$H_2O_2 \xrightarrow{h\nu} 2\ \bullet OH \qquad \text{(Eq. 3.1)}$$

The radicals react with organic molecules to yield water and carbon dioxide as the main reaction products. In addition to producing hydroxyl radicals, the UV radiation either decomposes or activates organic complexes as well, since most organic compounds absorb in the UV region. The UV irradiation thus makes the organic compounds more easily oxidized by the hydroxyl radicals.

A complex set of reactions occur when O_3 is added to H_2O_2, giving the hydroxyl radical and oxygen (Equation 3.2). In addition, ozone itself and ozone-activated hydrogen peroxide also trigger other reactions that result in the

decomposition of organic compounds. Since water is relatively impermeable to UV, the use of H_2O_2/O_3 is particularly desirable for the treatment of aqueous solution.

$$H_2O_2 + 2\,O_3 \longrightarrow 2\,{\bullet}OH + 3\,O_2 \qquad \text{(Eq. 3.2)}$$

As shown in Table 3.1, the standard reduction potential of hydroxyl radicals (OH•) is much higher than that of ozone, hydrogen peroxide, or Cl_2, three well known oxidants. The reaction times of hydroxyl radicals with organic compounds are short, usually less than a millisecond.[8b] In addition to the formation of hydroxyl radicals from the UV irradiation of H_2O_2 and addition of O_3 to H_2O_2, these reactions yield several other reactive species such as hydroperoxyl or peroxyl radicals. These radicals also decompose organic compounds. In other words, the activation of hydrogen peroxide by UV irradiation or ozone produces several radicals, all of which help decompose organic compounds.

The photo Fenton process[8a-b,10a-b] is an adaptation of the Advanced Oxidation Process. The photo Fenton process utilizes a catalytic amount of Fe^{2+} or Fe^{3+} in addition to H_2O_2 and UV radiation. Iron species have been shown to act as a catalyst in these oxidation reactions, promoting the decomposition of H_2O_2 and formation of active hydroxyl radicals (Equations 3.3 and 3.4). This process has been shown to improve the effectiveness of the oxidation of certain organic compounds compared to AOP alone.[10a-b]

Table 3.1. Comparison of standard (reduction) potentials of OH•, O_3, H_2O_2, and Cl_2.

Oxidizing Agent	Chemical Formula	Standard Potential (V)
hydroxyl radical	OH•	2.8
ozone	O_3	2.07
hydrogen peroxide	H_2O_2	1.78
chlorine	Cl_2	1.35

$$Fe^{3+} + H_2O + h\nu \longrightarrow Fe^{2+} + \bullet OH + H^+ \quad \text{(Eq. 3.3)}$$

$$Fe^{2+} + H_2O_2 \longrightarrow Fe^{3+} + \bullet OH + OH^- \quad \text{(Eq. 3.4)}$$

The hydroxyl radicals generated in AOP have been shown to oxidize even relatively stable substances.[8b] AOP has thus been widely used in the decomposition (and removal) of organic compounds that are difficult to degrade such as contaminants in drinking water and industrial wastewater.[8] Substances that have been oxidized (and thus decomposed) include methyl *t*-butyl ether (MTBE),[9a] mecoprop,[9b] ethylene glycol,[9c] polyethylene glycol,[9c] sodium dodecyl sulfate,[9c] and explosives.[9d] Ozone and hydrogen peroxide, as well as the UV irradiation process, when properly used, are safe and environmentally benign. The decomposition of ozone and hydrogen peroxide leads to the formation of oxygen and/or water. Both UV radiation and ozone have long been used to sterilize fish tanks by killing harmful microscopic organisms such as bacteria and parasites.[15] Although AOP has been used extensively for the oxidation of organic compounds, to our knowledge, AOP has not been used for the oxidation of metal species.

There are many factors that contribute to the efficiency of the Advanced Oxidation Process. Factors contributing most to the overall efficiency are choice of O_3 or UV to activate H_2O_2, power of the UV source, length of UV irradiation, use of a catalyst during UV irradiation, H_2O_2 concentration, sample pH, and reactor design. Each of these parameters has been investigated in the

conversion of chromium(III) propionate to chromate/dichromate, and the results are discussed below.

3.3.2. Comparison of AOP and the Photo Fenton Process

Cr(III) propionate, $[Cr_3O(O_2CCH_2CH_3)_6(H_2O)_3]NO_3$ (Figure 3.1), has been shown to mimic the ability of chromodulin[5a,11] to act as an insulin production trigger in vivo. It was for its biomimetic properties that this Cr(III) complex was chosen for the current studies. This complex was found to readily dissolve in aqueous solution. Our other work in Part 4 of this dissertation shows that good solubility of the compound in aqueous solution is critical in the AOP treatment.

We have found in the current studies that Cr(III) propionate readily undergoes oxidation by H_2O_2 under UV irradiation (Equation 3.5). UV-vis spectra of a Cr(III) propionate solution were

$$[Cr_3O(O_2CCH_2CH_3)_6(H_2O)_3]NO_3 + \text{excess } H_2O_2 \xrightarrow{h\nu} CrO_4^{2-} + CO_2 + H_2O + H^+ + NO_3^- \quad \text{(Eq. 3.5)}$$

collected before and after AOP treatment using the 450-W UV lamp and 500-mL photoreactor. A comparison of the UV-vis spectra of the Cr(III) propionate solution after AOP to that of a potassium dichromate solution (Figure 3.3) shows qualitatively that the Cr(III) complex has been oxidized to Cr(VI). In comparison, control experiments (Section 3.2.4.2) using solutions of Cr(III) propionate, H_2O_2 and a catalytic amount of $Fe_2(SO_4)_3$ as a catalyst *without* UV irradiation showed

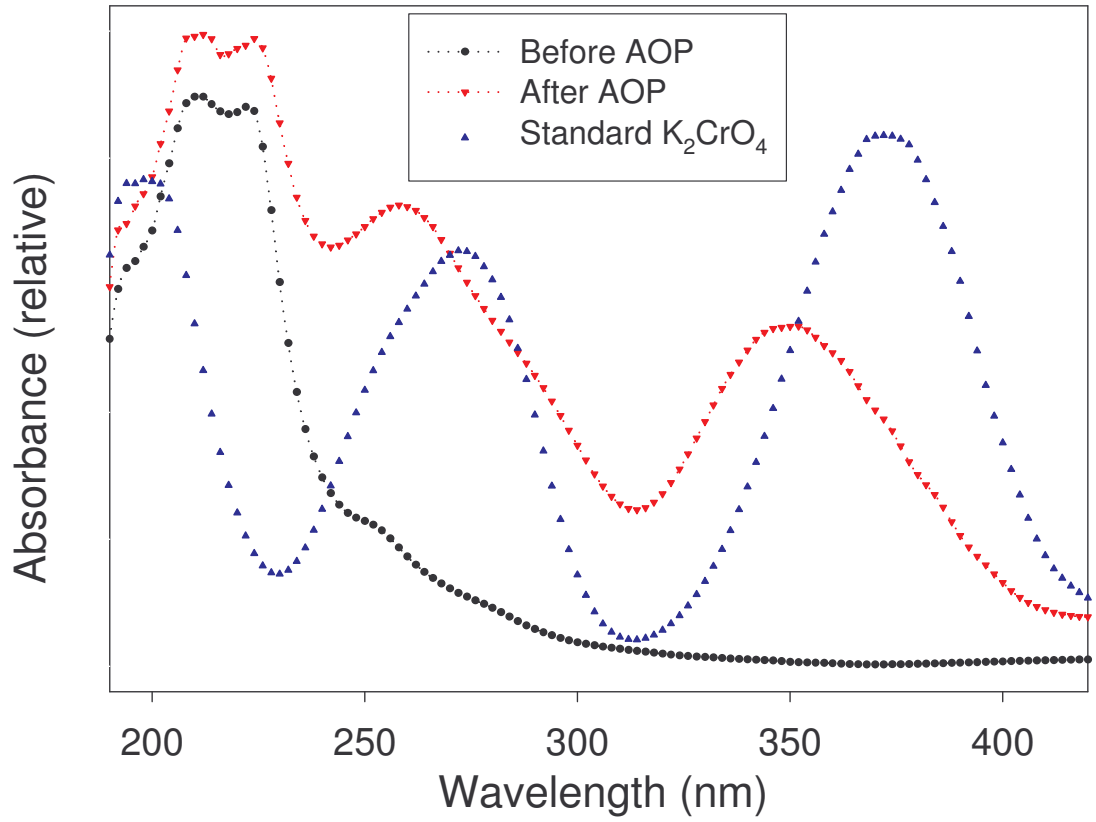

Figure 3.3. UV-vis spectra of a chromium(III) propionate solution before AOP (●) and after AOP (▼) compared to the spectrum of a standard potassium dichromate solution (▲). Sample was treated in the 500-mL photoreactor using the 450-W UV lamp and H_2O_2.

no conversion of Cr(III) propionate to chromate/dichromate. The control studies indicate that hydroxyl radicals from AOP are critical to the Cr(III) → Cr(VI) conversion.

Preliminary AOP experiments using ozone and H_2O_2 showed qualitative conversion of Cr(III) propionate to chromate in over 48 hours. Ozone was not used in our subsequent AOP studies for the following reasons: (a) Ozone generation *in a research laboratory* usually requires an ozone generator (and a supply of O_2), which gives an O_3/O_2 flow through a solution containing H_2O_2 for a limited amount of time; (b) The excess O_3 in the O_3/O_2 flow was found to be corrosive to laboratory equipment containing plastics, and O_3 itself in air is a health hazard.

A set of experiments were also conducted to see if direct analysis of Cr(III) propionate by atomic absorption (AA), *without prior AOP treatment*, would give accurate Cr analysis. These tests show the direct AA analysis of chromium in these Cr(III) propionate samples using an air acetylene flame gives an error of 50.6%. The studies here underscore the importance of AOP treatment of metal complexes to remove their ligands prior to metal analysis.

A direct comparison of the Advanced Oxidation Process and the photo Fenton process for the oxidation of Cr(III) propionate samples is shown in Figure 3.4. The photo Fenton process was found to be more efficient than AOP for the oxidation of Cr(III) propionate solutions. In other words, Fe^{3+} ions play the catalytic role in the AOP treatment of Cr(III) propionate. After 60 min of UV irradiation by the 5.5-W quartz mercury lamp in the 15-mL photoreactor, samples

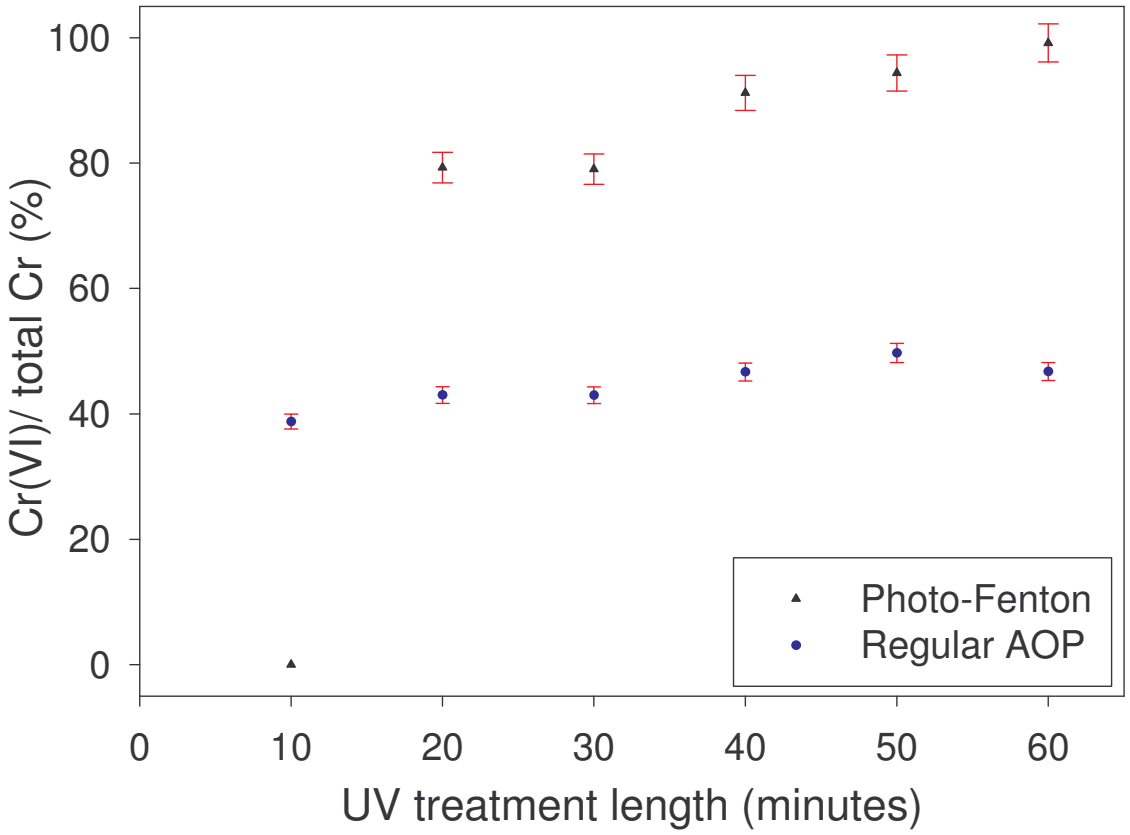

Figure 3.4. A comparison of the Advanced Oxidation Process (●) and the photo Fenton process (▲) for the oxidation of Cr(III) to Cr(VI) as a function of time. Samples were treated in the 15-mL photoreactor using the 5.5-W UV lamp and H_2O_2.

from the photo Fenton process showed (99 ± 3)% conversion of Cr(III) propionate to Cr(VI), whereas the control samples treated by regular AOP only showed approximately 50% conversion of Cr(III) propionate to Cr(VI). The Fe^{3+} catalysts likely yield larger quantities of active •OH radicals in the photo Fenton process. The majority of the current studies were thus conducted with the Fe^{3+} Fenton catalyst.

3.3.3. The Length of UV Irradiation and Advanced Oxidation Process

The length of UV irradiation of AOP samples has been found to play a major role in the degree of oxidation of the samples in earlier studies.[8b,9b-c,10a-b] In the current studies, identical solutions of Cr(III) propionate were prepared, and their pH was adjusted to 9.9 by NaOH (Section 3.2.4.3). After addition of H_2O_2, the 15-mL samples were UV-irradiated for varied lengths of time using the 5.5-W UV lamp. Increasing the length of UV irradiation from 0 to 60 min was found to increase the conversion of Cr(III) in the sample to Cr(VI) ions. After 60 min of UV irradiation, approximately 50% of the total Cr in the sample was in the Cr(VI) oxidation state (Figure 3.5).

3.3.4. The Length of UV Irradiation and the Photo Fenton Process

Studies similar to those discussed in Part 3.3.3 were conducted, this time with the addition of a Fe^{3+} catalyst. These studies also showed that the length of UV irradiation in the photo Fenton process samples play a major role in the

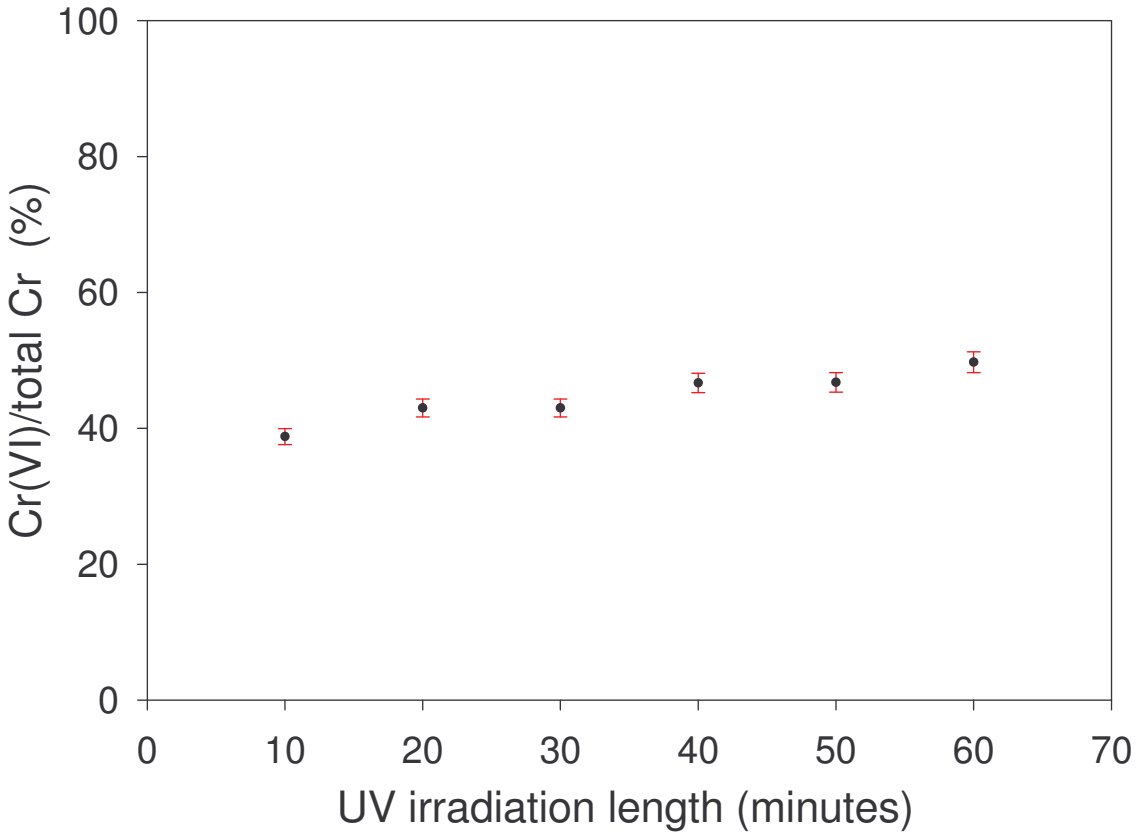

Figure 3.5. Conversion of Cr(III) in chromium(III) propionate to Cr(VI) as chromate/dichromate by the Advanced Oxidation Process as a function of the length of UV irradiation. Samples were treated in the 15-mL photoreactor using the 5.5-W UV lamp and H_2O_2.

amount of Cr(III) oxidized to Cr(VI). With longer exposure to UV radiation, larger quantities of active •OH radicals are generated thus increasing the overall efficiency of the oxidation process. To determine the optimum length of UV irradiation for the current photo Fenton process samples, experiments were conducted in which the length of UV irradiation (5.5-W UV lamp) of multiple identical Fe^{3+}-containing, Cr(III) propionate samples (pH 9.9) was varied (Section 3.2.4.4). Experimental results (Figure 3.6) show that, with increasing lengths of UV irradiation from 0 to 60 min, the amount of Cr(III) oxidized to Cr(VI) also increased. After 60 min of UV irradiation, (99 ± 3)% of the total chromium has been converted Cr(VI) chromate/dichromate.

3.3.5. Optimum H_2O_2 Concentration in the Photo Fenton Process

One critical factor regarding Advanced Oxidation Processes and the photo Fenton process is the concentration of hydrogen peroxide during the UV irradiation of the sample. Studies have been conducted to determine the optimum concentration of H_2O_2 for the oxidation of various organic compounds, and different optimum concentrations of H_2O_2 have been reported for the treatment of different chemicals.[8,9] At high concentrations of H_2O_2, the AOP and photo Fenton process efficiency is reported to decrease in some instances.[8b,10b] The decrease in efficiency is suspected to arise from the recombination of two •OH radicals, thus effectively lowering the number of •OH radicals in solution as well as the efficiency of the overall oxidation process. At low concentrations of

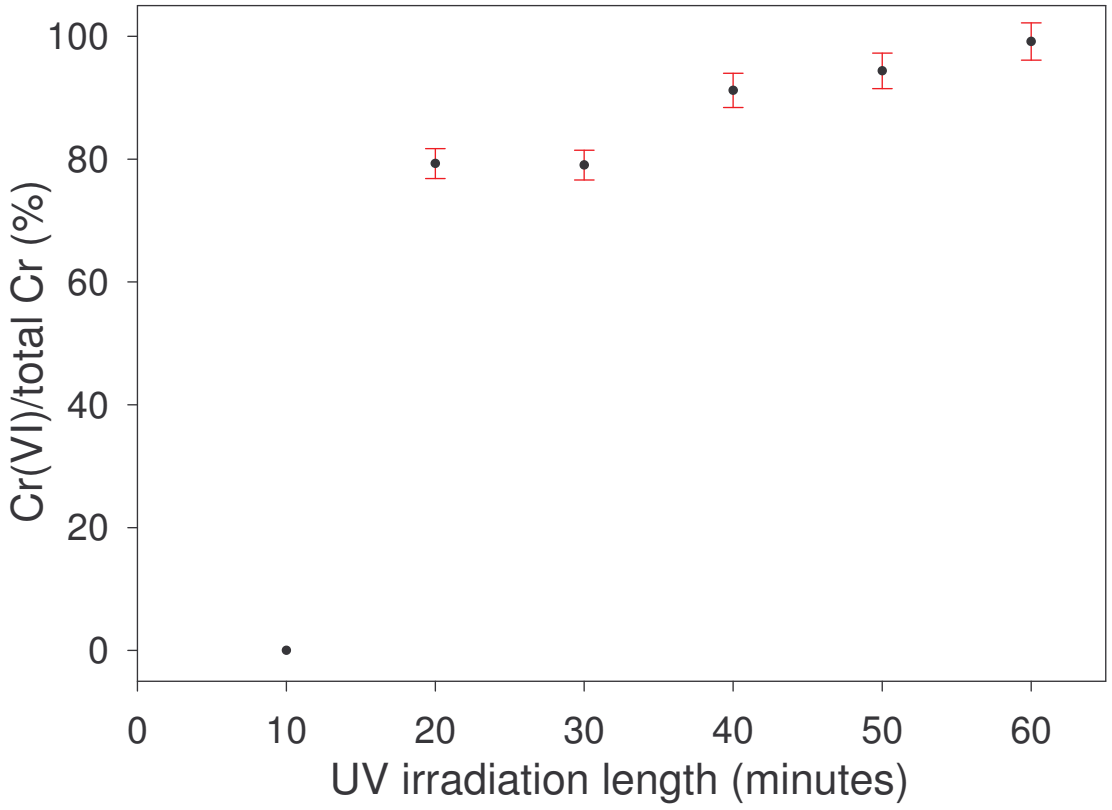

Figure 3.6. Conversion of Cr(III) propionate to chromate/dichromate by the photo Fenton process as a function of the length of UV irradiation. Samples were treated in the 15-mL photoreactor using the 5.5-W UV lamp and H_2O_2.

H_2O_2 there is not enough H_2O_2 to generate the adequate concentration of •OH radicals for the oxidation.

Several experiments in the current studies were conducted to determine the optimum concentration of H_2O_2 during the photo Fenton process (Section 3.2.4.5). Cr(III) propionate samples at approximately pH 9.0 (by NaOH) were prepared containing a catalytic amount of $Fe_2(SO_4)_3$. The H_2O_2 concentration was varied from 0.09 g/L to 0.44 g/L. Each sample was UV-irradiated in the 15-mL photoreactor for 30 min using the 5.5-W UV lamp. Our results show that the H_2O_2 concentration during the UV irradiation has a direct influence on the amount of Cr(III) oxidized to Cr(VI) in a given period of time (Figure 3.7). Samples at the H_2O_2 concentration of 0.26 g/L were found to show the highest Cr(III) to Cr(VI) conversion and were thus considered to be the optimum concentration for use in the current system.

3.3.6. Optimum pH in the Advanced Oxidation Process

In order to establish the optimum pH during AOP treatment of these samples, AOP experiments were carried out using a 100-mL photoreactor with a 450-W UV lamp. Samples containing a constant concentration of Cr(III) propionate and H_2O_2 were prepared and UV-irradiated for 30 min. Sample pH was varied from 0.23 to 9.97 during AOP (Figure 3.8). An increase of pH was found to enhance the conversion of Cr(III) propionate to chromate/dichromate. At higher pH, increased conversion rates were achieved. At pH < 4, no Cr(VI) was detected in the AOP-treated samples. As shown in Equation 3.6, the Cr(III)

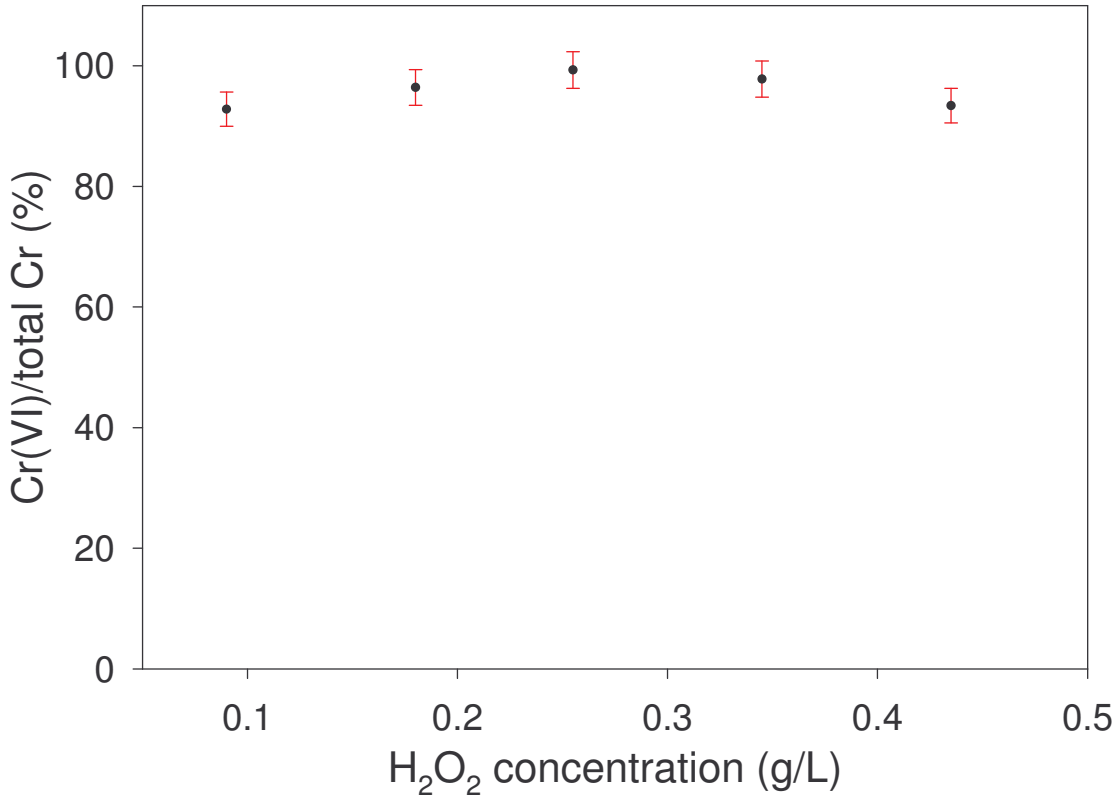

Figure 3.7. Conversion of chromium(III) propionate to chromate/dichromate as a function of H_2O_2 concentration during UV irradiation. Samples were treated in the 15-mL photoreactor using the 5.5-W UV lamp.

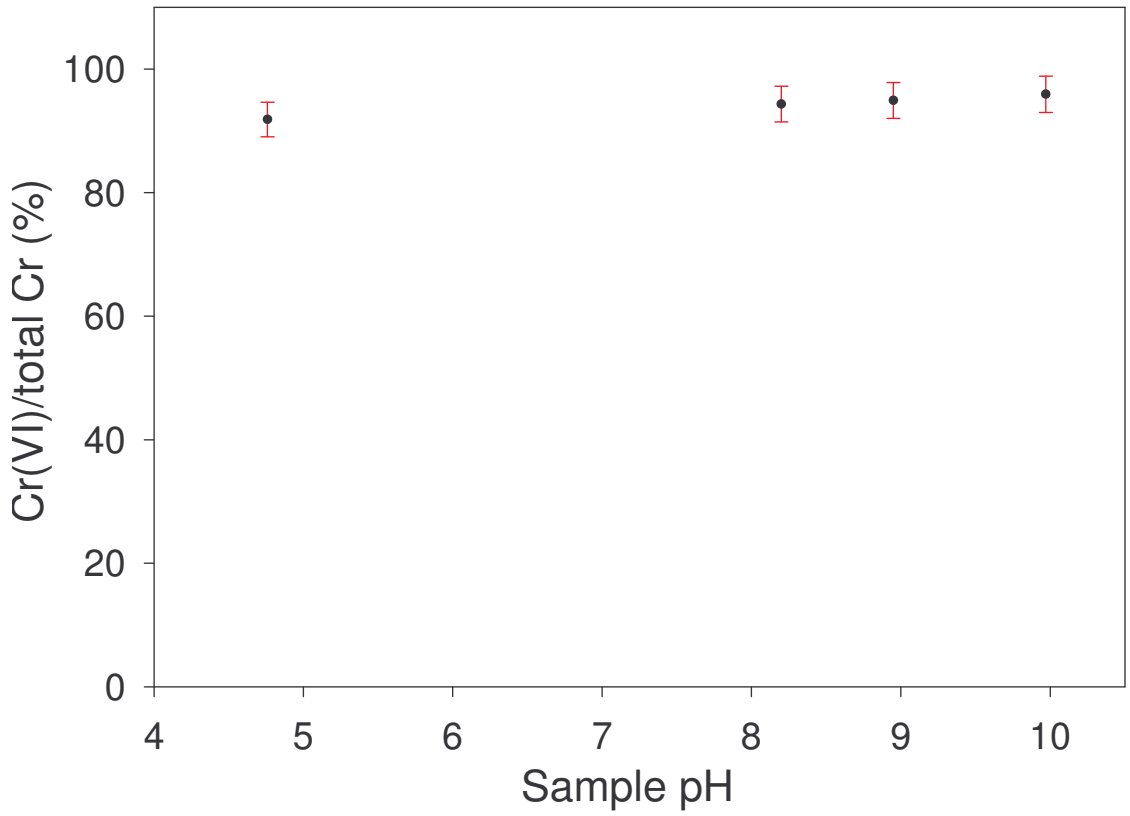

Figure 3.8. Conversion of Cr(III) in chromium(III) propionate to Cr(VI) present as chromate/dichromate as a function of sample pH during UV irradiation. Samples were treated in the 100-mL photoreactor using the 450-W UV lamp.

to Cr(VI) conversion yields acid, and OH^- ions in solutions of higher pH remove the H^+ ions generated from the Cr oxidation. The pH in these solutions after AOP was measured to be between pH 7.0 and 8.0.

$$2Cr^{3+} + 3H_2O_2 + H_2O \rightleftharpoons Cr_2O_7^{2-} + 8H^+ \qquad \text{(Eq. 3.6)}$$

3.3.7. Reactor Sizes and UV Lamps

Various reactor designs and sizes have been used in the current AOP and photo Fenton process reactions. One of the most important factors in the design of a reactor is the ability to adequately stir/mix the sample in the reactor. Thorough mixing of the sample is required to ensure that the contents are in the path of the UV radiation for the activation of H_2O_2. Another important factor regarding reactor design is the pathlength of UV radiation through the sample.[9c] With longer pathlengths, the UV intensity is decreased towards the outer portion of the sample. This is due to the fact that a large portion of the UV radiation is often absorbed by the inner portion of the sample. It is for this reason that our second- and third-generation reactors were designed so that the length between the outer wall of the immersion well and the inner wall of the reactor was minimal.

Large-scale photoreactors (100 and 500 mL, Figure 3.9) have the advantage of use with relatively large, higher wattage UV lamps and the ability to treat large samples. However they also require large samples and intense UV irradiation from, e.g., a 450-W lamp. The drawback with larger reactors is the large pathlength through which the UV radiation must travel to treat the sample.

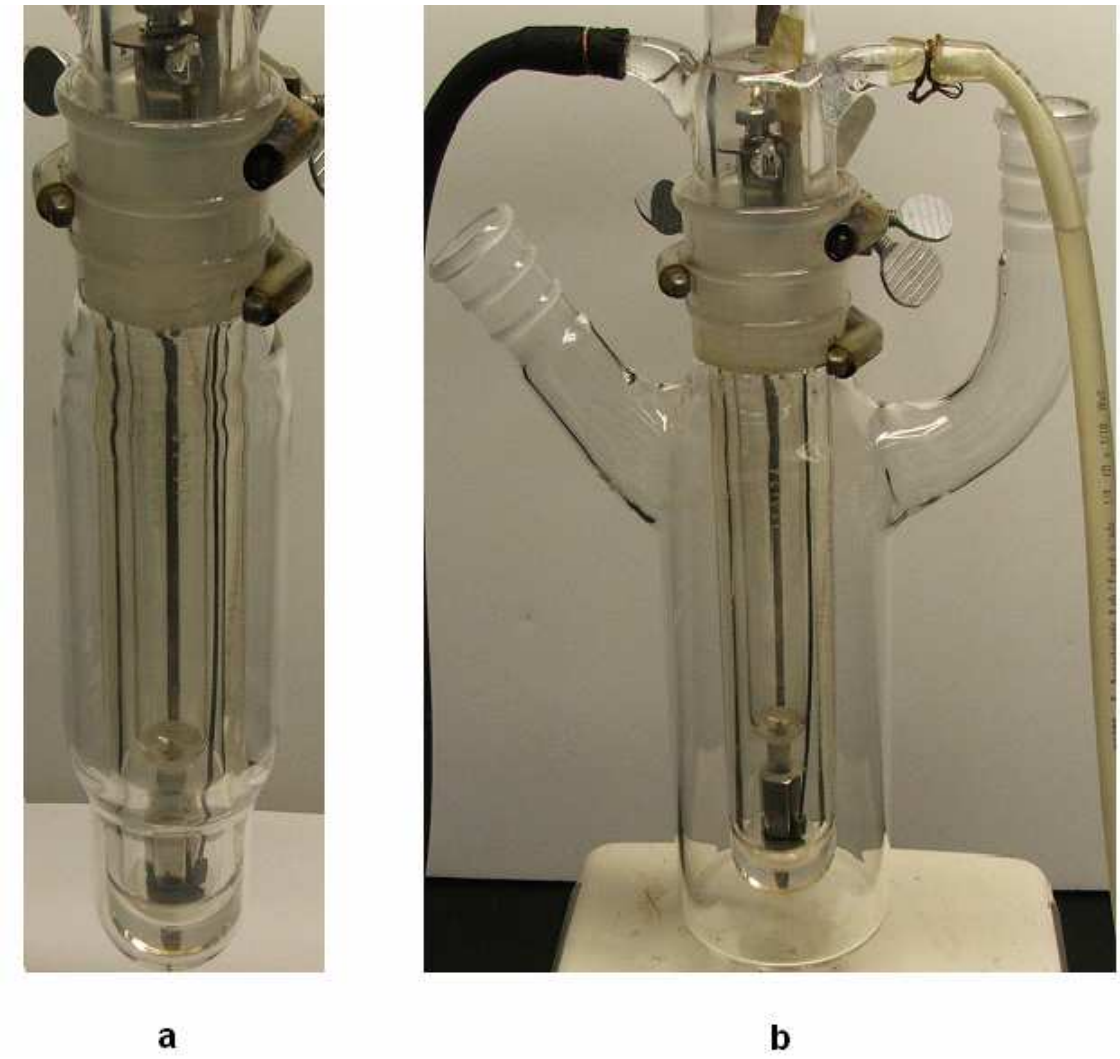

Figure 3.9. Images of the large-scale photochemical reactors used in the current studies. The 100-mL (**a**) and 500-mL (**b**) photoreactors are shown.

As discussed earlier this leads to decreased efficiency towards the outer portions of the sample due to decreased UV intensity.

The photoreactor in Figure 3.9b is capable of treating samples with volume up to 500 mL using a 450-W UV lamp. This is the first-generation reactor, and the efficiency is decreased due to the fact that a large portion of the sample is often out of the direct path of the UV radiation. The photoreactor in Figure 3.9a was designed for treating samples up to 100 mL using a 450-W UV lamp. Although this reactor is only useful for smaller volumes, the efficiency is greatly increased due to the fact that the pathlength is shortened and the entire sample is contained directly in the path of continuous UV radiation.

Small-scale photoreactors (Figure 3.10) have the advantage of a shorter UV pathlength through the sample, and better mixing of the sample, which both lead to increased efficiency of the oxidation process. These smaller reactors also require smaller sample volumes. The primary disadvantage of using a smaller reactor is that often, only small, low wattage UV lamps may be used.

The small-scale photoreactor in Figure 3.10 is capable of treating samples up to 15 mL in volume using a 5.5-W UV lamp. This photoreactor was designed so that the sample could be stirred to maximize the sample residence time in the UV radiation path. Studies using this photoreactor in combination with the 5.5-W UV lamp gave very good yields for the oxidation of the Cr(III) complex. This reactor was used in many of the current studies due to its efficiency.

Figure 3.10. Image of the small-scale photochemical reactor used in the current studies.

3.4. Concluding Remarks

The Advanced Oxidation Process and photo Fenton process have been proven as viable methods to oxidize a Cr(III) complex to Cr(VI) chromate/dichromate. Experiments in which the photo Fenton process was applied to a Cr(III) biomimetic compound have shown that a large majority of the total chromium has been converted to Cr(VI). This has been accomplished using a very low power UV lamp and a small-scale reactor. The success of this process has thus eliminated the need for using harsh oxidation procedures for these samples.

References

1. (a) Schwarz, K.; Mertz, W. *Arch. Biochem. Biophys.* **1959**, *85*, 292. (b) Mertz, W.; Schwarz, K. *J. Physiol.* **1959**, *196*, 614.
2. (a) Striffler, J. S.; Polansky, M. M.; Anderson, R. A. *Metabolism* **1999**, *48*, 1063. (b) Striffler, J. S.; Polansky, M. M. *Metabolism* **1998**, *47*, 396.
3. (a) Vincent, J. B. *Acc. Chem. Res.* **2000**, *33*, 503. (b) Jacquamet, L.; Sun, Y.; Hatfield, J.; Gu, W.; Cramer, S. P.; Crowder, M. W.; Lorigan, G. A.; Vincent, J. B.; Latour, J.-M. *J. Am. Chem. Soc.* **2003**, *125*, 774 and references therein.
4. (a) Granadillo, V. A.; de Machado, L. P.; Romero, R. A. *Anal. Chem*. **1994,** *66*, 3624. (b) Rukgauer M.; Zeyfang, A. *Biol. Trace Elem. Res*. **2002**, *86*, 193. (c) Enrique, A.-C. C.; Wrobel, K.; Marchante Gayon, J. M.; Sanz-Medel, A. *J. Anal. Atom. Spectrom*. **1994**, *9*, 117. (d) Rydberg D.

Acta Pharm. Technol. **1986**, *59*, 624. (e) Chen, S.; Jiang, Z.; Hu, B.; Liao, Z.; Peng, T. *Atom. Spectrosc*. **2002**, *23*, 86. (f) Ezer, M.; Elwood, S. A.; Simeonsson, J. B. *J. Anal. Atom. Spectrom*. **2001**, *16*, 1126. (g) Vaughan, M. A.; Baines, A. D.; Templeton, D. M. *Analyst* **1990**, *115*, 817. (h) Morris, B. W.; Kemp, G. J. *Clin. Chem*. **1985**, *31*, 171 (i) Welch, C. M.; Nekrassova, O.; Compton, R. G. *Talanta* **2005**, *65*, 74. (j) Smart, N. G.; Hitchman, M. L.; Ansell, R. O.; Fortune, J. D. *Anal. Chim. Acta* **1994**, *292*, 77. (k) Cox, J. A.; Kulesza, P. J. *Anal. Chim. Acta* **1983**, *154*, 71. (l) Turyan, I.; Mandler, D. *Anal. Chem*. **1997**, *69*, 894.

5. (a) National Institutes of Health (NIH) Program Announcement (PA) No. PA-01-114. (b) Anderson, R. A. *J. Am. Coll. Nutr.* **1998**, *17*, 548. (c) Ryan, G. J.; Wanko, N. S.; Redman, A. R.; Cook, C. B. *Ann. Pharmacotherapy* **2003**, *37*, 876. (d) Katz, S. A.; Salem, H. *The Biological and Environmental Chemistry of Chromium*, VCH, Weinheim, 1994.

6. Skoog, D. A.; Holler, F. J.; Nieman, T. A. *Principles of Instrumental Analysis*, 5th Ed., Harcourt Brace, Philadelphia, 1998, p.218.

7. Bock, R. *A Handbook of Decomposition Methods in Analytical Chemistry*, Wiley, New York, 1979, Ch. 5.

8. (a) *Advanced Photochemical Oxidation Processes*, US EPA **1998** (b) Schulte, P.; Bayer, A.; Kuhn, F.; Luy, Th.; Volkmer, M. *Ozone-Sci. Eng*. **1995**, *17*, 119. (c) Sapach, R.; Viraraghavan, T. *J. Environ. Sci. Health, Part A* **1997**, *A32*, 2355. (d) Acero, J. L.; Von Gunten, U. *Ozone-Sci. Eng*.

2000, *22*, 305. (e) Gunukula, R. V. B.; Tittlebaum, M. E. *J. Environ. Sci. Health, Part A* **2001**, *A36*, 307.

9. (a) Safarzadeh-Amiri, A. *Water Res*. **2001**, *35*, 3706. (b) Beltran, F. J.; Gonzalez, M.; Rivas, J.; Marin, M. *Ind. Eng. Chem. Res*. **1994**, *33*, 125. (c) Sigman, M. E.; Buchanan, A. C., III; Smith, S. M. *J. Adv. Oxid.Technol*. **1997**, *2*, 415. (d) Castaldi, F. J.; Richardson, C. F. Payne, B. *Proceedings – WEFTEC '96* **1996**, *3*, 275.

10. (a) Kavitha, V.; Palanivelu, K. *Chemosphere* **2004**, *55*, 1235. (b) Ghaly, M. Y.; Hartel, G.; Mayer, R.; Haseneder, R. *Waste Management* **2001**, *21*, 41.

11. (a) Sun, Y.; Mallya, K.; Ramirez, J.; Vincent, J. B. *J. Biol. Inorg. Chem*. **1999**, *4*, 838. (b) Davis, C. M.; Royer, A. C.; Vincent, J. B. *Inorg. Chem*. **1997**, *36*, 5316.

12. (a) Earnshaw, A.; Figgis, B. N.; Lewis, J. *J. Chem. Soc. (A)* **1966**, 1656. (b) Johnson, M. K.; Powell, D. B.; Cannon, R. D. *Spectrochim. Acta* **1981**, *37A*, 995.

13. Perkin-Elmer Corporation, *Analytical Methods for Atomic Absorption Spectroscopy*, 1996.

14. (a) Allen, T. L. *Anal. Chem*. **1958**, *30*, 447. (b) Urone, P. F. *Anal. Chem*. **1955**, *27*, 1354. (c) Dedkova, V. P.; Shvoeva, O. P.; Savvin, S. B. *J. Anal. Chem.* **2001**, *56*, 758.

15. Monroe, D. W.; Key, W. P. *Ozone: Sci. Eng*. **1980**, *2*, 203.

Part 4

Studies of the Oxidation of Palladium Complexes by the Advanced Oxidation Process. Pretreatment of Model Catalysts for Precious Metal Analysis

4.1. Introduction

Over the past few decades, organometallic complexes have gained widespread use in catalysis. In particular, precious metal complexes have been used extensively as catalysts in many synthetic organic reactions,[1-4] including ethylene to vinyl acetate conversion,[1a] oxidation of alcohols,[1b] coupling reactions,[1c,2a,3a] hydrogenation,[1e] silylation reactions,[2b] and isomerization reactions.[2c] Due to the success of these catalysts, they are becoming more commonly used in industrial-scale reactions.

As a result of the use of homogeneous and heterogeneous precious metal catalysts, low concentrations of spent catalysts are often contained in waste solutions from industrial-scale reactions. Before recycling the spent catalyst solutions to collect the spent precious metals, it is often necessary to determine the amount of precious metals in the solutions. When concentrations of the precious metals are low, it may not be economically feasible to recycle the precious metals.

Metal catalysts often contain organic ligands, and standard analyses of metals by ion selective electrodes (ISEs) and other electrochemical techniques are, however, for metal ions free of organic ligands.[5] The organic ligands usually need to be decomposed or removed to free the metals prior to the qualitative and quantitative analysis of the metals. High-temperature processes such as graphite furnace atomic absorption spectroscopy or inductively coupled plasma atomic emission or mass spectrometry may be used to directly analyze metal complexes containing organic ligands.[6,7] These methods are usually costly and

not suitable as a metal probe. In addition to organic ligands in precious metal catalysts, the presence of large amounts of organic species in spent catalyst solutions also makes quantitative analysis of precious metals a challenge.

Studies have been conducted to remove organic species in spent catalyst solutions. Johnson-Matthey has reported a method involving the use of supercritical water for oxidation of organic species.[8] Other methods require the use of harsh acids to digest organic species.[3e,9] Although these methods have proven effective for the oxidation of metals as well as organic species, more environmentally benign and cost effective methods are desirable.

The Advanced Oxidation Process (AOP) has recently been investigated to convert organic compounds to CO_2 and H_2O. This process utilizes a combination of hydrogen peroxide (H_2O_2) and ozone (O_3) or ultraviolet (UV) radiation to generate highly potent hydroxyl radicals (•OH)[10a] that oxidize even relatively stable substances.[10b] AOP has thus been widely used in the decomposition of organic compounds and contaminants in drinking water and industrial wastewater.[10] Many organic compounds have been oxidized and thus decomposed using the Advanced Oxidation Processes.[10c,11a-c] Although AOP has been used extensively for the oxidation of organic compounds, to our knowledge, it has not been used for the oxidation of metal complexes.

When H_2O_2 is UV irradiated at wavelengths $\lambda < 300$ nm, homolytic splitting of the oxygen-oxygen bonds occurs, yielding hydroxyl radicals (Equation 4.1).

$$H_2O_2 \xrightarrow{h\nu} 2\ \bullet OH \qquad \text{(Eq. 4.1)}$$

The radicals react with organic molecules to yield H_2O and CO_2 as main products. In addition to producing hydroxyl radicals, the UV radiation either decomposes or activates organic complexes as well, since most organic compounds absorb in the UV region. The UV radiation thus makes the organic compounds more easily oxidized by the hydroxyl radicals.

Addition of ozone or UV radiation to a solution of hydrogen peroxide results in the activation of H_2O_2 and the formation of hydroxyl radicals, •OH.[10b] The reaction times of hydroxyl radicals with organic compounds are short, usually less than a millisecond.[10b] In addition to the formation of hydroxyl radicals from the UV irradiation of H_2O_2, these reactions yield several other reactive species such as hydroperoxyl or peroxyl radicals. These radicals also decompose organic compounds. In other words, the activation of hydrogen peroxide by UV irradiation or ozone produces several radicals, all of which help decompose organic compounds.

Two-stage analyzers for precious metals in spent industrial catalysts are of interest. One design of an analyzer may involve a first stage to pre-treat the spent catalyst by AOP to remove ligands and organic species, and convert precious metals such as palladium to aqueous Pd(II) ions. The second stage of the analyzer would consist of an electrochemical or optical sensing element selective for the precious metal. To our knowledge, there has been no report of

using AOP in the oxidation of metal complexes to remove ligands. We have investigated the conversion of palladium complexes to aqueous Pd(II) ions by the AOP reactions. The three Pd catalyst complexes in Figure 4.1 were chosen as model precious metal complexes: palladium(II) acetate $Pd(OAc)_2$ (**4a**), palladium(II) acetylacetonate $Pd(acac)_2$ (**4b**), and tris(dibenzylideneacetone)dipalladium(0) $Pd_2(dba)_3$ (**4c**). These three complexes are common catalysts in synthetic organic chemistry.[1-3] $Pd_2(dba)_3$ was chosen in part to test AOP as a means by which to oxidize Pd(0) to Pd(II). A summary of our studies is reported here.

4.2. Experimental

4.2.1. Reagents

The chemicals used in the current studies, including hydrogen peroxide (Fisher, 30%; Kroger brand, 3%); N,N-dimethyl-4-nitrosoaniline (Acros, 99%); acetone (Fisher, certified ACS); glacial acetic acid (Mallinckrodt, analytical reagent); concentrated hydrochloric acid (Fisher, certified ACS); concentrated nitric acid (Fisher, certified ACS); sodium dodecyl sulfate (Fisher, certified ACS); Triton® X-100 (Acros); palladium(II) acetate (Strem, 98+%); palladium(II) acetylacetonate (Strem, 99%); tris(dibenzylideneacetone)dipalladium(0) (Strem, 98%); palladium atomic absorption standard solution (Acros, 1000.6 ppm Pd) were used as received. Deionized water (18 MΩ) was used in the preparation of all aqueous solutions and standards.

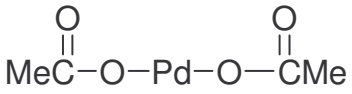

4a

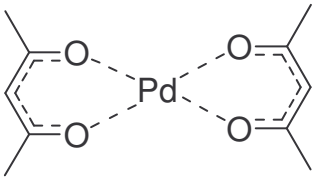

4b

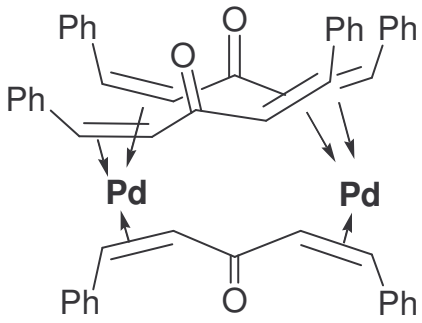

4c

Figure 4.1. Chemical structures of the model palladium complexes studied in the current work: palladium(II) acetate (**4a**); palladium(II) acetylacetonate (**4b**); tris(dibenzylideneacetone)dipalladium(0) (**4c**).

4.2.2. Analytical Instrumentation

All UV-visible spectra were collected using a Hewlett-Packard 8452 photodiode array UV-visible spectrophotometer and a standard 1.0-cm quartz cuvette. Blank spectra of solutions containing all matrix components other than the analyte were recorded and subtracted from all subsequent spectra.

Atomic absorption (AA) analyses were performed using a Perkin-Elmer 5100 atomic absorption spectrophotometer using an air/acetylene flame under standard conditions[6] unless otherwise noted.

4.2.3. Photochemical Reactor and UV Lamp Used in the Current Studies

The photoreactor used in the current studies consists of an outer vessel containing the sample, into which a quartz immersion well/water jacket housing the UV lamp is immersed. The sample capacity of the photoreactor is approximately 500 mL. This reactor was designed and built in house, except for the quartz immersion well, which was purchased from Ace Glass. The UV lamp used in these studies was a 450-W quartz medium-pressure mercury-vapor immersion lamp with a 5-in. arc length (Ace Glass 7825-34).

4.2.4. Preparation and AOP Treatment of Samples

4.2.4.1. Studies of the Solubilities of the Pd Complexes 4a-4c

The three Pd complexes **4a-4c** were found *insoluble* in water. Studies were conducted to determine their solubilities in various organic solvents by the

following process. Pd complex (20 mg) was weighed into each of several small glass vials. A minimal volume (< 1 mL) of an organic solvent was added to each vial (one solvent per vial). The vials containing solvents with low solubilities of the Pd complex were discarded. The vials containing the solvent in which the Pd complex was soluble were kept for further investigation. The contents of these vials were then added to 100 mL of deionized water to determine if phase separation would occur. Suitable organic solvents were determined to be those in which the Pd catalyst would readily dissolve, and would exhibit no phase separation upon addition of water.

4.2.4.2. AOP Treatment of Palladium(II) Acetate (4a)

In the preparation of a typical sample of **4a** for AOP treatment, $Pd(OAc)_2$ (**4a**, 31.7 mg) was dissolved in acetone (700 µL). The solution was then added to deionized water (200 mL) in the photochemical reactor. A 3:1 mixture of concentrated HCl and HNO_3 was then added to adjust pH to 0.75. H_2O_2 (30%, 5.0 mL) was added to the reactor to bring the H_2O_2 concentration to 5.0 g/L. After shielding the photochemical reactor with aluminum foil, the sample was UV irradiated using a 450-W UV lamp for 4.1 hours. During the UV irradiation, H_2O_2 (5%, 100 mL) was added dropwise to replenish H_2O_2. After UV irradiation of the sample, the contents of the reactor were quantitatively transferred to a 500-mL volumetric flask so that the total volume of the sample could be accurately measured. Repeated $Pd(H_2O)_n^{2+}$ analyses by the N,N-dimethyl-4-nitrosoaniline method showed that (98.5 ± 1.2)% of **4a** had been converted to aqueous

$Pd(H_2O)_n^{2+}$ ions. In a control sample of **4a** that was *not* treated by AOP, only (79.1 ± 1.2)% of **4a** existed as $Pd(H_2O)_n^{2+}$ ions. These results indicate that AOP treatment of the $Pd(OAc)_2$ sample is necessary for the accurate detection and quantification of Pd(II) in **4a**.

Atomic absorption (AA) was found to be a good method for total Pd analysis for samples of **4a** that were and were *not* treated by AOP. AA analyses of an AOP-treated sample and its control that was not treated by AOP detected (97 ± 3)% and (99 ± 3)% of palladium, respectively, in the samples of **4a**.

4.2.4.3. AOP Treatment of Palladium(II) Acetylacetonate (4b)

$Pd(acac)_2$ (**4b**, 19.1 mg) was dissolved in glacial acetic acid (9.00 mL). The solution was added to deionized water (250 mL) in the photochemical reactor. A 3:1 mixture of concentrated HCl and HNO_3 was then added to adjust pH to 0.75. H_2O_2 (30%, 6.3 mL) was added to the reactor to make the H_2O_2 concentration 5.0 g/L. After shielding the photochemical reactor with aluminum foil, the solution was UV irradiated using a 450-W UV lamp for 4.0 hours. During the UV irradiation of the sample, H_2O_2 (5%, 100 mL) was added dropwise to replenish H_2O_2. After UV irradiation, the contents in the reactor were quantitatively transferred to a 500-mL volumetric flask so that the total volume of the sample could be accurately measured. Repeated $Pd(H_2O)_n^{2+}$ analyses by the N,N-dimethyl-4-nitrosoaniline method showed that (98.2 ± 0.6)% of **4b** had been converted to aqueous $Pd(H_2O)_n^{2+}$ ions. In a control sample of **4b** that was *not* treated by AOP, only (89.5 ± 1.2)% of **4b** existed as $Pd(H_2O)_n^{2+}$ ions. These

results indicate that AOP treatment of the $Pd(OAc)_2$ sample gives more accurate detection and quantification of Pd in **4b**.

AOP was also found necessary for the accurate quantification of Pd in **4b** by atomic absorption (AA). AA analyses of an AOP-treated sample and its control that was *not* treated by AOP detected (99 ± 3)% and (89 ± 3)% of palladium, respectively, in the samples of **4b**.

4.2.4.4. AOP Treatment of Tris(dibenzylideneacetone)dipalladium(0) (4c)

$Pd_2(dba)_3$ (**4c**, 21.5 mg) was mixed with triton X-100 (0.150 mL) in a glass vial. This mixture was then added quantitatively to deionized water (300 mL) in the photochemical reactor. A 3:1 mixture of concentrated HCl and HNO_3 was then added to adjust pH to 0.13. H_2O_2 (30%, 5.0 mL) was added to the reactor to make the H_2O_2 concentration 5.0 g/L. After shielding the photochemical reactor with aluminum foil, the sample was UV irradiated using a 450-W UV lamp for 5.8 hours. During the UV irradiation, H_2O_2 (4.7%, 125 mL) was added dropwise to replenish H_2O_2. After UV irradiation, the contents of the reactor were quantitatively transferred to a 500-mL volumetric flask so that the total volume of the sample could be accurately measured.

$Pd(H_2O)_n^{2+}$ analyses by the N,N-dimethyl-4-nitrosoaniline method showed that (90.0 ± 1.2)% of **4c** had been converted to aqueous $Pd(H_2O)_n^{2+}$ ions. In a control sample of **4c** that was *not* treated by AOP, *no* $Pd(H_2O)_n^{2+}$ ions were detected by the N,N-dimethyl-4-nitrosoaniline method. AOP treatments of $Pd_2(dba)_3$ (**4c**) were repeated many times. However, quantitative oxidation of **4c**

was not reproducible. These results indicate that the oxidation of **4c** and removal of its ligands is possible, but the process is not complete.

AOP was also found necessary for the accurate quantification of Pd in **4c** by atomic absorption (AA). AA analyses of an AOP-treated sample and its control that was not treated by AOP detected (99 ± 3)% and (16 ± 3)% of palladium, respectively, in the samples of **4c**.

4.2.4.5. Continuous Addition of H_2O_2 during UV Irradiation

Continuous addition of H_2O_2 during UV irradiation was conducted by using an addition funnel that was offset from the photoreactor and shielded by aluminum foil. Such a design was made so that UV radiation from the photoreactor would not prematurely decompose H_2O_2 in the funnel. The flow rate was adjusted prior to the start of the UV irradiation.

4.2.4.6. Studies of the pH during AOP Treatment of the Pd Complexes

In order to determine the optimum pH and acid/acid combination for use during AOP, samples of $Pd(acac)_2$ (**4b**) were investigated. $Pd(acac)_2$ (**4b**, 19 mg) was dissolved in glacial acetic acid (9.00 mL). The solution was added to deionized water (250 mL) in the photochemical reactor. Sample pH was varied from 0-1 by addition of H_2SO_4, HCl, HNO_3, or aqua regia (a 3:1 mixture of HCl and HNO_3). H_2O_2 (30%, 6.3 mL) was added to each sample to make the H_2O_2 concentration 5.0 g/L. After shielding the photochemical reactor with aluminum foil, the solution was UV irradiated using a 450-W UV lamp for 4.0 hours. During

the UV irradiation of the sample, H_2O_2 (5%, 100 mL) was added dropwise to replenish H_2O_2. After UV irradiation, the contents in the reactor were quantitatively transferred to a 500-mL volumetric flask so that the total volume of the sample could be accurately measured. Samples in which the pH was adjusted to 0.75 by addition of aqua regia showed the lowest errors in both aqueous Pd(II) [(1.8 ± 0.6)%] and total Pd [(1 ± 3)%] analyses. Aqua regia was thus chosen for use in further experiments.

A control sample was prepared by adding $Pd(acac)_2$ (**4b**, 19 mg) dissolved in glacial acetic acid (9.00 mL) to deionized water (250 mL) in a volumetric flask. Sample pH was adjusted to 0.75 by addition of aqua regia. There was *no* AOP treatment of this sample. Analyses of this control sample showed (10.5 ± 1.2)% and (11 ± 3)% errors in aqueous Pd(II) and total Pd contents, respectively.

4.2.5. Analysis of Total Pd and Pd(II)

All AOP samples and standards were prepared gravimetrically using standard analytical techniques. At the conclusion of the UV irradiation step, samples were quantitatively transferred and diluted in volumetric flasks. After dilution, samples were then analyzed for total palladium and aqueous Pd(II) content.

Total palladium in each sample was analyzed by AA spectroscopy using an air-acetylene flame. Standard solutions were prepared by serial dilution of a 1000.6 ppm Pd(II) AA standard solution and addition of necessary sample matrix components to each standard before diluting to the proper volume. The standard

curves were made by measuring the absorbance at 244.8 nm using a slit width of 0.20 nm with a lamp current of 15 mA during analysis of the standards and samples for total Pd.[6]

Pd(II) in each sample was analyzed by UV-vis spectrometry using N,N-dimethyl-4-nitrosoaniline, a ligand selective for Pd(II).[12] Upon addition of the ligand to a Pd(II) solution, a colored complex is formed. Pd(II) content in the standards and samples was determined by monitoring the absorbance at 496 nm in the UV-vis spectrum. Standards were prepared by serial dilution of a 1000.6 ppm Pd(II) AA standard solution and addition of the ligand and necessary sample matrix components to a volumetric flask.

Detailed procedures and errors in the determination of total Pd and Pd(II) are given in Appendix C.

4.3. Results and Discussion

4.3.1. The Advanced Oxidation Process

Palladium acetate (**4a**) and palladium acetylacetonate (**4b**) are Pd(II) complexes. Our tests have shown that *direct* analysis of Pd *before* AOP treatment by the UV-vis and AA methods discussed in Part 4.2.5 result in large errors, suggesting that the ligands in these complexes may interfere with detection of Pd(II). $Pd_2(dba)_3$ contains Pd(0) and thus requires both oxidation of Pd(0) to Pd(II) and the removal of the organic ligands before quantitative analysis of palladium by established electrochemical or optical methods. The Advanced

Oxidation Process (AOP) has thus been investigated to treat these Pd complexes.

Our work reveals that, among the factors contributing to the efficiency of Advanced Oxidation Processes, solubility of the complex in aqueous solution is the most important. Other factors include power of the UV source, reactor design, H_2O_2 concentration, length of UV irradiation, and sample pH. Our studies of these factors are discussed herein.

4.3.2. Optimization of Parameters in an AOP Treatment

4.3.2.1. Improving Solubility of the Pd Complexes in Aqueous Solution

AOP is an oxidation process conducted in aqueous solution using dilute H_2O_2 in water and UV radiation or O_3 as oxidants. Our studies have shown that, for the successful treatment of compounds by AOP, it is necessary that the compound be soluble or at least well dispersed in aqueous solution. For compounds that are water soluble, AOP may be readily applied, as demonstrated in the AOP treatment of a water-soluble chromium complex in Part 3. For compounds that are sparingly soluble in water, their AOP treatments may be challenging.

Most palladium complexes that are good catalysts are only soluble in organic solvents.[3e] The Pd catalyst complexes (Figure 4.1) investigated in the current studies, palladium acetate (**4a**), palladium acetylacetonate (**4b**), and tris(dibenzylideneacetone)dipalladium(0) (**4c**), are insoluble in water.[13]

Significant effort was made to investigate methods to incorporate these complexes into aqueous solution.

4.3.2.2. Solubility and AOP Treatment of Palladium(II) Acetate (4a)

Initial attempts to disperse/dissolve $Pd(OAc)_2$ (**4a**) in aqueous solution involved addition of various surfactants to solids of **4a**. Sodium dodecylsulfate (SDS), an ionic surfactant (**4d**, Figure 4.2), was first investigated. The addition of SDS (850 mg) to **4a** (10 mg) in water (200 mL) was found to make a clear dispersion of **4a** in the solution. The AOP treatment of this solution was found to give poor analyses of both total Pd and Pd(II). Unknown black solids were found in the AOP-treated mixture.

Triton X-100 (**4e**, Figure 4.2), a nonionic surfactant, was next investigated to disperse $Pd(OAc)_2$ (**4a**) in aqueous solution. There is a long, oxygen-containing tail in **4e**, and it was thought that the oxygen atoms may allow easier oxidation of the carbon atoms in the tail. In comparison, the tail in SDS is hydrocarbon in nature. It was found that ca. 2.0 g of Triton X-100 was required to disperse 10 mg of $Pd(OAc)_2$ (**4a**) in ca. 200 mL of water. The AOP treatment of this solution was also unsuccessful, yielding poor analyses of both total Pd and Pd(II).

The two surfactants **4d** and **4e** were found to disperse the Pd complex in aqueous solution. However, in the AOP treatment, the large amounts of the organic surfactants are also oxidized by H_2O_2 and UV irradiation. The amounts

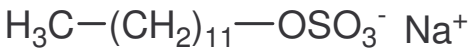

4d

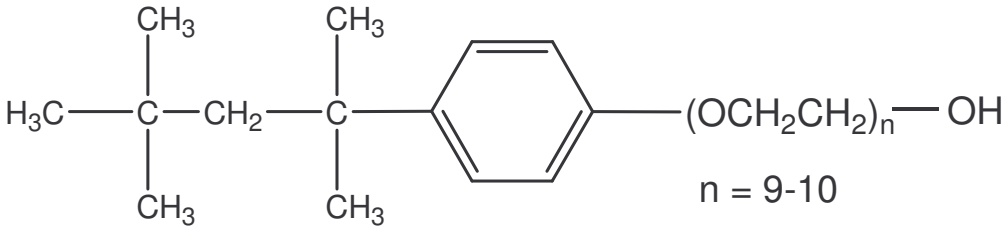

4e

Figure 4.2. Chemical structures of sodium dodecyl sulfate (SDS, **4d**) and Triton® X-100 (**4e**).

of the surfactants needed to reach the critical micelle concentration to disperse the Pd complex likely exceeded the amount of organics that could be completely oxidized by AOP in our work. The incomplete oxidation of surfactant molecules could have led to the formation of black particles that were observed in some instances. The use of surfactants thus made the complete oxidation of all organic species difficult.

We next investigated the approach using solvent mixtures of an organic solvent and water to dissolve $Pd(OAc)_2$ (**4a**). After investigating several organic solvents, acetone was found to work well in this approach. $Pd(OAc)_2$ in acetone and water was found to give a clear solution. In one solubility test, the sample was prepared by dissolving $Pd(OAc)_2$ (30 mg) in a minimum amount of acetone (700 µL). The solution was then added to 300 mL of deionized water to give a homogeneous solution. Subsequent AOP treatment of this sample was successful, yielding values for total Pd and Pd(II) that were in a close agreement.

The results here indicate that this is a good method to dissolve $Pd(OAc)_2$ in aqueous solution. The following may contribute to its success: (1) Acetone molecules are much smaller than the bulky surfactant molecules used earlier; (2) Acetone contains a carbonyl group that may have helped the oxidation of acetone in the AOP; (3) In the sample using acetone, the total amount of organics (700 µL) is lower than in samples containing the surfactants (SDS: 850 mg; Triton X-100: 2.0 g).

4.3.2.3. Solubility of Palladium(II) Acetylacetonate (4b)

Studies in Part 4.3.2.2 showed that mixed solvents containing water and an organic solvent miscible with water dissolves $Pd(OAc)_2$. A similar method was used to dissolve $Pd(acac)_2$ (**4b**) in mixed solvents. Several organic solvents were investigated, and $Pd(acac)_2$ was found to be soluble in glacial acetic acid. In one test, $Pd(acac)_2$ (**4b**, 20 mg) was dissolved in 9 mL of glacial acetic acid. This solution was then mixed with 300 mL of water to give a homogeneous solution. Subsequent AOP treatment of this sample was successful, yielding values for total Pd and Pd(II) that were in a close agreement.

Acetic acid, as acetone, contains a carbonyl group, and is thus easier to oxidize than bulky surfactants. Even though a relatively large amount of glacial acetic acid was used here, it apparently did not cause a problem for subsequent AOP treatment.

4.3.2.4. Solubility of Tris(dibenzylideneacetone)dipalladium(0) (4c)

Tris(dibenzylideneacetone)dipalladium(0) [$Pd_2(dba)_3$, **4c**] is soluble in few organic solvents.[3e] Of the solvents such as chloroform and toluene in which $Pd_2(dba)_3$ is soluble, *none are miscible with water*. The use of a surfactant was found to be the *only* method to disperse the complex in aqueous solution. Both SDS and triton X-100 were investigated for dispersion of $Pd_2(dba)_3$ (**4c**) in aqueous solution. Triton X-100 was found to work well for the dispersion of the complex. However, attempts to disperse the complex using SDS did not work as well as those using triton X-100.

Subsequent AOP treatment of the $Pd_2(dba)_3$ (**4c**)/triton X-100 samples show qualitatively that the ligand in **4c** was removed from the metal, and Pd(0) in the complex was oxidized to Pd(II). However the conversion during AOP was not complete, and unknown black solids were found in the AOP-treated mixture. As in the samples involving $Pd(OAc)_2$ (**4a**) and surfactants (Part 4.3.2.2), the amount of surfactant (Triton X-100: 0.162 g) needed to reach the critical micelle concentration to disperse the Pd complex likely exceeded the amount of organics that could be oxidized by AOP. The use of surfactants thus made the complete oxidation of all organic species difficult.

4.3.2.5. UV Irradiation vs. Ozone in the AOP Treatment of the Pd Complexes

Many AOP studies have been conducted using both ozone and UV radiation to generate active hydroxyl radicals from H_2O_2. Although both methods have been thoroughly tested, UV radiation was chosen as the method for activating H_2O_2 in the current studies. Advantages of using UV in our studies include the ease of generating UV radiation, low cost, and its potential for use in a portable sensor. Primary reasons for not using ozone include the need for an ozone generator, health risks associated with ozone in a research laboratory, and corrosion that ozone causes to laboratory equipment.

4.3.2.6. Hydrogen Peroxide Concentration during the AOP Treatment

Earlier AOP studies showed that a H_2O_2 concentration of 5 g/L during the UV irradiation process was sufficient for the oxidation of several organic compounds.[10b] A H_2O_2 concentration of 5 g/L was also found to work well in the current studies. As is the case with other AOP systems, replenishing H_2O_2 during UV irradiation of the sample has been found to contribute to the overall efficiency of the process.

In many reported AOP studies, H_2O_2 is added at the beginning of the experiment before UV irradiation of the sample.[10b-c,14] Our initial experiments were carried out similarly. H_2O_2 was added into the reactor immediately before UV irradiation of the sample so that the H_2O_2 concentration was 5 g/L. These experiments showed *incomplete* oxidation of the organic species and thus poor Pd(II) analysis. It is suspected that the H_2O_2 was depleted during the reaction, and thus not enough hydroxyl radicals were generated to complete the oxidation.

We subsequently investigated continuous addition of H_2O_2 during the UV irradiation of $Pd(OAc)_2$ samples. H_2O_2 (30%, 5.0 mL) was added to samples i and ii (total volume: 300 mL) in Figure 4.3 before UV irradiation to give a H_2O_2 concentration of 5 g/L. During the UV irradiation of samples i and ii (Figure 4.3), a 5% H_2O_2 solution (100 mL) was added dropwise to replenish H_2O_2. In control samples (iii and iv) *without* continuous H_2O_2 addition (Figure 4.3), H_2O_2 was added prior to the UV irradiation so that the H_2O_2 concentration was 5 g/L. The continuous addition of H_2O_2 was found to greatly increase the efficiency of the oxidation process and the removal of organic ligands. Nearly quantitative [(99.0

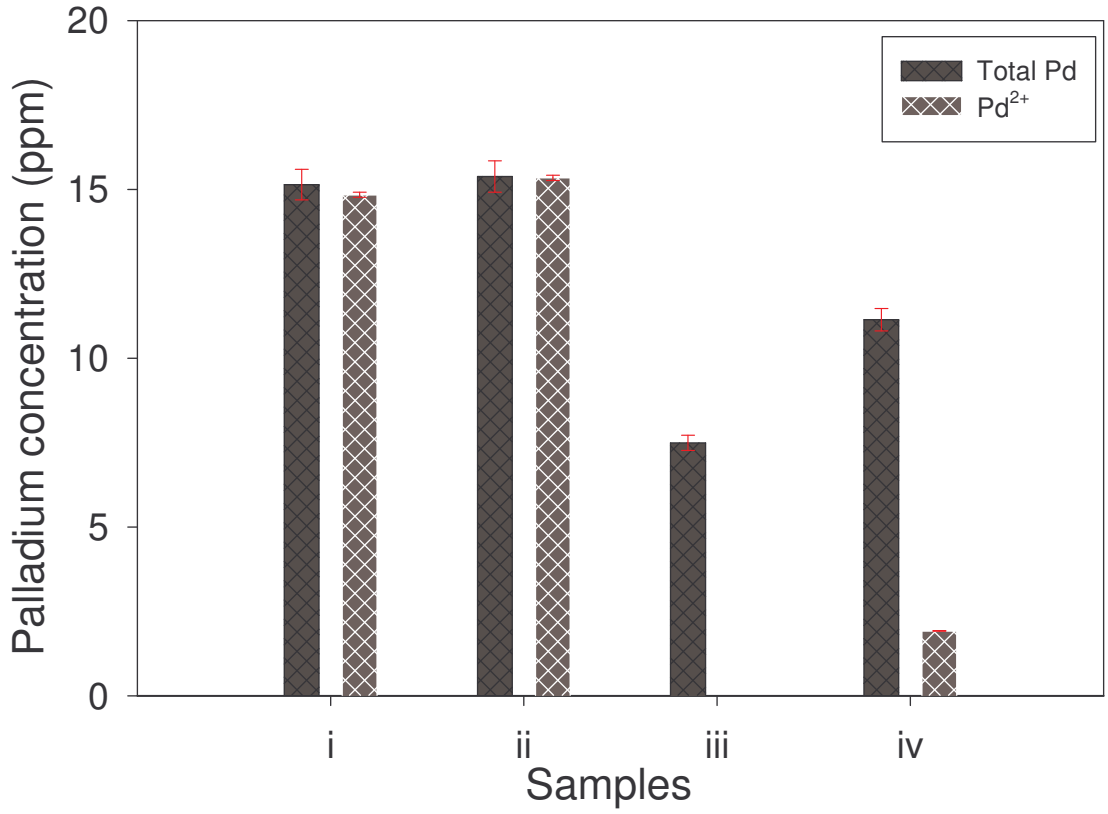

Figure 4.3. Comparison of the total Pd and aqueous Pd(II) concentration after the AOP treatment of $Pd(OAc)_2$ samples i, ii, iii, and iv. H_2O_2 was continuously added during UV irradiation of samples i and ii. In control samples iii and iv, H_2O_2 was *not* continuously added during UV irradiation.

± 0.5)%] conversion of the Pd complex in samples i and ii to aqueous Pd(II) was achieved, as the Pd(II) analysis revealed. In comparison, (0.0 ± 0.1)% and (17.8 ± 0.1)% of the Pd complex in samples iii and iv were converted to aqueous Pd(II).

4.3.2.7. Length of UV Irradiation and Related Effects

Unlike the water-soluble chromium complex discussed in Part 3, longer UV irradiation is required to treat the water-*insoluble* palladium complexes, even when continuous addition of H_2O_2 is used during UV irradiation. Each of the three Pd complexes (**4a**, **4b**, **4c**) was investigated separately to determine the optimum UV irradiation length. Incomplete oxidation of the tris(dibenzylideneacetone)dipalladium(0) (**4c**)/micelle mixture was observed even after 15 hours of UV irradiation, as stated earlier, and **4c** was thus not studied further. Identical Pd samples of **4a** or **4b** were UV irradiated from one to six hours. Samples treated for less than four hours often did not yield quantitative analysis of aqueous Pd(II) by UV-vis spectroscopy using N,N-dimethyl-4-nitrosoaniline. UV irradiation of four hours resulted in (99.0 ± 0.5)% oxidation and removal of the ligands to give quantitative analysis of aqueous Pd(II) by UV-vis spectroscopy using N,N-dimethyl-4-nitrosoaniline. Longer UV irradiation was thus not investigated.

Several factors may contribute to the increase in UV irradiation time here (in comparison to the AOP treatment of the Cr complex in Part 3): (1) There are organic solvents in **4a** and **4b**, and they need to be oxidized as well; (2) The Pd

complexes **4a** and **4b** are insoluble in water, and, in mixed organic solvent/water, may have higher kinetic barriers for oxidation by water-based hydroxyl radicals •OH; (3) The volume of samples in the current work (~300-400 mL) is much larger than that (~15 mL) in the Cr sample, and the larger volume is expected to require longer AOP treatment.

4.3.2.8. Effect of pH during AOP Treatment

Initial AOP experiments involving the palladium complexes were conducted without adjustment of pH. Coatings and/or unknown black particles were often observed on the inside walls of the photoreactor. Analysis of the coatings/particles showed a significant amount of Pd content. In an attempt to prevent formation of the coatings, variation of solution pH during AOP treatment of $Pd(acac)_2$ (**4b**) was investigated.

These studies show that lowering pH during the AOP treatment eliminates the formation of coatings and/or particles. Optimum results were obtained when sample pH was maintained in the range of 0.5-0.8. Several acids including HCl, HNO_3, and aqua regia (a 3:1 mixture of HCl and HNO_3) were used to lower pH. While neither HCl nor HNO_3 alone was found to greatly increase the amount of free Pd(II), the use of the combination of acids as aqua regia was found to give the best results [(1.8 ± 0.6)% and (1 ± 3)% errors in Pd(II) and total Pd analyses, respectively].

A control sample of **4b** was prepared similarly, and its pH was adjusted to 0.75 by addition of aqua regia. There was *no* H_2O_2 addition or UV irradiation of

this sample. The (10.5 ± 1.2)% and (11 ± 3)% errors in aqueous Pd(II) and total Pd analyses, respectively, in this control sample are larger than those in the sample of **4b** that was treated by AOP. This finding indicates that the combination of low pH and AOP treatment are required for accurate Pd analysis. It should be noted that low pH (pH < 2) is often used in standard analytical procedures.[15]

4.3.2.9. UV Lamp and Photoreactor Used in the Current Studies

A large-scale photoreactor and high-intensity UV lamp were used to treat large quantities of samples in the current work. A 500-mL photoreactor (Figure 4.4) was designed and built in house. A large Teflon-coated magnetic stir bar was used during the UV irradiation process. A port was incorporated into the design to allow the use of a continuous addition funnel for H_2O_2 addition during UV irradiation. A second port allows air to enter the photoreactor. For the large photoreactor, the path of the UV irradiation through the sample is relatively long. Solution in the inner portion of the photoreactor absorbs much of the radiation, thus reducing the amount of UV radiation reaching the solution in the outer portion of the photoreactor. A high intensity UV source (450-W) (Figure 4.5) was therefore used to provide adequate radiation intensity for activation of the H_2O_2 near the outer portion of the sample.

Although the 15-mL small-scale photoreactor and the 5.5-W UV lamp were proven effective for the oxidation processes discussed in Part 3, sample treatment using this combination was not attempted. As discussed earlier in the

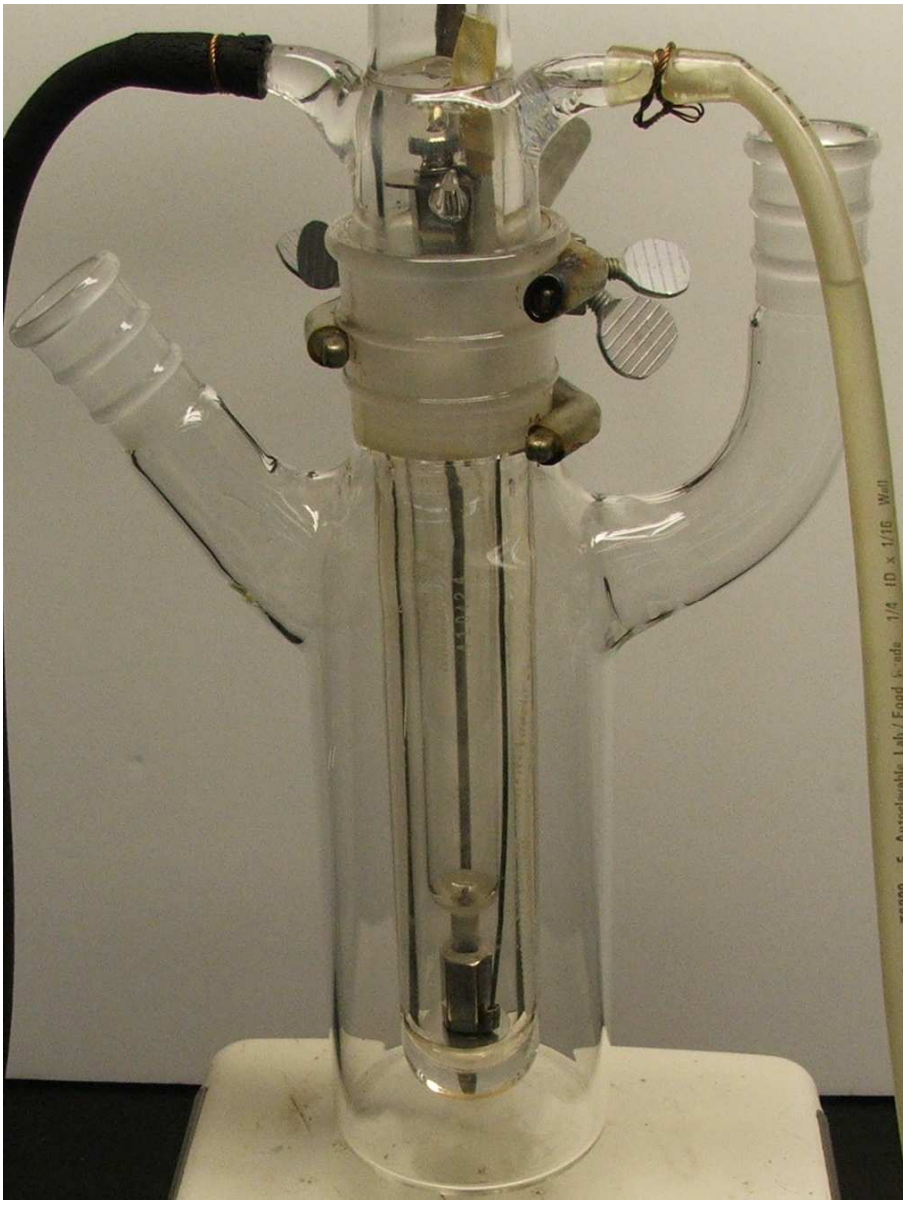

Figure 4.4. Photo of the photochemical reactor with an immersion well and a 450-W UV lamp.

Figure 4.5. Photo of the 450-W UV lamp used in the current studies.

current work, the Pd complexes **4a**-**4c** require long UV irradiation, as well as continuous addition of H_2O_2 for good results. Much longer UV treatment would have been expected if the microscale photoreactor had been used. Thus the 15-mL photoreactor and the 5.5-W UV lamp were not used in the current work.

4.4. Concluding Remarks

The Advanced Oxidation Process has proven to be a viable method to oxidize the ligands and organic species contained in model Pd catalyst complexes. The low solubility of these complexes in aqueous solution was a major challenge in the AOP treatment. The use of mixed organic solvent/water for $Pd(OAc)_2$ (**4a**) and $Pd(acac)_2$ (**4b**) is a good method to dissolve water-insoluble complexes for subsequent AOP treatment. Although treatment of Pd(0) complex **4c** did not give good Pd analysis results, oxidation of **4c** and removal of its ligands by AOP did occur. Its low solubility in many organic solvents makes it difficult to find mixed organic/water solvents for **4c**.

References

1. (a) Kragen, D. D.; Rutger, A. V. S. *Inorg. Chem*. **1999**, *38*, 331. (b) Hallman, K.; Moberg, C. *Adv. Synth. Catal*. **2001**, *343*, 261. (c) Singh, R.; Viciu, M. S.; Kramareva, N.; Navarro, O.; Nolan, S. P. *Org. Lett*. **2005**, *7*, 1829. (d) Schultz, M. J.; Hamilton, S. S.; Jensen, D. R.; Sigman, M. S. *J. Org. Chem.* **2005**, *70*, 3343. (e) Ikawa, T.; Sajiki, H.; Hirota, K. *Tetrahedron* **2005**, *61*, 2217. (f) Grasa, G. A.; Hillier, A. C.; Nolan, S. P.

Org. Lett. **2001**, *3*, 1077.

2. (a) Stefani, H. A.; Cella, R.; Dorr, F. P.; Pereira, C. M. P.; Zeni, G.; Gomes Jr., M. *Tetrahedron Lett*. **2005**, *46*, 563. (b) Terao, J.; Oda, A.; Kambe, N. *Org. Lett*. **2004**, *6*, 3341. (c) Myagmarsuren, G.; Tkach, V. S.; Shmidt, F. K. *React. Kinet. Catal. Lett*. **2004**, *83*, 337.

3. (a) Yoo, W.-J.; Tsui, G. C.; Tam, W. *Eur. J. Org. Chem*. **2005**, *6*, 1044. (b) Hay, M. B.; Hardin, A. R.; Wolfe, J. P. *J. Org. Chem*. **2005**, *70*, 3099. (c) Dominczak, N.; Damez, C.; Rhers, B.; Labrosse, J.-R.; Lhoste, P.; Kryczka, B.; Sinou, D. *Tetrahedron* **2005**, *61*, 2589. (d) Nakamura, H.; Onagi, S.; Kamakura, T. *J. Org. Chem*. **2005**, *70*, 2357. (e) Heck, R. F. *Palladium Reagents in Organic Syntheses*, Harcourt Brace Jovanovich, New York, 1985.

4. (a) Evans, D. A.; Morrissey, M. A. *Tetrahedron Lett*. **1984**, *25*, 4637. (b) Kiener, C. A.; Shu, C.; Incarvito, C.; Hartwig, J. F. *J. Am. Chem. Soc*. **2003**, *125*, 14272. (c) May, J. A.; Stoltz, B. M. *J. Am. Chem. Soc*. **2002**, *124*, 12426. (d) Wender, P. A.; Barzilay, C. M.; Dyckman, A. J. *J. Am. Chem. Soc*. **2001**, *123*, 179. (e) Yonehara, K.; Hashizume, T.; Mori, K.; Ohe, K.; Uemura, S. *J. Org. Chem*. **1999**, *64*, 5593. (f) Chatani, N.; Tatamidani, H.; Ie, Y.; Kakiuchi, F.; Murai, S. *J. Am. Chem. Soc*. **2001**, *123*, 4849. (g) Trost, B. M.; Pinkerton, A. B.; Seidel, M. *J. Am. Chem. Soc*. **2001**, *123*, 12466. (h) Trost, B. M.; Ball, Z. T. *J. Am. Chem. Soc*. **2003**, *125*, 30.

5. (a) Aghamohammadi, M.; Alizadeh, N. *Anal. Chim Acta* **2003**, *480*, 299. Wang, J.; Varughese, K. *Anal. Chim. Acta* **1987**, *199*, 185. (b) Bharathibai, J. B.; Rajagopalan, S. R. *Analyst* **1992**, *117*, 1623. (c) Raber, G.; Kalcher, K.; Neuhold, C. G.; Talaber, C.; Kolbl, G. *Electroanalysis* **1995**, *7*, 138.

6. (a) Welz, B.; Sperling, M. *Atomic Absorption Spectrometry*, 3rd Ed., Wiley, New York, 1999 (b) Perkin Elmer Corporation, *Analytical Methods for Atomic Absorption Spectroscopy*, 1996. (c) Skoog, D. A.; Holler, F. J.; Nieman, T. A. *Principles of Instrumental Analysis*, 5th Ed., Harcourt Brace, Philadelphia, 1998.

7. (a) Taylor, H. E. *Inductively Coupled Plasma-Mass Spectrometry*, Academic Press, New York, 2001. (b) Qi, L.; Zhou, M.-F.; Wang, C. Y. *J. Anal. Atom. Spectrom*. **2004**, *19*, 1335.

8. Grumett, P. *Platinum Metals Rev*. **2003**, *47*, 163.

9. Bock, R. *A Handbook of Decomposition Methods in Analytical Chemistry*, Wiley, New York, 1979, Ch. 5.

10. (a) *Advanced Photochemical Oxidation Processes*, US EPA **1998** (b) Schulte, P.; Bayer, A.; Kuhn, F.; Luy, Th.; Volkmer, M. *Ozone-Sci. Eng*. **1995**, *17*, 119. (c) Sigman, M. E.; Buchanan, A. C., III; Smith, S. M. *J. Adv. Oxid.Technol*. **1997**, *2*, 415. (d) Castaldi, F. J.; Richardson, C. F. Payne, B. *Proceedings – WEFTEC '96* **1996**, *3*, 275.

11. (a) Safarzadeh-Amiri, A. *Water Res*. **2001**, *35*, 3706. (b) Beltran, F. J.; Gonzalez, M.; Rivas, J.; Marin, M. *Ind. Eng. Chem. Res*. **1994**, *33*, 125.

(c) Castaldi, F. J.; Richardson, C. F. Payne, B. *Proceedings – WEFTEC '96* **1996**, *3*, 275.

12. Sarkar, P.; Paria, P. K.; Majumdar, S. K. *J. Indian Chem. Soc*. **1988**, *65*, 117.

13. (a) O'Neil, M. J.; Smith, A.; Heckelman, P. E., Eds. *The Merck Index*, 13th Ed., Merck and Co., Whitehouse Station, NJ, 2001, p. 7056. (b) Takahashi, Y.; Ito, T.; Sakai, S.; Ishii, Y. *Chem. Comm*. **1970**, 1065. (c) Kawazura, H.; Tanaka, H.; Yamada, K.-I.; Takahashi, T.; Ishii, Y. *B. Chem. Soc. Jpn*. **1978**, *51*, 3466.

14. (a) Kavitha, V.; Palanivelu, K.; *Chemosphere* **2004**, *55*, 1235. (b) Ghaly, M. Y.; Hartel, G.; Mayer, R.; Haseneder, R. *Waste Manage*. **2001**, *21*, 41.

15. For example, in the ICP-AE or ICP-MS analysis of aqueous samples, the pH of the solutions is adjusted to < 2 prior to analysis to minimize analyte precipitation. Varnes, A. W. in *Handbook of Instrumental Techniques for Analytical Chemistry*, Settle, F. A., Ed.; Prentice Hall: Upper Saddle River, NJ, Chs. 21 and 22.

Part 5

Spectroscopic Detection of Halocarbons Using Modified Fujiwara Reactions

5.1. Introduction

Halocarbons such as chloroform[1] and carbon tetrachloride[2] have been used extensively in many industries and are produced on the scale of thousands of tons per year worldwide. These chemicals, which are also called halogenated hydrocarbons (HHCs), are known to cause damage to the liver, kidneys, and the neurological system, and most are suspected carcinogens.[3] The levels of these chemicals in the environment need to be closely monitored.[4] Chromatography has been used in the analysis of these compounds.[5,6]

The Fujiwara reaction for the spectroscopic detection of chloroform was first reported in 1916.[7] This reaction, as originally reported, relies on a two-phase system consisting of an aqueous layer of NaOH along with a liquid pyridine layer to which chloroform was added. This mixture was then heated to give an intense red color that was monitored spectroscopically for chloroform detection and quantification. Although this reaction is irreversible and nonspecific with respect to the detection of halocarbons, it has great utility when analyzing solutions containing a single analyte. Kowalski and coworkers have developed procedures based on the Fujiwara reactions for the multicomponent determination of halocarbons and mixtures of halocarbons using tetra-*n*-butylammonium hydroxide as the base.[8-10]

Several modifications[11-21] of the original Fujiwara procedure, including a single-phase Fujiwara system,[11] have been reported for the detection of halogenated compounds. Many of these methods rely on the use of excess

pyridine for the detection and quantification of the halogenated compounds. Pyridine is a toxic, offensive-smelling liquid,[22-23] and, in the state of California, it is legally known to the state to cause cancer.[24] The vapor of pyridine often adheres to skin and clothing persistently. The systems involving pyridine for detection of halogenated compounds are often comprised of two phases, since the commonly used alkalis in water are insoluble in pyridine. Complicated procedures are thus often required to extract the analyte compound into the pyridine layer for detection.

We have recently studied new reagents for the Fujiwara reactions. Solid pyridine derivatives such as 2,2′-dipyridyl or 4,4′-dipyridyl are easier to handle. We have also replaced aqueous NaOH, the traditional base, with aqueous tetra-*n*-butylammonium hydroxide (*n*-Bu_4NOH)[8-11] or potassium *tert*-butoxide (KO-*t*-Bu), which are both soluble in tetrahydrofuran (THF). By replacing liquid pyridine and NaOH with reactants that are soluble in THF, we have eliminated the two-phase system and developed a less complicated experimental procedure. THF, with a moderate health effect,[25] is used as a solvent in these reactions to incorporate the more user-friendly reagents.

Unlike the traditional Fujiwara reaction that requires the use of an aqueous base solution, the use of KO-*t*-Bu and the solid pyridine derivatives require no water. These reactions may thus potentially allow the detection of halocarbons in water-sensitive systems as well. Our studies using these new reagents in the Fujiwara reactions to spectrophotometrically detect chloroform and carbon tetrachloride are reported here.

5.2. Experimental

5.2.1. Reagents

Chloroform $HCCl_3$ (Burdick and Jackson, high purity), carbon tetrachloride CCl_4 (99.5+% anhydrous, Sigma), tetrahydrofuran (THF) (Fisher, certified), 2,2′-dipyridyl (Acros, 99+%), 4,4′-dipyridyl (Acros, 98%), and tetra-*n*-butylammonium hydroxide (*n*-Bu_4NOH, Lancaster, 40 w/w% aqueous solution) were used as received. KO-*t*-Bu was prepared from potassium metal and *tert*-butanol (HO-*t*-Bu) and freshly sublimed at 120 °C and 0.1 torr before use.[26]

5.2.2. Instrumentation

A Hewlett-Packard 8452 photodiode array UV-visible spectrophotometer or a Thermo Spectronic BioMate 5 scanning UV-visible spectrophotometer were used in the current studies. All blank and sample spectra were collected in standard 1.0 cm quartz cuvettes.

5.2.3. Preparation of Standards

Each standard was prepared by weighing 0.3128 g (2 mmol) of 2,2′-dipyridyl or 4,4′-dipyridyl into a 10-mL volumetric flask, and the dipyridyl was dissolved using a minimal amount of THF. *n*-Bu_4NOH (40% aqueous solution, 100 µL, 0.1 mmol) or KO-*t*-Bu (75.8 mM in THF, 8.00 mL, 0.606 mmol) was then added to the volumetric flask containing the dipyridyl. THF was added to the

volumetric flask to obtain the desired concentration. Standard $HCCl_3$ or CCl_4 solutions were prepared from their stock solutions that had been prepared gravimetrically.

Unless specified otherwise, all studies were carried out using solutions containing 0.015 M *n*-Bu_4NOH and 0.200 M 2,2′-dipyridyl at 25 °C. For each measurement, the UV-visible spectrum of a blank containing the dipyridyl and the base at the desired concentrations was used as the reference. Error estimation is given in Appendix D. In some cases, the error bars in the measurements may not be visible in the plots.

5.3. Results and Discussion

The Fujiwara reaction and mechanism have been described in the literature using trihalogenated methanes (HCX_3) as representative halocarbons.[12,27-28] First, a strong base removes the acidic proton in HCX_3 to yield a trihalomethyl anion $:CX_3^-$ (Equation 5.1). This unstable anion loses a halide anion (Equation 5.2) and gives a reactive carbene species ($:CX_2$) that reacts with pyridine (Py), yielding a highly conjugated colored product. The traditional Fujiwara chemistry (pyridine/OH^-) is a two-phase system, since the commonly used alkalis (NaOH and KOH) in water are insoluble in pyridine. Therefore, the reaction product is formed only at the interface.[11,14]

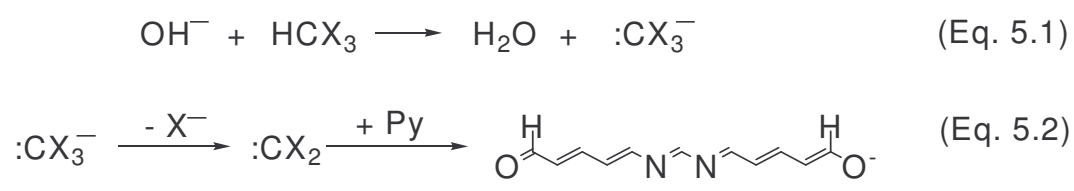

(Eq. 5.1)

(Eq. 5.2)

In many Fujiwara reactions, a small amount of water (or OH^-) is required both for the hydroxide (OH^-) base and in the reaction of the carbene $:CX_2$ with pyridine to give the colored product.[27] When a large amount of water is present, it competes with pyridine for the carbene intermediate, decomposing $:CX_2$ before it reacts with pyridine to give the colored product.[29] It should be pointed out that, when the base KO-*t*-Bu was used, colored products were obtained *without* water, as shown in the current work.

5.3.1. Solvent and Reagents

Tetrahydrofuran was used as a solvent mainly because of high solubilities of reactants such as *n*-Bu_4NOH, KO-*t*-Bu, 2,2′-dipyridyl and 4,4′-dipyridyl in THF.[25] One-phase Fujiwara reactions are thus feasible in THF. When conducting this modified Fujiwara reaction, it was found to be of paramount importance to strictly control the concentrations of dipyridyl and base. The concentrations of dipyridyl and base significantly affected the amount of products from the Fujiwara reactions, and the detection limit of these reactions. Studies were carried out to optimize the amount of the reagents used in these reactions and the detection limits of the new processes.

n-Bu_4NOH is commercially available as a 40 w/w% aqueous solution. In the determination of the optimum *n*-Bu_4NOH concentration, standard solutions were prepared containing 0.200 M 2,2′-dipyridyl and 20 mg/L $HCCl_3$ in THF. The concentration of *n*-Bu_4NOH in these standards was varied from 0.0061 M, 0.015 M, 0.030 M, 0.050 M, 0.075 M, 0.100 M to 0.150 M. The absorbance of the colored products at 440 nm in the UV spectrum (Figure 5.1) for these solutions was the greatest when the *n*-Bu_4NOH concentration was at 0.015 M.

At a lower *n*-Bu_4NOH concentration of 6.10×10^{-3} M, a drop in absorbance was observed. Thus, the *n*-Bu_4NOH concentration of 0.015 M was used in most of the current studies. An adequate amount of the base is needed for the Fujiwara reaction. However, as noted earlier, excess water in the more concentrated *n*-Bu_4NOH solutions may intercept the carbene intermediate $:CCl_2$,[29] and thus reduce the yield of the colored product between $:CCl_2$ and 2,2′-dipyridyl. In other words, excess water has detrimental effects on the reaction. Both 2,2′-dipyridyl and 4,4′-dipyridyl were found to react with $HCCl_3$ or CCl_4 and *n*-Bu_4NOH to give colored species. Typical UV-visible spectra of the products from the Fujiwara reactions of $HCCl_3$ with *n*-Bu_4NOH and 2,2′-dipyridyl or 4,4′-dipyridyl are given in Figure 5.2. Such UV-visible spectra of the products from the reactions of CCl_4 are given in Figure 5.3. In reactions involving both $HCCl_3$ and CCl_4, UV-visible peaks at 438-444 nm and 364 nm were observed for the solutions containing 2,2′-dipyridyl and 4,4′-dipyridyl, respectively. The products from the Fujiwara reactions involving 4,4′-dipyridyl were found to

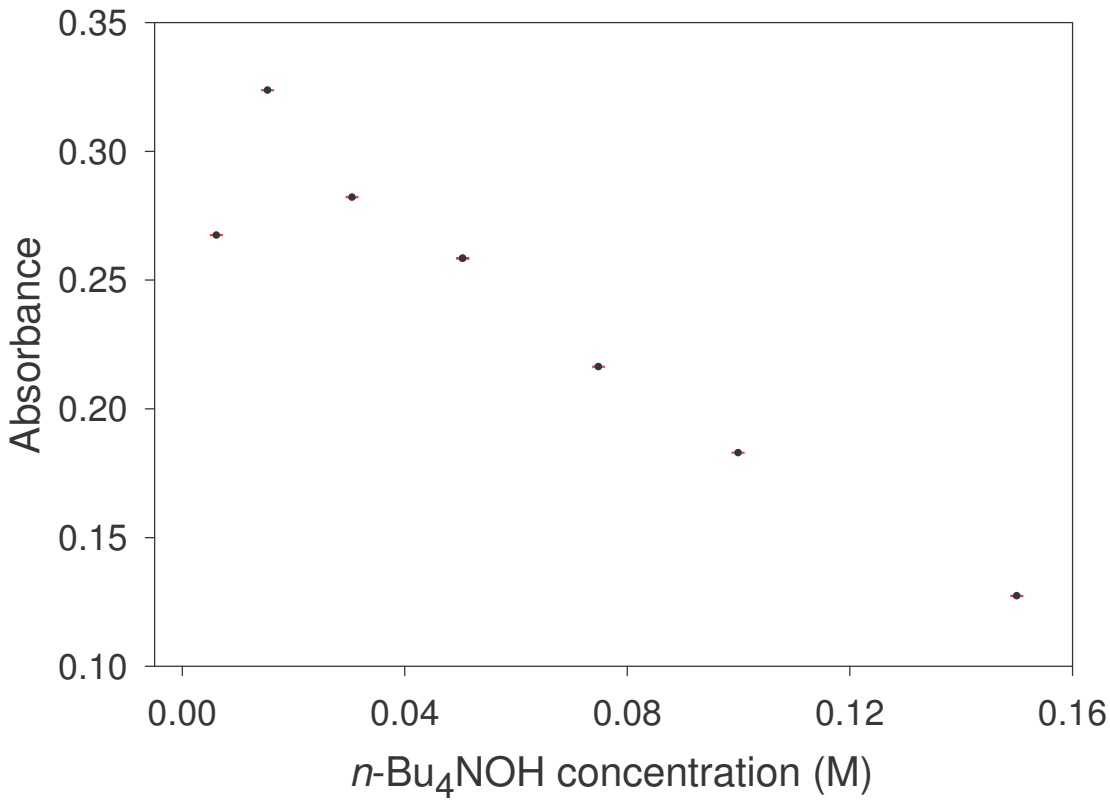

Figure 5.1. Absorbance of the colored products at 438 nm as a function of *n*-Bu_4NOH concentration.

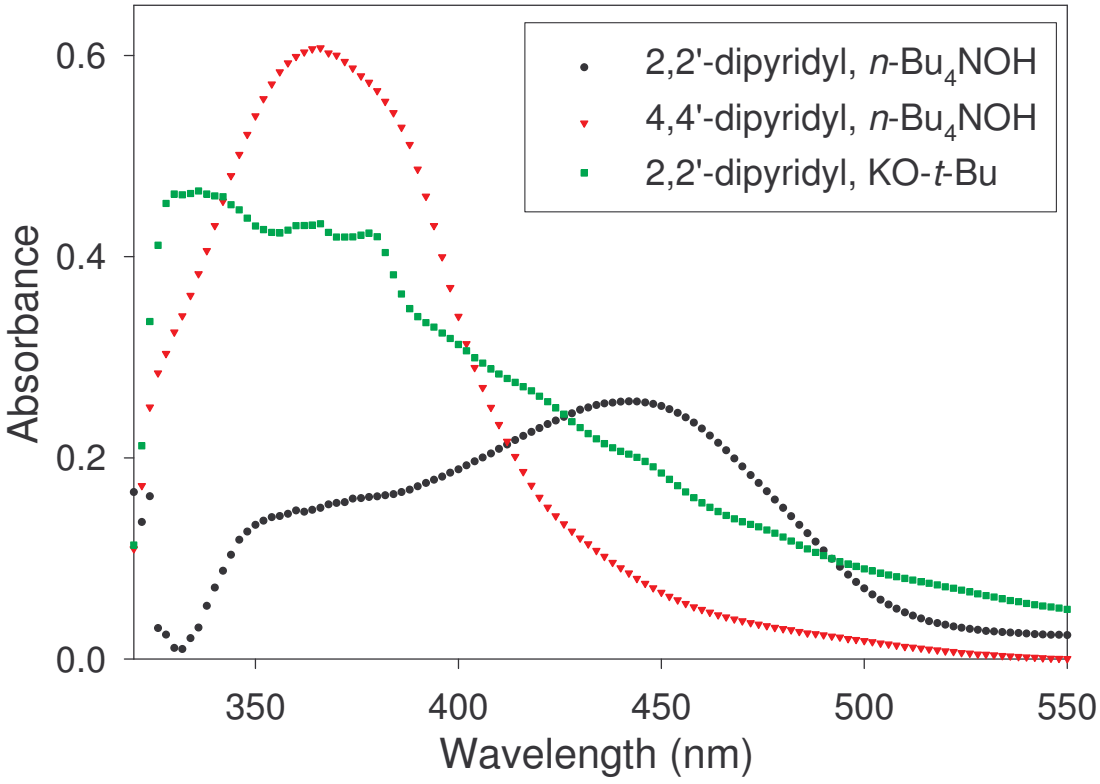

Figure 5.2. UV-visible spectra of the products from the Fujiwara reactions involving chloroform. (●) 18.54 mg/L $HCCl_3$ with 0.200 M 2,2′-dipyridyl and 0.050 M *n*-Bu_4NOH; (▼) 18.54 mg/L $HCCl_3$ with 0.200 M 4,4′-dipyridyl and 0.050 M *n*-Bu_4NOH; (■) 16.10 mg/L $HCCl_3$ with 0.200 M 2,2′-dipyridyl and 0.060 M KO-*t*-Bu.

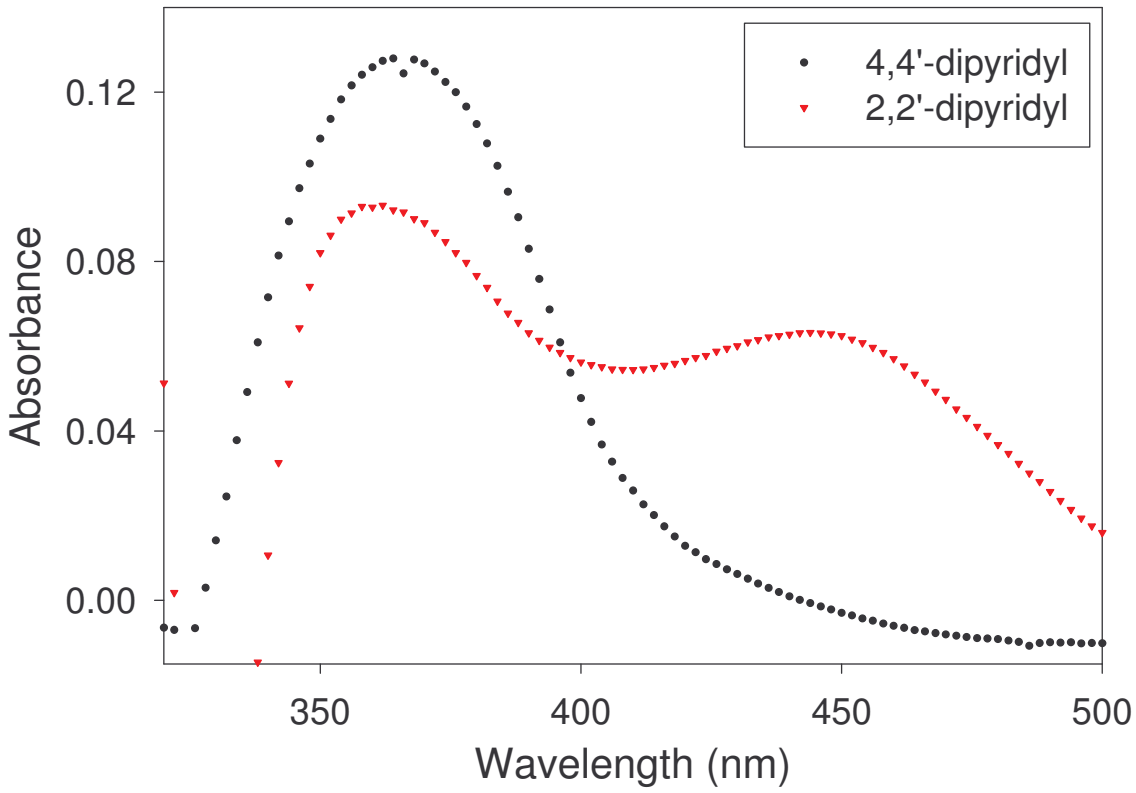

Figure 5.3. UV-vis spectra of the products from the Fujiwara reactions involving carbon tetrachloride. (▼) 27.78 mg/L CCl_4 with 0.200 M 2,2′-dipyridyl and 0.050 M *n*-Bu_4NOH; (●) 11.11 mg/L CCl_4 with 0.200 M 4,4′-dipyridyl and 0.050 M *n*-Bu_4NOH.

contain unknown solids, and were more difficult to handle than those involving 2,2′-dipyridyl. Thus our current studies were focused on the use of 2,2′-dipyridyl with limited tests conducted using 4,4′-dipyridyl for comparison.

Studies were also conducted using KO-*t*-Bu as the base in the Fujiwara reaction involving $HCCl_3$ and 2,2′-dipyridyl. This reaction involves no water, and thus allows for the detection of the halocarbons in systems sensitive to water. A large peak at 340 nm in the UV spectrum (Figure 5.2) was observed for the product(s) from the reaction.

Other experiments were conducted to determine the optimum concentration of 2,2′-dipyridyl in the current Fujiwara reactions. Standard solutions were prepared so that each contained 0.050 M *n*-Bu_4NOH and 20 mg/L $HCCl_3$ in THF. The concentration of 2,2′-dipyridyl was varied from 0.050 M, 0.075 M, 0.100 M, 0.125 M, 0.150 M, 0.175 M to 0.200 M. The highest absorbance and thus highest sensitivity were achieved with the solution containing 0.200 M 2,2′-dipyridyl (Figure 5.4). These seven points yield the following linear plot: $Absorbance$ (440 nm) = 0.02752 + 1.122 $C_{2,2'\text{-dipyridyl}}$ (R^2 = 0.99). Increasing the concentration of 2,2′-dipyridyl was limited by its solubility in THF.

5.3.2. Change of Absorbance at λ_{max} as a Function of Time

Color development was noticed immediately after the reagents were mixed in the Fujiwara reactions involving $HCCl_3$. In a study involving 20 mg/L

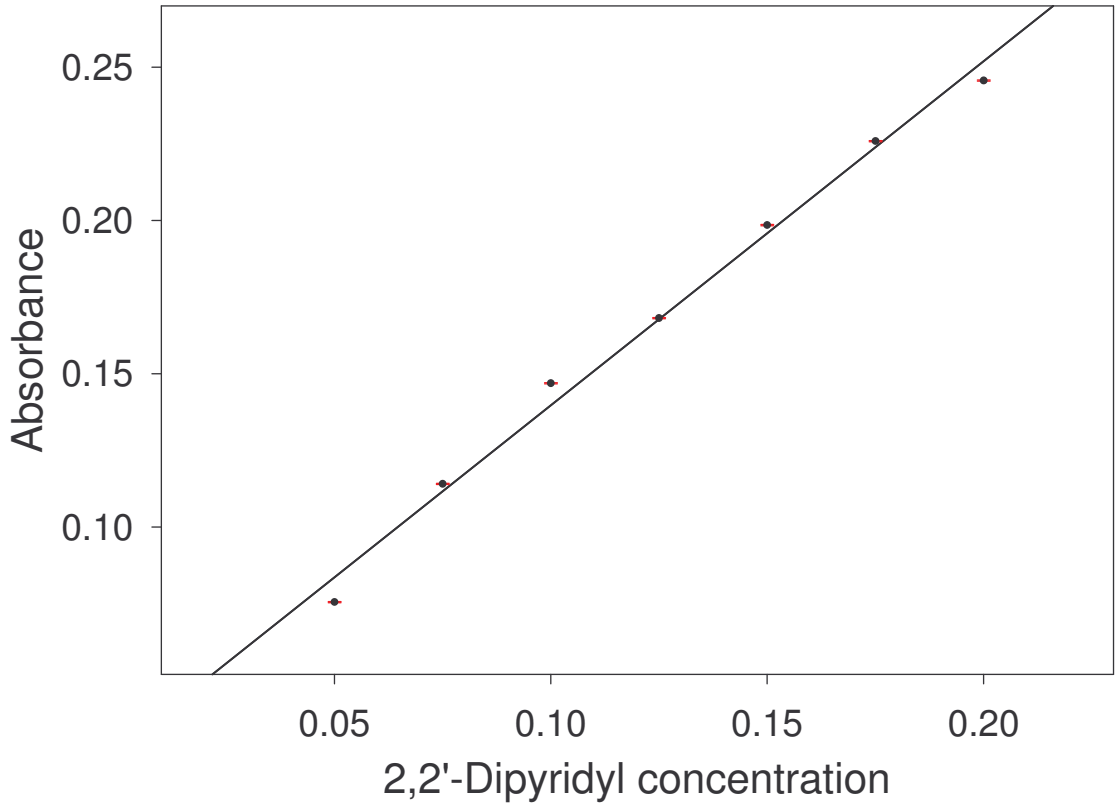

Figure 5.4. Absorbance of colored products at 440 nm as a function of 2,2′-dipyridyl concentration.

$CHCl_3$, 0.05 M *n*-Bu_4NOH and 0.200 M 2,2′- dipyridyl, the absorbance of the product at λ_{max} reached the maximum at time (*t*) = 10 min, and subsequently decreased linearly by the following equation: *Absorbance* = 0.162 – (2.72×10^4) *t* (min) (R^2 = 0.99; range of *t*: 10-60 min; spectrum recording interval: 1 min). A control study ruled out the photodecomposition of the colored products by the irradiation of the light source in the Hewlett-Packard 8452 photodiode array UV-visible spectrophotometer. It would thus be desirable to take the spectra of this Fujiwara reaction at 10 min after the reagents are mixed. We have found however that, for a typical test involving, e.g., 8 standards to establish the calibration plot, it usually takes 20 min to prepare the test solutions, and that recording the spectra of the 8 standards normally takes 20 min as well. We thus chose in the current studies to start recording the spectra of the test solutions at 30 min, so that the spectrum of each test solution was recorded approximately 30 min after the reagents were mixed. Such tests were found to give linear calibration plots of absorbance vs. $HCCl_3$ concentrations, as discussed below.

Color development was also noticed immediately after the reagents were mixed in the Fujiwara reactions involving CCl_4. However, unlike in the reaction involving $HCCl_3$, *no* change of the absorbance vs. time was observed. In a test involving 2.00 mg/L CCl_4, 0.015 M *n*-Bu_4NOH and 0.200 M 2,2′-dipyridyl, the absorbance of the product reached the maximum at *t* = 6 min, and did not change (range of *t*: 0-114 min; spectrum recording interval: 6 min). In the current studies, spectra of the product in the tests with CCl_4 were recorded 90 min after the reagents were mixed.

5.3.3. Test Solutions for $HCCl_3$ and CCl_4

5.3.3.1. Detection of $HCCl_3$ Using *n*-Bu_4NOH and 2,2′-Dipyridyl or 4,4′-Dipyridyl

In the detection of $HCCl_3$ using 0.015 M *n*-Bu_4NOH and 0.200 M 2,2′-dipyridyl in THF, $HCCl_3$ concentrations were tested in the range of 0.17-0.98 mg/L. Under these optimum concentrations of the reagents, a linear calibration plot ($R^2 > 0.99$) was observed using the UV-visible peak at 438 nm. The $HCCl_3$ detection limit was found to be 0.17 mg/L (Table 5.1). Additional tests were conducted using 0.050 M *n*-Bu_4NOH, 0.200 M 2,2′-dipyridyl in THF, and 0.23-18.54 mg/L $HCCl_3$. As shown in Figures 5.5 and 5.6, linear calibration plots ($R^2 > 0.99$) were prepared by plotting the absorbance at 444 nm and 364 nm vs. $HCCl_3$ concentration in this range when using 2,2′-dipyridyl and 4,4′-dipyridyl, respectively. The $HCCl_3$ detection limits in these tests were 0.23 mg/L for the tests using both 2,2′-dipyridyl and 4,4′-dipyridyl, and this concentration using 0.050 M *n*-Bu_4NOH was higher than the 0.17 mg/L detection limit when using 0.015 M *n*-Bu_4NOH.

5.3.3.2. Detection of $HCCl_3$ Using KO-*t*-Bu and 2,2′-Dipyridyl

In the studies using 0.200 M 2,2′-dipyridyl and KO-*t*-Bu (0.060 M) in THF, $HCCl_3$ concentrations were tested in the range of 4.00-40.00 mg/L. As shown in Figure 5.7, linear calibration plots ($R^2 > 0.99$) were thus prepared by plotting the

Table 5.1. Comparison of the $HCCl_3$ and CCl_4 detection limits using the modified Fujiwara reactions.

Analyte	Base	Pyridine Derivative	Detection Limit (mg/L)
$HCCl_3$	*n*-Bu_4NOH (0.015 M)	2,2′-dipyridyl (0.200 M)	0.172 ± 0.002
$HCCl_3$	KO-*t*-Bu (0.060 M)	2,2′-dipyridyl (0.200 M)	4.00 ± 0.09
CCl_4	*n*-Bu_4NOH (0.015 M)	2,2′-dipyridyl (0.200 M)	0.50 ± 0.02

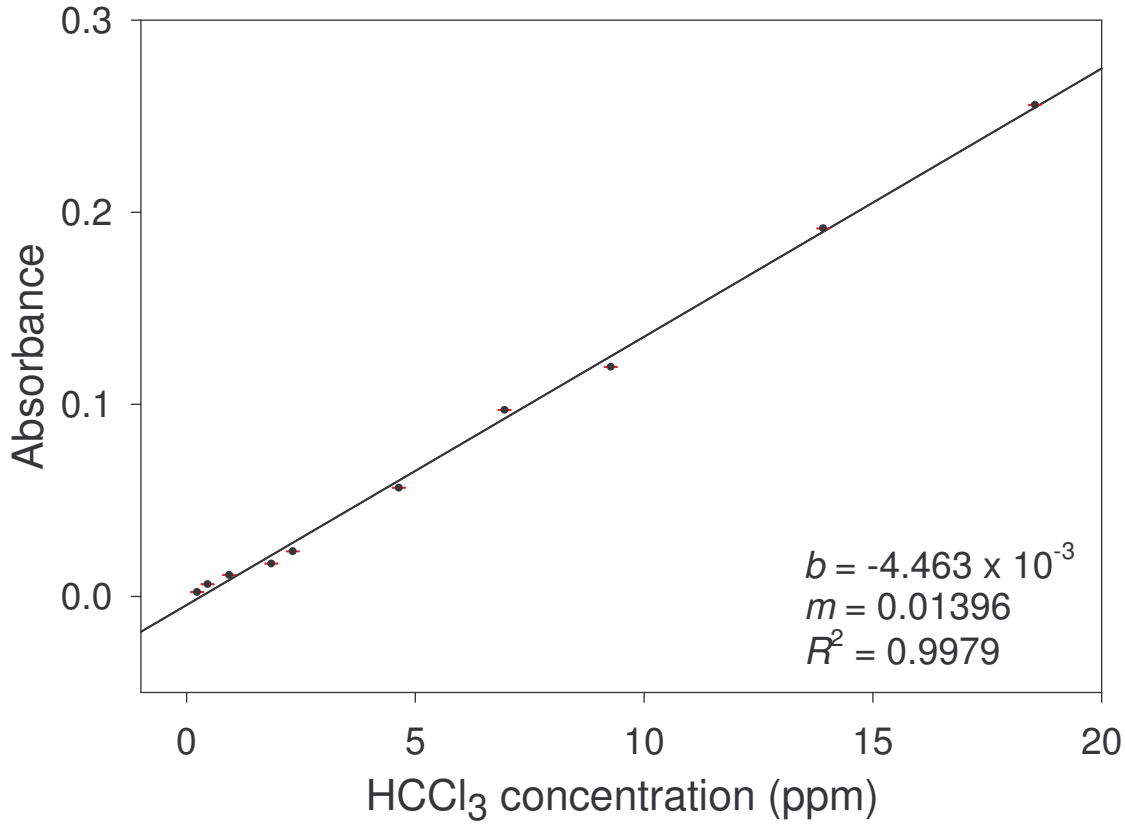

Figure 5.5. Calibration plot for the analysis of $HCCl_3$ by the modified Fujiwara reaction using 2,2′-dipyridyl and *n*-Bu_4NOH.

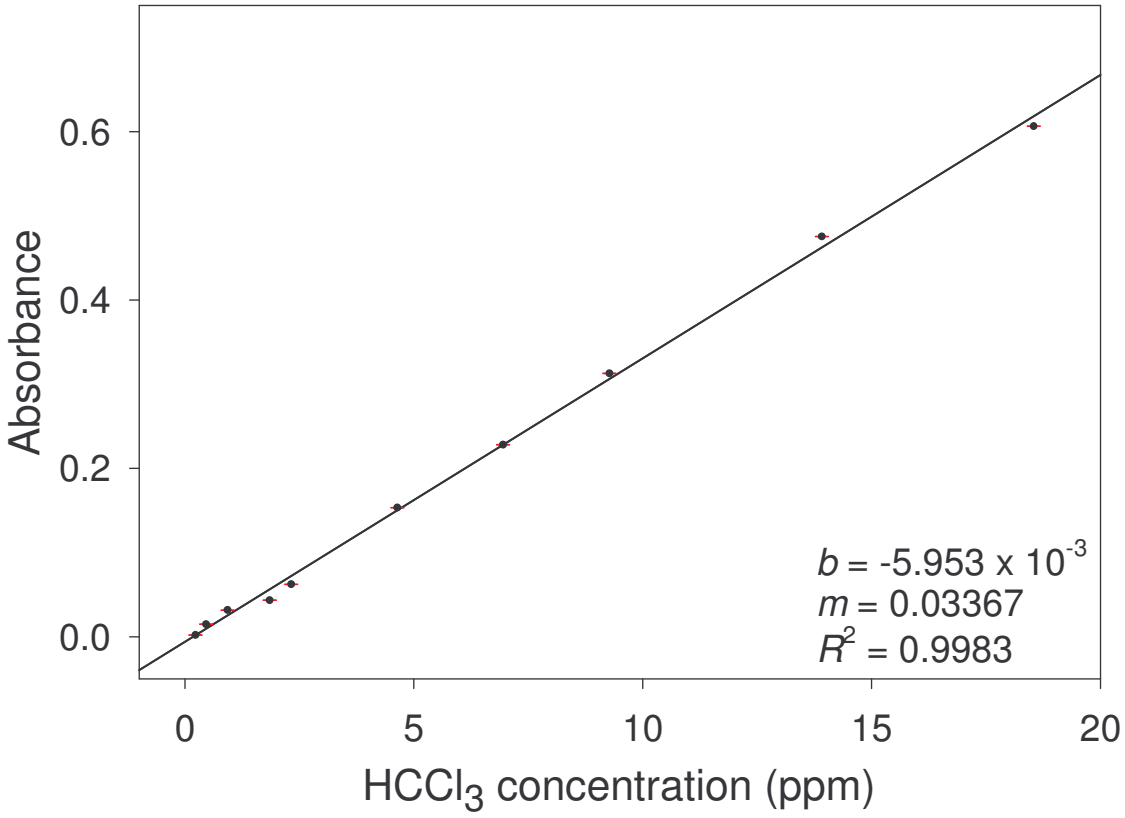

Figure 5.6. Calibration plot for the analysis of $HCCl_3$ by the modified Fujiwara reaction using 4,4′-dipyridyl and *n*-Bu_4NOH.

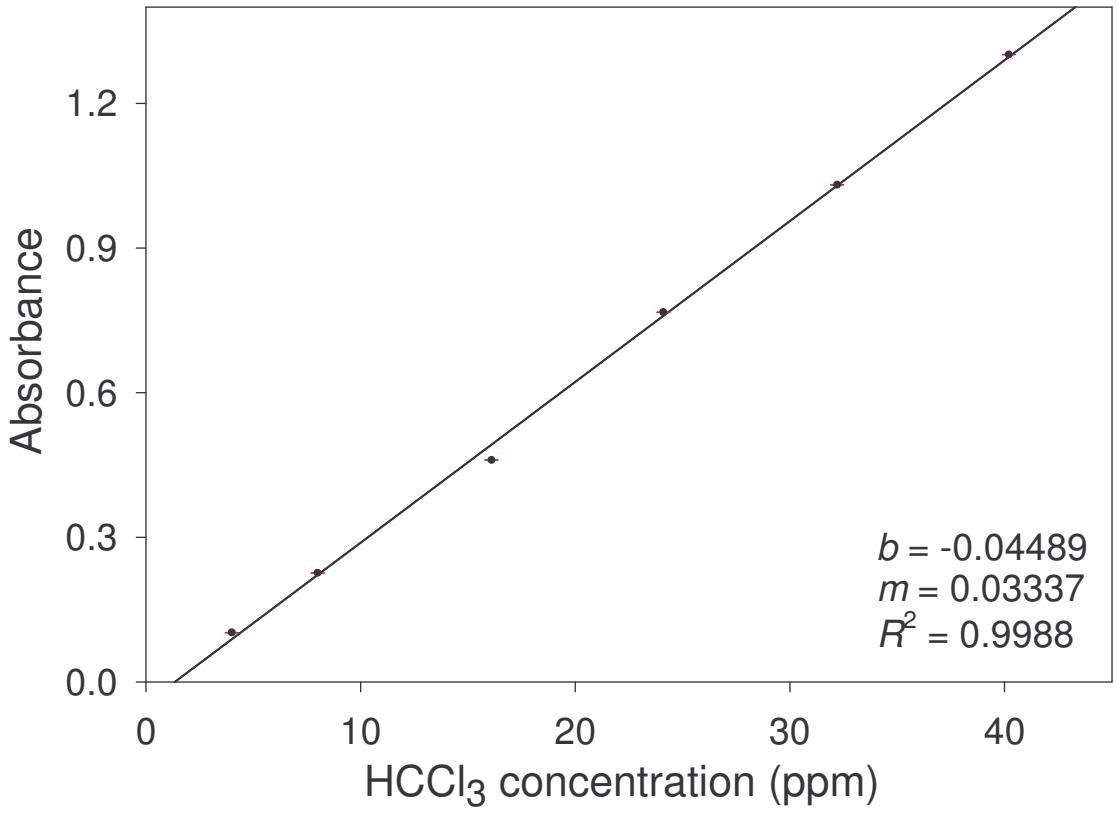

Figure 5.7. Calibration plot for the analysis of $HCCl_3$ by the modified Fujiwara reaction using 2,2′-dipyridyl and KO-*t*-Bu.

absorbance at 340 nm vs. $HCCl_3$ concentration in the range from 4.00-40.00 mg/L. The $HCCl_3$ detection limit by this method was found to be 4.00 mg/L (Table 5.1). It is noted that the reaction here was conducted in water-free solutions, and the procedure here allows the $HCCl_3$ detection in water-sensitive systems.

5.3.3.3. Detection of CCl_4 Using *n*-Bu_4NOH and 2,2′-Dipyridyl or 4,4′-Dipyridyl

In the detection of CCl_4 using 0.015 M *n*-Bu_4NOH and 0.200 M 2,2′-dipyridyl in THF, CCl_4 concentrations were tested in the range of 0.50-2.00 mg/L. A linear calibration plot ($R^2 > 0.99$) was observed using the UV-visible peak at 444 nm. The CCl_4 detection limit was found to be 0.50 mg/L (Table 5.1). Additional studies were conducted using 0.050 M *n*-Bu_4NOH, 0.200 M 2,2′-dipyridyl or 4,4′-dipyridyl in THF, and CCl_4 (concentration ranges of 1.39-27.78 mg/L and 11.11-55.55 mg/L for 2,2′-dipyridyl and 4,4′-dipyridyl, respectively). Linear calibration plots (Figures 5.8 and 5.9; $R^2 > 0.98$) were prepared by plotting the absorbance at 444 nm and 364 nm vs. CCl_4 concentration when using 2,2′-dipyridyl and 4,4′-dipyridyl, respectively. The detection limits were 0.50 and 11.11 mg/L for the tests involving 2,2′-dipyridyl and 4,4′-dipyridyl, respectively.

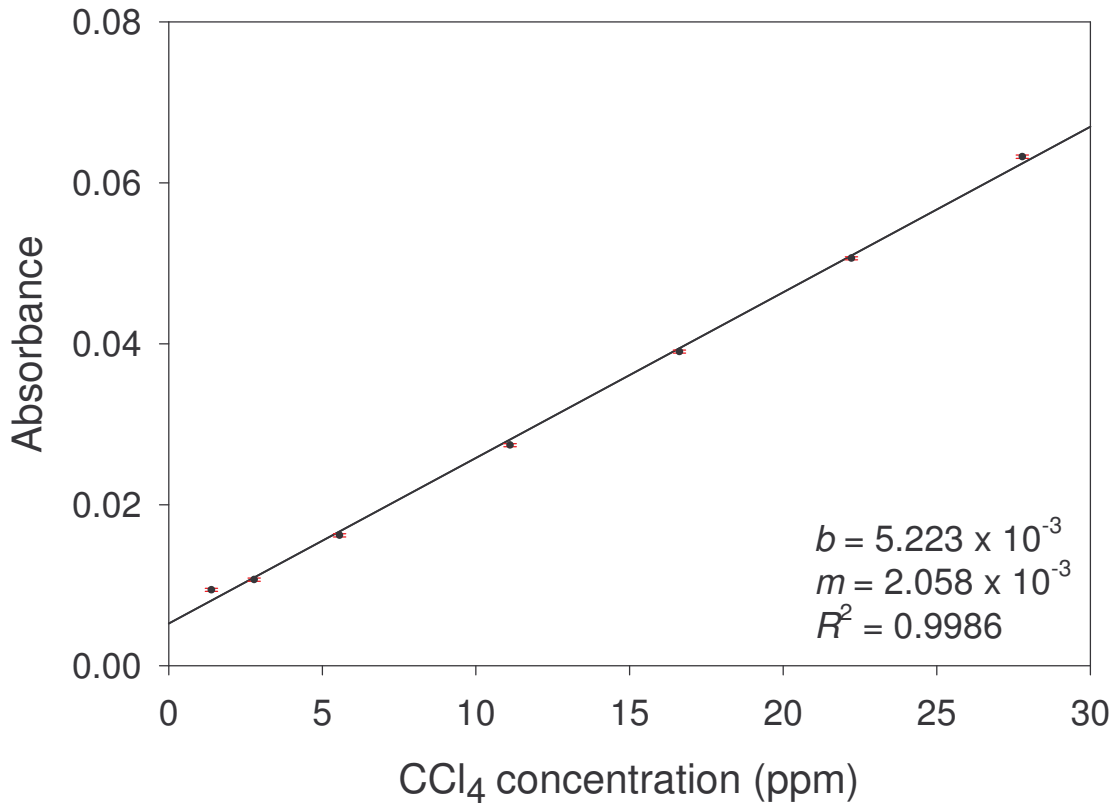

Figure 5.8. Calibration plot for the analysis of CCl_4 by the modified Fujiwara reaction using 2,2′-dipyridyl and *n*-Bu_4NOH.

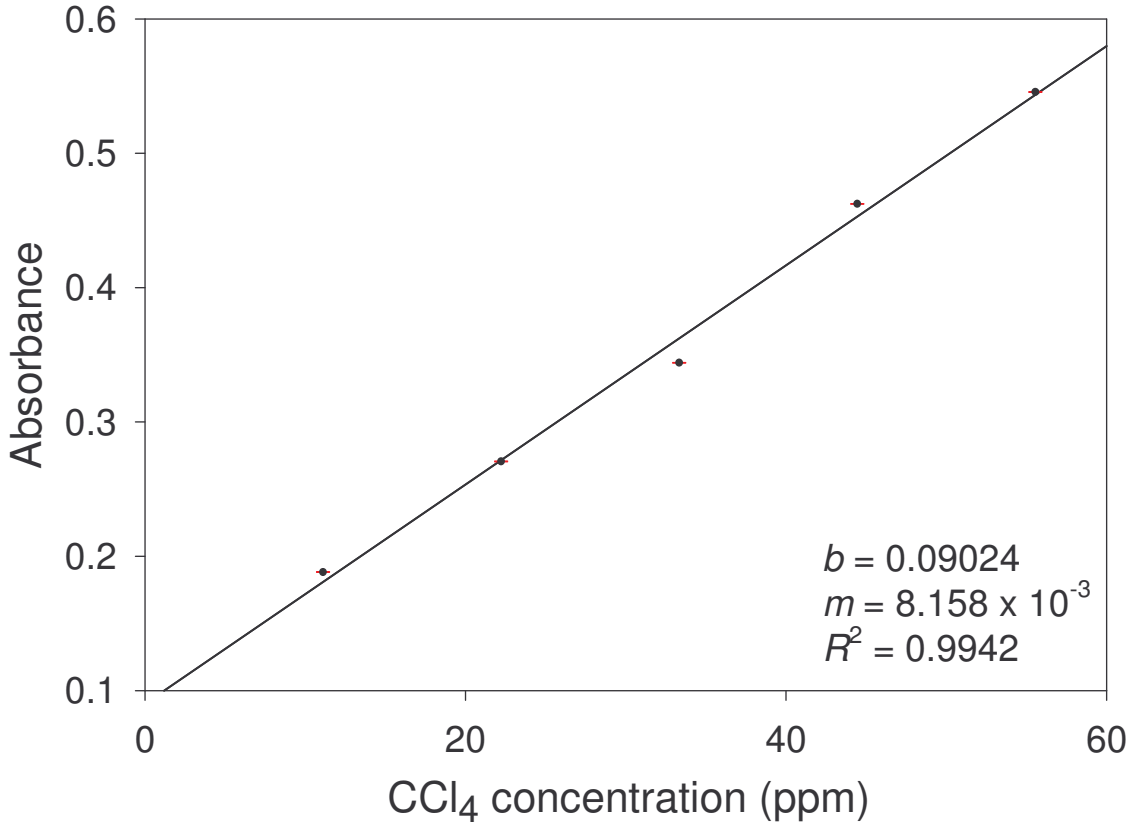

Figure 5.9. Calibration plot for the analysis of CCl_4 by the modified Fujiwara reaction using 4,4′-dipyridyl and *n*-Bu_4NOH.

5.3.4. A Comparison of the Current Modified Fujiwara Reactions with the Standard Fujiwara Reactions

There have been many reports outlining the use of pyridine with various bases for the Fujiwara reactions.[7-21] These reported methods have detection limits in the range of 1-100 mg/L and response times varying from 15 min to several hours. The dynamic range of these methods also varies, but is often on the order of 5-100 mg/L.

In comparison to these previously reported methods, the detection limit of chloroform with the current modified Fujiwara reactions is as low as 0.17 mg/L (Table 5.1). Calibration plots for the analysis of $HCCl_3$ using *n*-Bu_4NOH and 2,2′-dipyridyl were shown to be linear ($R^2 \geq 0.99$) in the range from 0.17-18.54 mg/L. In the analysis of $HCCl_3$ using 2,2′-dipyridyl and KO-*t*-Bu, calibration plots were shown to be linear ($R^2 > 0.99$) in the range of 2.00-40.2 mg/L with a detection limit of 2.00 mg/L. These comparisons show that our modifications to the original Fujiwara reaction yield at least comparable results to those obtained when conducting the Fujiwara reaction using liquid pyridine. In addition to the comparable analytical figures of merit, the current modified reactions have eliminated the use of an undesirable reagent, pyridine.

Chloroform was found to have a lower detection limit than carbon tetrachloride, perhaps because the proton in $HCCl_3$ is easier to remove to yield the CCl_3^- anion. In addition, aqueous base *n*-Bu_4NOH offers a better $HCCl_3$ detection limit than water-free KO-*t*-Bu (Table 5.1).

5.4. Concluding Remarks

The proposed methods for detection/quantification of chloroform and carbon tetrachloride replace toxic, offensive-smelling liquid pyridine and allow the Fujiwara reactions in a single phase. Such one-phase, modified Fujiwara reactions offer detection limits comparable to the traditional two-phase Fujiwara reactions, the only known reactions for detecting halocarbons spectrophotometrically in the visible region. Minimal instrumentation is required, and the proposed methods may thus lead to an analytical procedure that could be readily employed in laboratories or in field tests using portable UV-visible spectrometers.

Our ultimate objective is to employ a membrane (e.g., silastic membrane) that would separate the Fujiwara reagent and the aqueous sample, and allow vapors of halogenated hydrocarbons to permeate selectively into the Fujiwara reagents. The use of a membrane, however, prolongs the response time. It is one of the reasons for our use of halogenated hydrocarbons samples in aqueous *n*-Bu_4NOH and dipyridyl systems without exceeding the threshold for water. The samples that we are targeting for these modified Fujiwara reagents include halogenated hydrocarbons in the vapor phase, dissolved in water, soaked in soil or mud, and as dense non-aqueous phase liquid (DNAPL).

References

1. Holbrook, M. J. in *Kirk-Othmer Encyclopedia of Chemical Technology*, 5th Ed., Wiley, New York, Vol. 6, 2004, pp. 279-290.

2. Holbrook, M. J. in *Kirk-Othmer Encyclopedia of Chemical Technology*, 4th Ed., Wiley, New York, Vol. 5, 1993, pp. 1017-1072.

3. Ferguson, J. F.; Pietary, J. M. H. *Environ. Pollut*. **2000**, *107*, 209.

4. McCulloch, A. *Chemosphere* **2003**, *50*, 1291.

5. Cardinali, F. L.; Ashley, D. L.; Morrow, J. C.; Moll, D. M.; Blount, B. C. *J. Chromatogr. Sci.* **2004**, *42*, 200.

6. Carpi, M.; Zufall, C. *LCGC N. Am*. **2003**, *21*, 60.

7. Fujiwara, K. *Sitz. Nat. Ges. Rostock* **1916**, *6*, 33.

8. Henshaw, J. M.; Burgess, L. W.; Booksh, K. S.; Kowalski, B. R. *Anal. Chem*. **1994**, *66*, 3328.

9. Tauler, R.; Smilde, A. K.; Henshaw, J. M.; Burgess, L. W.; Kowalski, B. R. *Anal. Chem*. **1994**, *66*, 3337.

10. Smilde, A. K.; Tauler, R.; Henshaw, J. M.; Burgess, L. W.; Kowalski, B. R. *Anal. Chem*. **1994**, *66*, 3345.

11. Anderson, W. G.; Anderson, J. S. US Patent No. 4,929,562, **1990**.

12. Milanovich, F. P.; Brown, S. B.; Colston, B. W.; Daley, P. F.; Langry, K. C. *Talanta* **1994**, *41*, 2189.

13. Goswami, K.; Dandge, D. K.; Klainer, S. M.; Ejiofor, C. H. US Patent No. 5,358,875, **1994**.

14. Klainer, S. M.; Butler, M. S. International Patent No. WO 9304368, **1993**.

15. Shivhare, P.; Gupta, V. K. *Fresenius' J. Anal. Chem*. **1992**, *343*, 612.

16. Bhattacharjee, M.; Cherian, L.; Gupta, V. K. *Microchem. J*. **1991**, *43*, 109.

17. Mantel, M.; Nothmann, R. *Analyst* **1977**, *102*, 672.

18. Mantel, M.; Molco, M.; Stiller, M. *Anal. Chem*. **1963**, *35*, 1737.

19. Reith, J. F.; Van Ditmarsch, W. C.; De Ruiter, T. *Analyst* **1974**, *99*, 652.

20. Lugg, G. A. *Anal. Chem*. **1966**, *38*, 1532.

21. Leibman, K. C.; Hindman, J. D. *Anal. Chem*. **1964**, *36*, 348.

22. The health rating for pyridine in the Materials Safety Data Sheet: 3-Severe (Life). http://www.jtbaker.com/msds/englishhtml/P7456.htm

23. *Toxicological Profile for Pyridine*, Agency for Toxic Substances and Disease Registry, U.S. Public Health Service, 1992. http://www.atsdr.cdc.gov/toxprofiles/tp52.pdf.

24. *The Safe Drinking Water and Toxic Enforcement Act of 1986*, The Office of Environmental Health Hazard Assessment of the California Environmental Protection Agency. http://www.oehha.ca.gov/prop65/out_of_date/51702notice.html

25. The health rating for THF in the Materials Safety Data Sheet: 2-Moderate (Life). http://www.jtbaker.com/msds/englishhtml/t1222.htm

26. Graves, B. B.; Vincent Jr., B. F. *Chem. Ind*. (London) **1962**, 2137.

27. Uno, T.; Okumura, K.; Kuroda, Y. *J. Org. Chem*. **1981**, *46*, 3175.

28. Kofron, W. G.; Kirby, F. B.; Hauser C. R. *J. Org. Chem*. **1963**, *28*, 873.

29. Hine, J. *J. Am. Chem. Soc*. **1950**, *72*, 2438.

Part 6

Development of a Controlled-Release Polymer for Delivery of Dipyridyls and a Tetraalkyl Ammonium Hydroxide

6.1. Introduction

Controlled-release polymers (CRPs) have been intensively investigated for the delivery of various drugs, reagents, and biological species.[1-7] Many different polymers including poly(vinyl alcohol), poly(ethylene-vinyl acetate), poly(ethylene), and poly(propylene) have been used for controlled release delivery.[1] Some CRPs have demonstrated the ability to deliver reagents at a constant rate over long periods of time.[2-5] Several attributes including ease of synthesis, lack of chemical reactivity, cost effectiveness, and consistent delivery of reagents make CRPs very attractive for delivery of reagents.

We have been interested in the delivery of 2,2′-dipyridyl (or 4,4′-dipyridyl) and tetra-*n*-butylammonium hydroxide (*n*-Bu_4NOH) using controlled-release polymers (CRPs). As reported in Part 5 of this dissertation, these chemicals are reagents for the detection and quantification of HHCs by the modified Fujiwara reactions, and they need to be replenished for continuous monitoring of HHCs. Studies have been conducted to replenish these reagents by a pump.[8] This dissertation part will discuss our recent studies to develop CRP monoliths of poly(vinyl alcohol) (PVA) for the delivery of 2,2′-dipyridyl, 4,4′-dipyridyl and *n*-Bu_4NOH.

6.2. Experimental

6.2.1. Reagents

Poly(vinyl alcohol) (Scientific Polymer Products, 99% hydrolyzed, MW 86,000), tetrahydrofuran (THF) (Fisher, certified), 2,2′-dipyridyl (Acros, 99+%), 4,4′-dipyridyl (Acros, 98%), and tetra-*n*-butylammonium hydroxide (*n*-Bu_4NOH) (Lancaster, 40 w/w% aqueous solution) were used as received. Deionized water was used in the preparation of all PVA gels.

6.2.2. Instrumentation

A Hewlett-Packard 8452 photodiode array UV-visible spectrophotometer was used in the current studies. All blank and sample spectra were collected in standard 1.0 cm quartz cuvettes.

6.2.3. Synthesis of the PVA Monolith and Incorporation of Reagents

The method used to make the PVA monolith (Figure 6.1) is similar to that reported in the literature.[3] Monoliths of various sizes were made using a 15 w/w% solution of PVA beads in deionized water contained in a 50-mL polyethylene vial. The vial containing the PVA beads and water was placed into a 90 ℃ water bath for six hours. Afterwards the contents of the vial were in the form of a viscous liquid. The vial was then removed from the water bath, and the mixture in the vial was stirred using a glass stirring rod. The viscous PVA solution was then loaded with up to 6.3 w/w% of 2,2′-dipyridyl, or 2.5 w/w% of

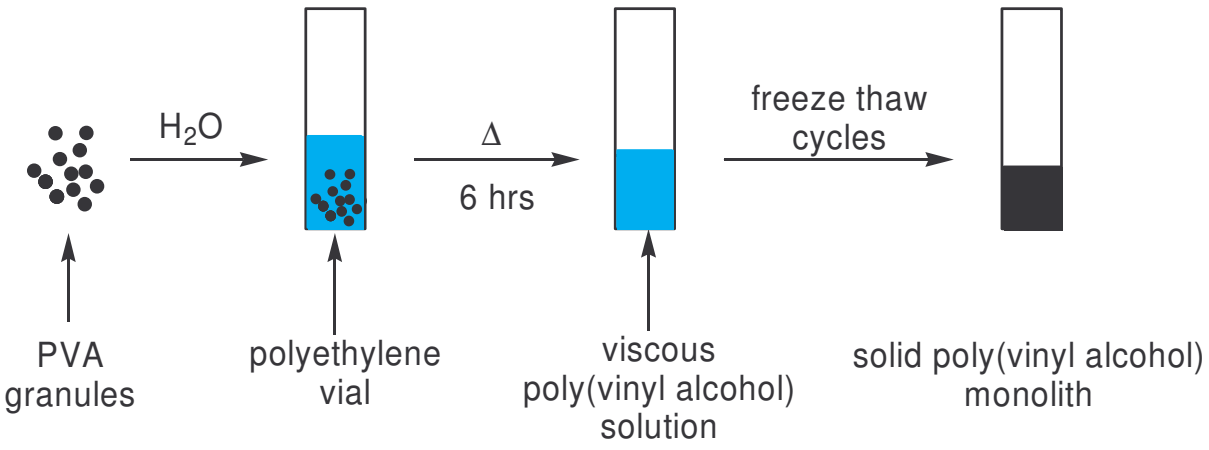

Figure 6.1. Schematic of the procedure used in the preparation of the PVA monoliths.

4,4′-dipyridyl, or 9.9 w/w% of *n*-Bu_4NOH, and stirred thoroughly to give a homogeneous reagent/PVA mixture. The vial was then reinserted into the 90 °C water bath for 15 min so that any bubbles trapped in the molten polymer could escape.

After the vials containing the polymer were removed from the water bath and allowed to slowly cool to room temperature for one hour, the gels were placed into a –20 °C freezer for 18 hours. The vials containing the gels were then removed from the freezer and allowed to thaw to 25 °C for 6 hours. This freeze-thaw cycle was repeated for a total of five times. At the conclusion of the freeze-thaw process, mechanically stable, reagent-loaded PVA monoliths were obtained (Figure 6.2).

6.2.4. Controlled-Release Experimental Design

Experiments were conducted in which the release of a reagent from a PVA monolith was monitored as a function of time. Tetrahydrofuran was chosen as the solvent for the release experiments due to its earlier use with modified Fujiwara reactions. A reagent-loaded PVA monolith was immersed in THF contained in a sealed Florence flask maintained at 25 °C (Figure 6.3). As a control, a monolith containing *no* reagents was immersed in the same volume of THF in a separate sealed Florence flask. Samples of a precisely measured volume were periodically removed from each flask by micropipette and replaced with fresh solvent thus maintaining perfect sink conditions. The samples were placed into separate 10-mL volumetric flasks and sealed so that the THF and

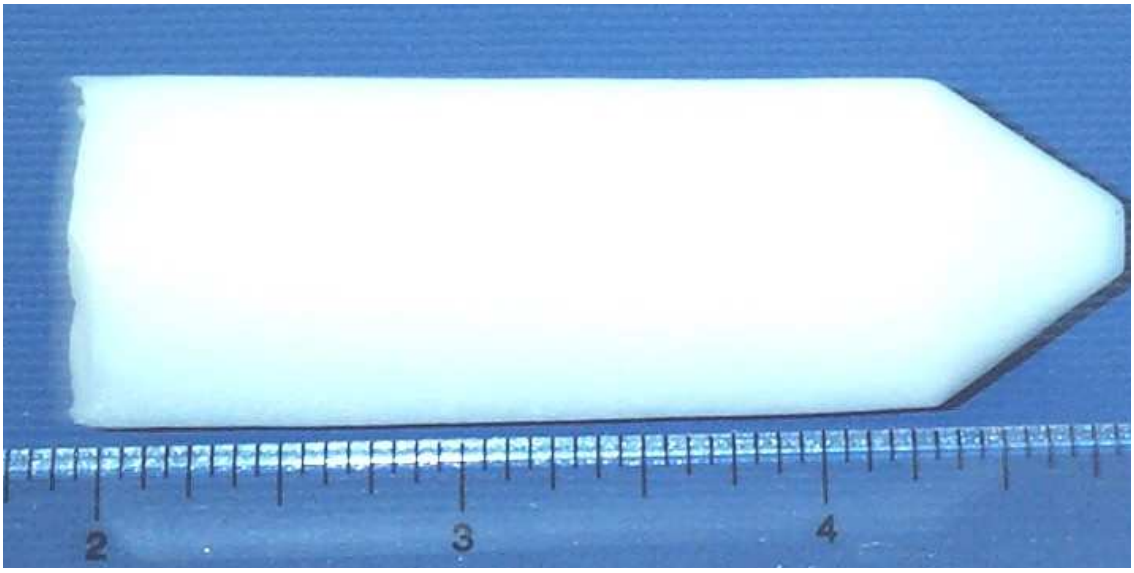

Figure 6.2. Image of a PVA monolith used in the current studies, units on scale are in inches.

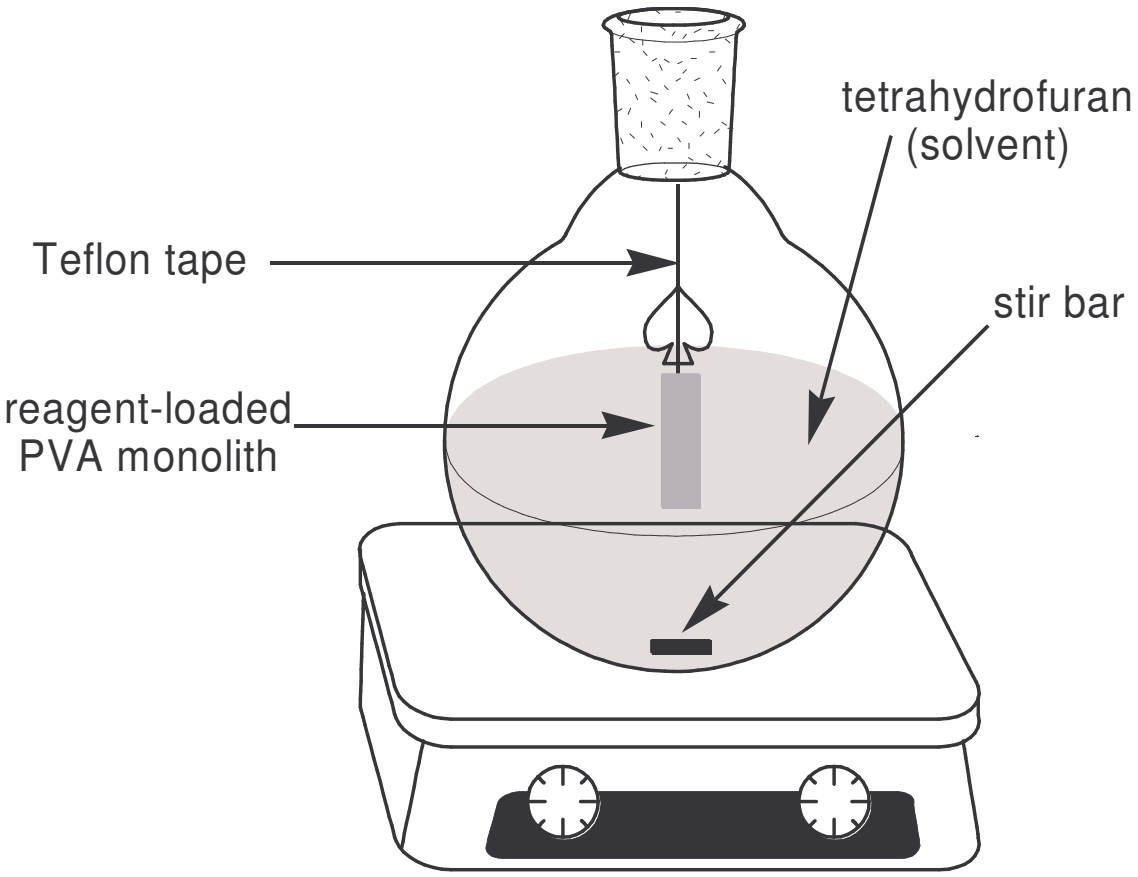

Figure 6.3. Schematic of the experimental setup used in the diffusion experiments with the PVA monoliths.

reagents could not evaporate. At the conclusion of the release study, all samples were diluted to the mark with THF. UV-visible spectra of all samples were collected in sequence to minimize the errors due to spectrometer drift. The UV-visible spectrum from each control sample was collected and stored as the reference for each corresponding reagent sample.

Estimation of errors in the analysis is given in Appendix E.

6.3. Results and Discussion

6.3.1. Factors Affecting the Mechanical Strength of the PVA Monoliths

It is well known that aqueous solutions of PVA gradually gel and exhibit a small increase in elasticity upon standing at room temperature.[9] The gelation of aqueous solutions of PVA through freeze-thaw cycles results in the formation of a viscoelastic polymer with increased mechanical strength compared to those not freeze-thaw processed. These polymers have been shown to exhibit very high elasticity, often stretching to 5-6 times their original size.[3,9-11]

During the freeze-thaw processing of PVA, small domains of crystalline polymer are formed.[10-15] These crystalline domains act as physical crosslinks between polymer chains.[3,9,11,12] As the number of freeze-thaw cycles is increased, the fraction of polymer in the crystalline domain increases, as does the mechanical strength of the polymer. The viscoelasticity of these polymers arises from polymer chains which are physically crosslinked connected by amorphous chain segments.[3,9,11,12] Many investigations into the morphology of

these polymers have been conducted using small angle neutron scattering (SANS),[12,15] X-ray diffraction (XRD),[10,15] and differential scanning calorimetry (DSC).[3,10,11]

Other factors such as the molecular weight of the polymer, percentage of polymer in the initial polymer-water solution, and freezing temperature have also been shown to contribute to the physical properties of the polymer monolith.[3,9-11] Studies have shown that the fraction of polymer in the crystalline domain was increased when PVA with increasing molecular weights was used in the monolith synthesis.[3,11] Increasing the percentage of polymer in the initial PVA-water solution was also shown to increase the mechanical strength of the polymer monolith.[11]

Due to the wealth of knowledge currently available regarding the morphology and mechanical properties of freeze-thawed PVA gels, none of these properties were investigated in the current studies. The mechanical properties of PVA monoliths produced by the current procedure were found to be adequate for the current application. Our current research has rather focused on development of a method for incorporating specific reagents into the PVA monoliths and monitoring the release characteristics of the reagents in a THF solution.

6.3.1.1. Effect of Reagent Loading on Mechanical Strength

Upon loading the PVA monoliths with reagent, changes in the physical and mechanical properties of the monoliths were expected to occur. The addition of reagents was expected to possibly retard the growth of the crystalline

domain, thus disrupting the physical crosslinks between polymer chains. This could lead to decreased mechanical strength. However, upon loading reagents according to the procedure in Section 6.2.3, no change in physical or mechanical properties was observed in the PVA monoliths.

6.3.2. Solubility of the PVA Monolith in THF

One goal of this project is the release of reagents into THF solution without dissolution of the PVA monolith. Literature data indicate that PVA is insoluble in THF.[16] PVA monoliths exposed to THF solution for long periods of time appeared to be completely insoluble in THF. In order to verify this observation, a PVA monolith was immersed in THF for one week. After one week, UV-visible spectra of the THF solution exposed to the PVA monolith and that of pure THF were collected. A comparison of the two spectra showed very little variation, indicating that there is indeed very little or no dissolution of the PVA monolith in THF.

6.3.3. Loading of the Reagents

Several methods of loading reagents into the PVA monoliths were tested. Methods investigated include addition of the reagent before and at various points during the initial heating of the PVA beads. Addition of *n*-Bu_4NOH before and during the heating process often resulted in chemical reactions of *n*-Bu_4NOH with PVA. Unlike addition of *n*-Bu_4NOH, incorporation of 2,2′-dipyridyl or 4,4′-dipyridyl in the early stages of the heating process resulted in no observable chemical

reaction between the dipyridyl and PVA. Addition of all reagents near the conclusion of the heating process resulted in no observable chemical reaction between the reagents and PVA. Reagents were therefore added near the conclusion of the heating process to avoid chemical reaction with PVA.

6.3.4. Controlled-Release Studies

PVA monoliths were loaded with either 2,2′-dipyridyl, 4,4′-dipyridyl, or *n*-Bu_4NOH. The diffusion properties of these reagents from the monoliths were tested by the method described in Part 6.2.4. In order to have a useful CRP, it is necessary that the concentration of reagents released into solution from the CRP monolith reach a constant value. In order to measure the rate at which the release of reagents occurs from these monoliths, the absorbance at λ_{max} in the UV-visible spectra of each specific reagent was monitored as a function of time that the reagent-loaded PVA monolith was immersed in THF.

6.3.4.1. Controlled-Release of 2,2′-Dipyridyl from a PVA Monolith

A control-release study using a PVA monolith loaded with 2,2′-dipyridyl was conducted by the method described in Part 6.2.4. The PVA monolith used in the current study (2.0243 g of PVA + 11.5 g H_2O) was loaded with 0.2525 g of 2,2′-dipyridyl according to the procedure in Part 6.2.3. The 2,2′-dipyridyl-loaded PVA monolith was immersed in 1000 mL of pure THF in a sealed flask. In order to quantify the release characteristics of the reagent-loaded PVA monolith, the

concentration of 2,2′-dipyridyl in the THF solution, calculated using Beer's law,[17] was monitored as a function of time.

As shown in Figure 6.4, the early stages of the study show rapid diffusion of 2,2′-dipyridyl from the PVA monolith. The rapid increase in concentration is likely due to the rapid diffusion of the 2,2′-dipyridyl molecules near the surface of the monolith. As the length of the study increases, the concentration of 2,2′-dipyridyl reaches a constant value with little change.

A study of the amount of 2,2′-dipyridyl released from a PVA monolith revealed that (93 ± 4)% of 2,2′-dipyridyl that had been loaded in the monolith was released into the solution. Details of the studies are provided in Appendix E.

In order to provide evidence that no chemical change has taken place in 2,2′-dipyridyl that had been previously loaded into the PVA monolith, a UV-visible spectroscopic study was conducted. The spectra of a freshly prepared solution of 2,2′-dipyridyl dissolved in THF was compared to the spectra of 2,2′-dipyridyl released into THF from a diffusion study. As shown in Figure 6.5, these spectra match very closely, thus indicating that there is no chemical change of 2,2′-dipyridyl during the control-release process.

6.3.4.2. Controlled-Release of 4,4′-Dipyridyl from a PVA Monolith

A control-release study using a PVA monolith loaded with 4,4′-dipyridyl was conducted by the method described in Section 6.2.4. The PVA monolith used in the current study (6.0014 g PVA + 34.0 g H_2O) was loaded with 0.9999 g

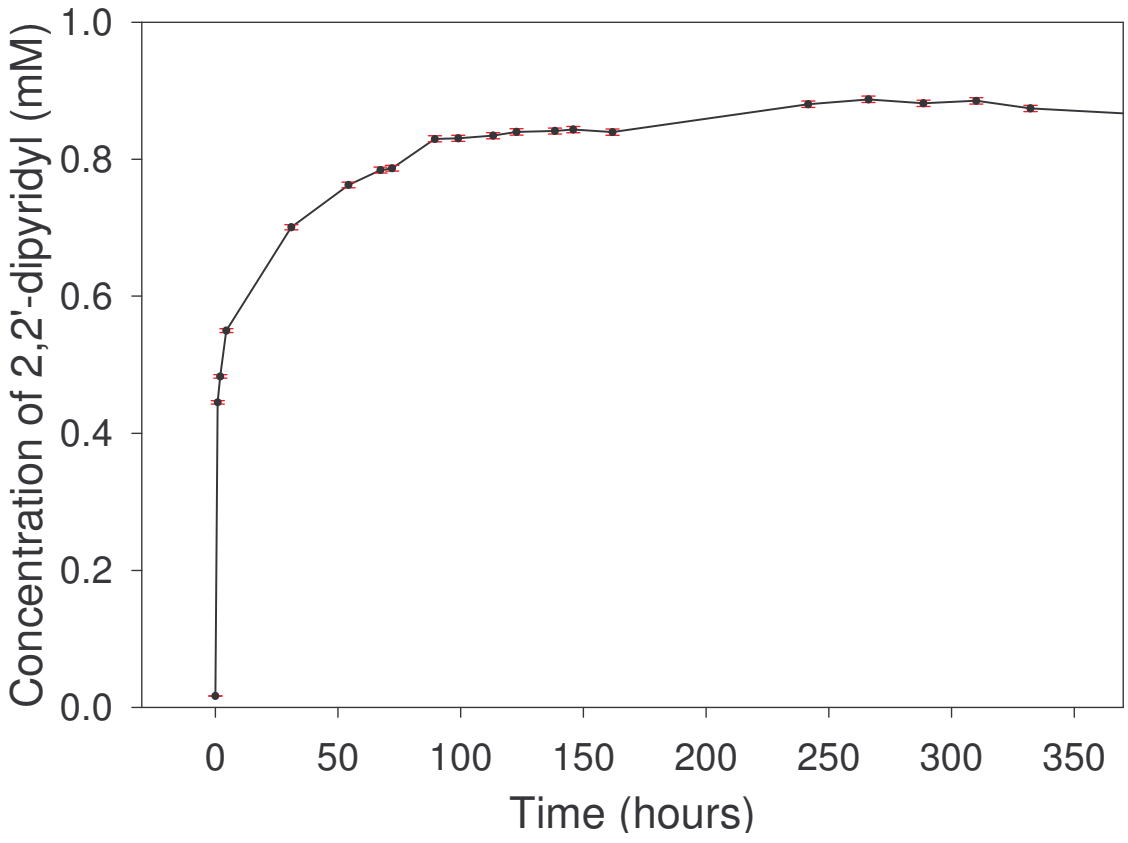

Figure 6.4. Concentration of 2,2′-dipyridyl in a THF solution during the release of 2,2′-dipyridyl from a PVA monolith.

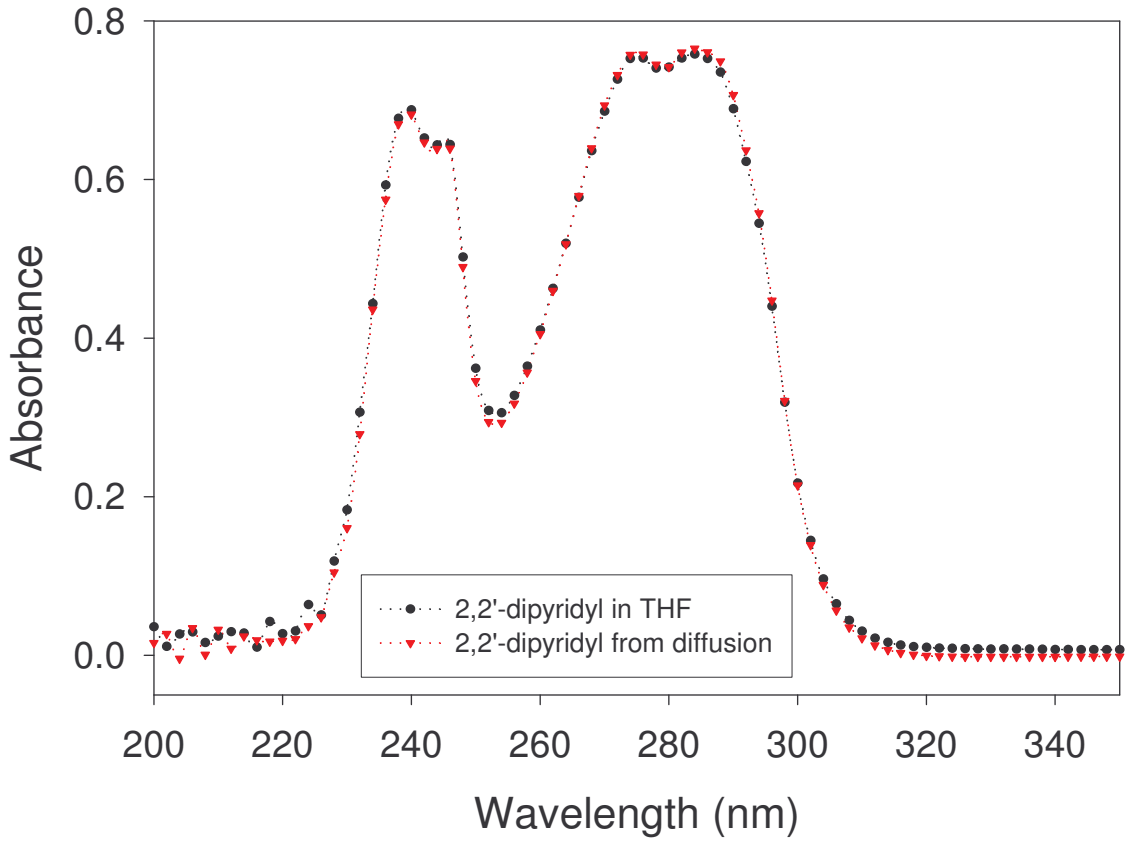

Figure 6.5. A comparison of the UV-visible spectrum of a freshly-prepared solution of 2,2′-dipyridyl dissolved in THF (●) with that of a solution of 2,2′-dipyridyl released into THF from a PVA monolith (▼).

of 4,4′-dipyridyl according to the procedure in Section 6.2.3. The 4,4′-dipyridyl-loaded PVA monolith was immersed in 100 mL of THF in a sealed flask. The concentration of 4,4′-dipyridyl in the THF solution, calculated using Beer's law,[17] was monitored as a function of time.

As shown in Figure 6.6, the early stages of the study show rapid diffusion of 4,4′-dipyridyl from the PVA monolith. The rapid increase in concentration is likely due to the rapid diffusion of the 4,4′-dipyridyl molecules near the surface of the monolith. As the length of the study increases, the 4,4′-dipyridyl concentration reaches a constant value with little change.

A study of the amount of 4,4′-dipyridyl released from a PVA monolith revealed that (6.7 ± 0.3)% of 4,4′-dipyridyl that had been loaded in the monolith was released into the solution, reaching a concentration of ca. 3.5 mM (for a 100-mL solution). In comparison, the end concentration of the diffusion studies involving 2,2′-dipyridyl was ca. 0.85 mM (for a 1000-mL solution). Perhaps the solution in the 4,4′-dipyridyl studies was so concentrated that the diffusion of 4,4′-dipyridyl into and out of the monolith had reached an equilibrium, thus reducing the percentage of 4,4′-dipyridyl released from the monolith. Details of the studies are provided in Appendix E.

In order to provide evidence that 4,4′-dipyridyl did not undergo chemical change in the loading and controlled-release process, a UV-visible experiment was conducted. The spectra of a freshly prepared solution of 4,4′-dipyridyl

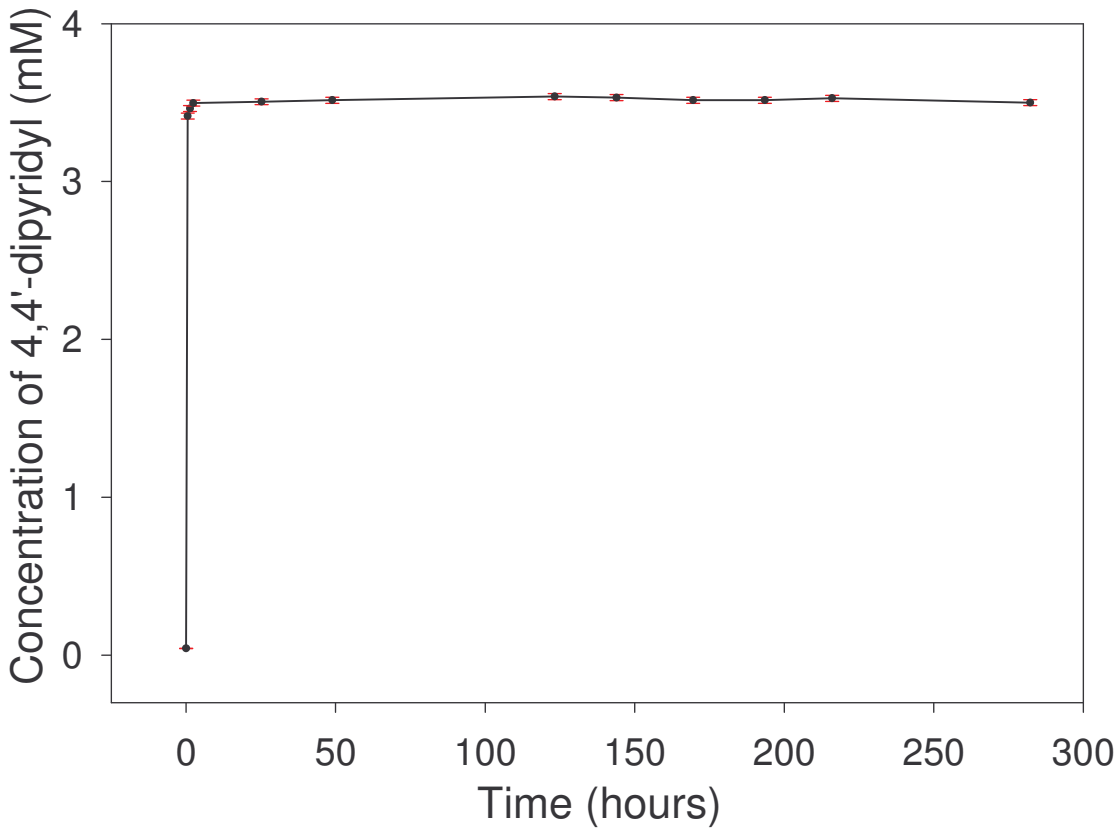

Figure 6.6. Concentration of 4,4′-dipyridyl in a THF solution resulting from the release of 4,4′-dipyridyl from a PVA monolith.

dissolved in THF was compared to the spectra of 4,4′-dipyridyl release into THF from a diffusion study. As shown in Figure 6.7, these spectra match very closely, thus indicating that there is likely no chemical change.

6.3.4.3. Controlled-Release of *n*-Bu_4NOH from a PVA Monolith

A control-release study using a PVA monolith loaded with *n*-Bu_4NOH was conducted by the method described in Part 6.2.4. The PVA monolith used in the current study (2.6497 g PVA + 13.0 g H_2O) was loaded with 2.000 g of 40 w/w% aqueous *n*-Bu_4NOH according to the procedure in Part 6.2.3. The *n*-Bu_4NOH-loaded PVA monolith was immersed in 100 mL of THF in a sealed flask. The concentration of *n*-Bu_4NOH in the THF solution, calculated using Beer's law,[17] was monitored as a function of time.

As shown in Figure 6.8, the early stages of the study show a slower diffusion of *n*-Bu_4NOH from the PVA monolith compared to those previously discussed in Parts 6.3.4.1 and 6.3.4.2. The increase in concentration later in the experiment also proceeded at a slower rate than in the previous two studies of the 2,2′- and 4,4′-dipyridyl release from PVA monoliths. Repetitions of this experiment showed similar data to those in Figure 6.8. Multiple factors are suspected to hinder the diffusion of the *n*-Bu_4NOH from the PVA monolith. *n*-Bu_4NOH may form hydrogen bonds with the –OH groups in the PVA monolith, making it difficult to release it from PVA monoliths. With *n*-Bu_4NOH being ionic, it may also dissociate into cation/anion, which could contribute to slower diffusion of the *n*-Bu_4NOH from the PVA monolith.

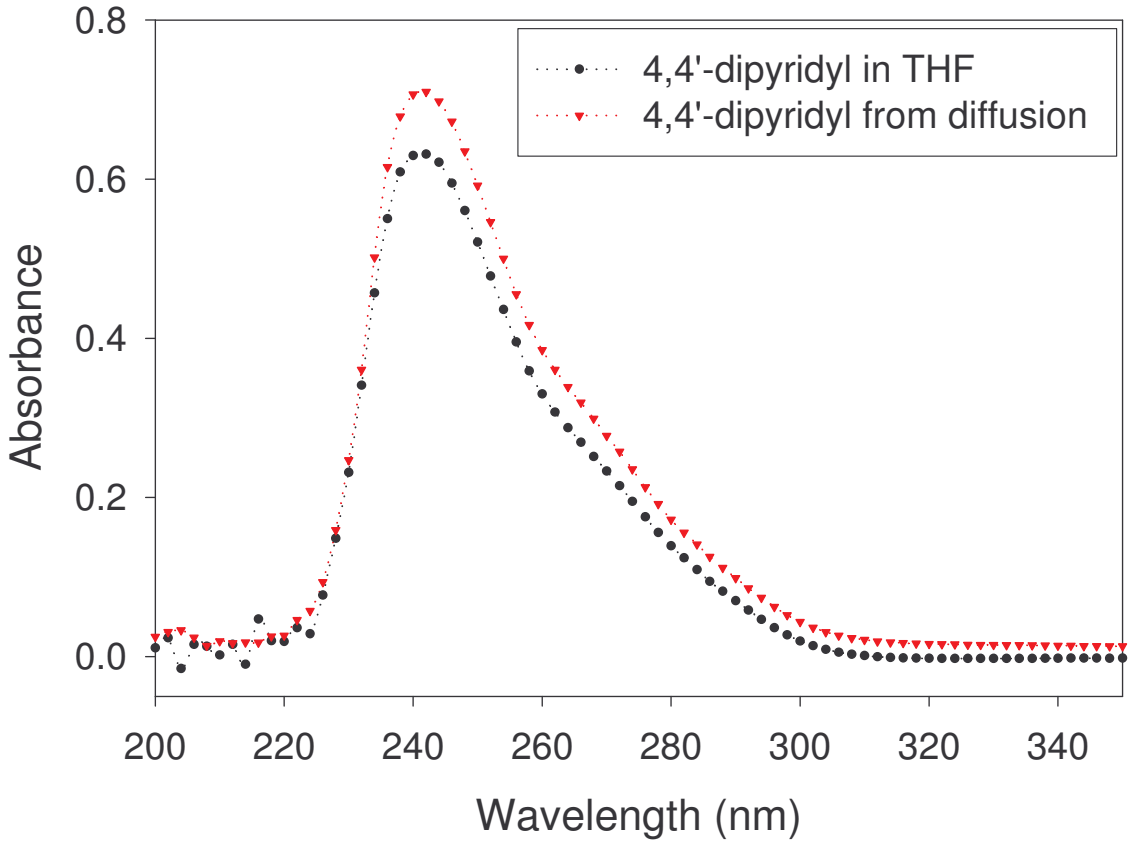

Figure 6.7. A comparison of the UV-visible spectrum of a freshly-prepared solution of 4,4′-dipyridyl dissolved in THF (●) with that of a solution of 4,4′-dipyridyl released into THF from a PVA monolith (▼).

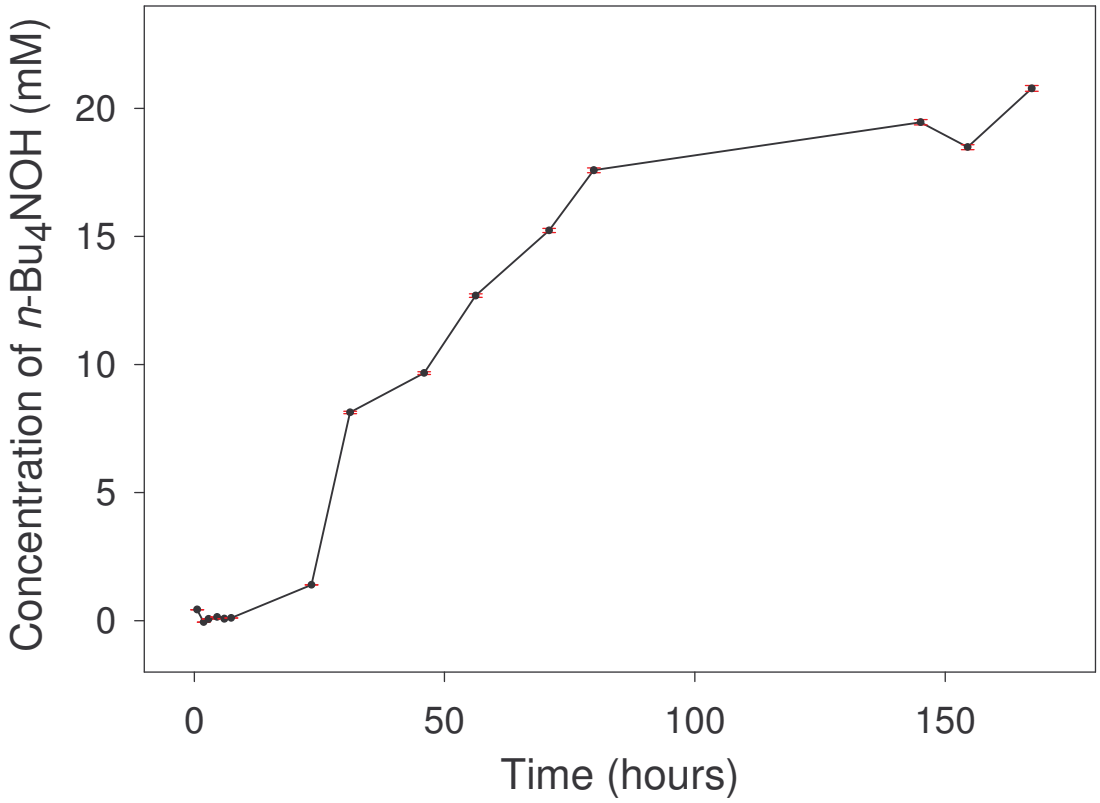

Figure 6.8. Concentration of *n*-Bu_4NOH in a THF solution from the release of *n*-Bu_4NOH from a PVA monolith.

A study of the amount of *n*-Bu_4NOH released from a PVA monolith revealed that (73 ± 3)% of *n*-Bu_4NOH that had been loaded in the monolith was released into the solution. Details of the studies are provided in Appendix E.

In order to provide evidence that *n*-Bu_4NOH did not undergo chemical change (other than dissociation into cation/anion in a polar solvent such as THF) during the loading and controlled-release process, a UV-visible experiment was conducted. The spectrum of a freshly prepared solution of *n*-Bu_4NOH dissolved in THF was compared to the spectrum of *n*-Bu_4NOH released into THF from a PVA monolith. As shown in Figure 6.9, these spectra match very closely, indicating that no chemical change has taken place.

6.3.4.4. Consistency of the Controlled-Release Rates

Studies were conducted in order to test the consistency in the rate of reagent release among different reagent-loaded PVA monoliths. Two identically prepared 4,4′-dipyridyl-loaded PVA monoliths were tested by the method described in Part 6.2.4. The results of the diffusion studies are shown in Figure 6.10. The diffusion properties of the two reagent-loaded monoliths are similar. Although not tested, similar consistency in results is expected for the diffusion properties of other reagent-loaded monoliths. The consistency in reagent release characteristics from these reagent-loaded monoliths indicates that at least in the case of 4,4′-dipyridyl, such reagent-loaded polymer monoliths may be mass-produced for delivery and/or sensing applications.

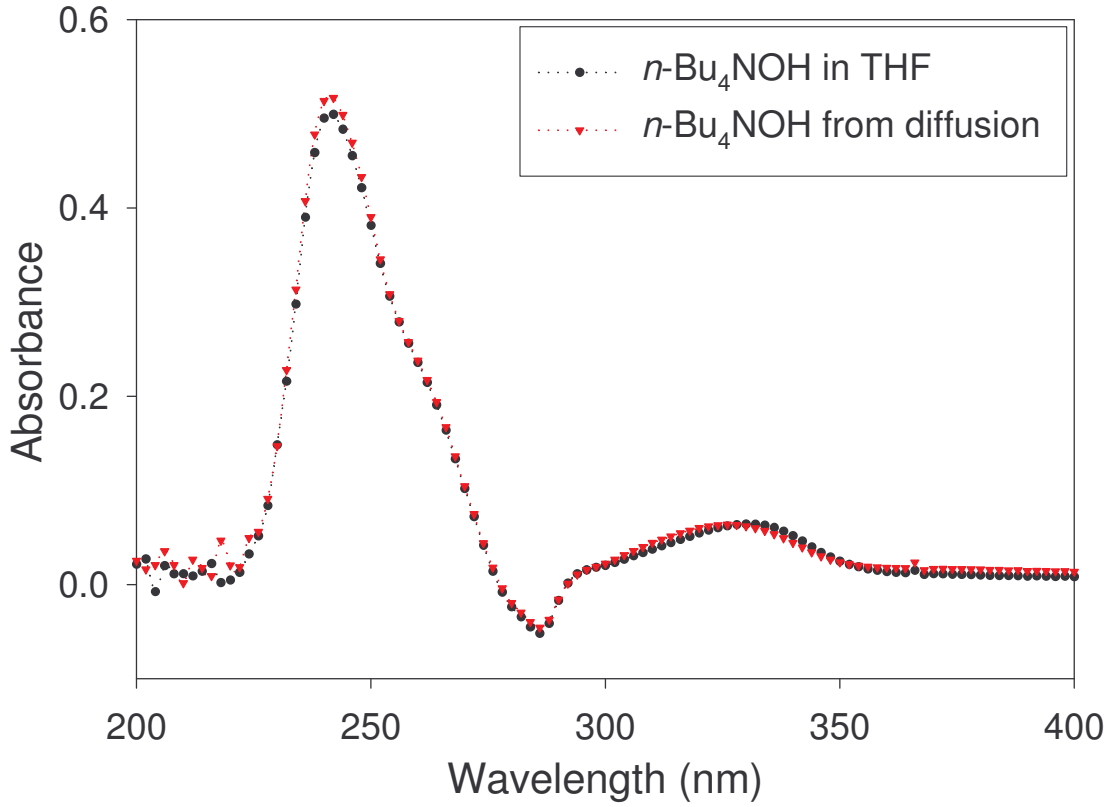

Figure 6.9. A comparison of the UV-visible spectrum of a freshly-prepared solution of *n*-Bu_4NOH dissolved in THF (●) with that of a solution of *n*-Bu_4NOH released into THF from a PVA monolith (▼).

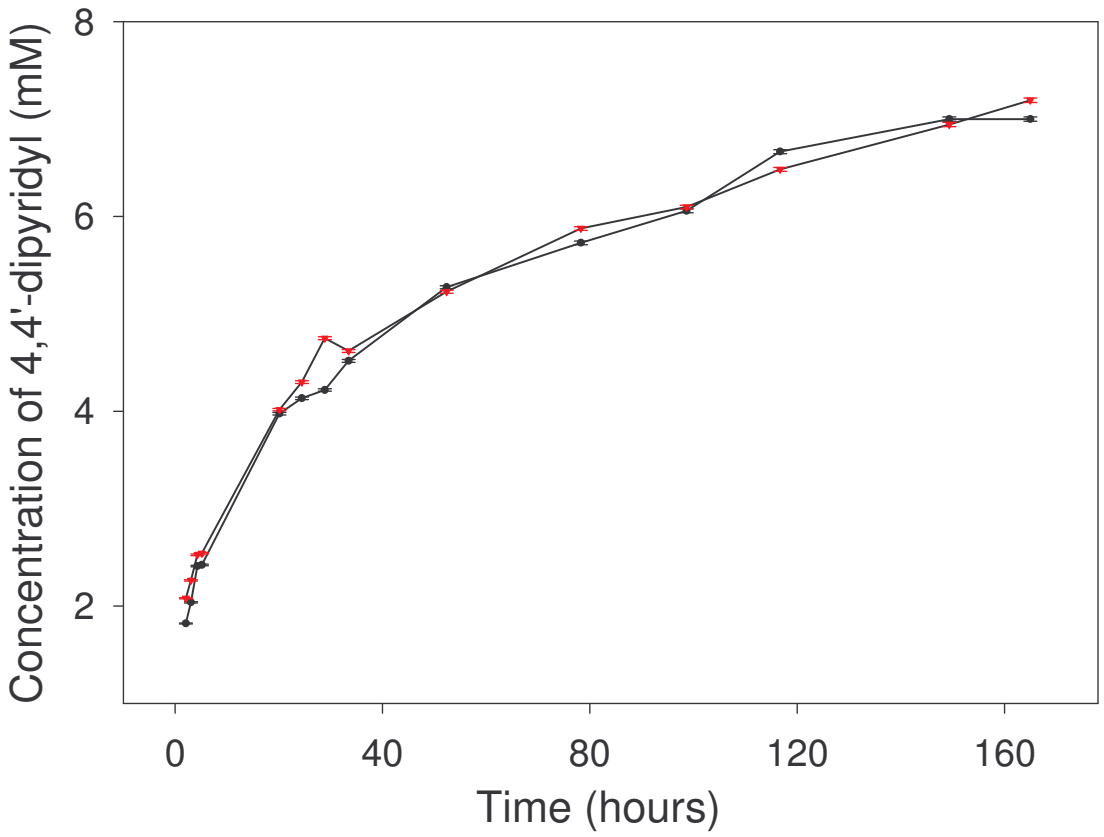

Figure 6.10. Comparison of the controlled-release study results of two similarly-prepared PVA monoliths containing 4,4′-dipyridyl.

6.3.5. Limitations of PVA Monoliths for Use in the Fujiwara Reaction

The PVA monoliths reported herein have been shown to release reagents at a consistent rate, making the monoliths attractive in chemical sensor development. However the PVA monoliths in this study are composed of 80-90 w/w% water.[9] As reported in Part 5 of this dissertation, the modified Fujiwara reactions must be conducted in a low-moisture environment. When a large amount of water is present, it competes with pyridine for the carbene $:CX_2$ intermediate, decomposing $:CX_2$ before it reacts with pyridine to give the colored product in the modified Fujiwara reactions.[18]

As a result, solutions of *n*-Bu_4NOH and 2,2′- or 4,4′-dipyridyl resulting from controlled-release studies were found to be unsuccessful for carrying out the modified Fujiwara reactions. No colored products were observed when chloroform was added to THF solutions of controlled-released *n*-Bu_4NOH and 2,2′- or 4,4′-dipyridyl.

In order to rule out interference of dry PVA beads with the Fujiwara reactions, experiments were carried out in which dry PVA beads *as received* were added to a mixture of 2,2′-dipyridyl and *n*-Bu_4NOH. This combination of PVA beads and reagents was allowed to stand for 24 hours. After 24 hours, a small amount of chloroform was added to the vessel, and subsequently the characteristic color of the modified Fujiwara reaction product was observed. This test rules out interference of PVA and indirectly suggests that the water released from PVA monoliths had decomposed carbene intermediates in the Fujiwara reactions. In other words, the process developed here and controlled-release of

the reagents could be used in other reactions that are *not* sensitive to the presence of water.

In an attempt to avoid the use of water, CRP monoliths containing 2,2′-dipyridyl, 4,4′-dipyridyl, or *n*-Bu_4NOH were prepared from polystyrene and THF.[19] Little release of the reagents from the polystyrene monoliths into organic solvents was however observed. Controlled release from polystyrene monoliths was not further investigated.

6.4. Concluding Remarks

A method for the development of controlled-release polymers containing reagents used in the modified Fujiwara reactions reported in Part 5 of this dissertation has been developed. The method by which the reagents were incorporated into the polymer matrix was found to be a critical step in the development of the CRPs. The release characteristics of the reagents from the polymer monoliths were also found to proceed in a controlled manner. Release characteristics of reagents from reagent-loaded PVA monoliths were also found to be consistent among different monoliths prepared similarly. The modified Fujiwara reactions were found to be unsuccessful using solutions of the reagents released from the PVA monoliths. However, the methodology for reagent delivery developed herein could have potential applications in other chemical sensing applications.

References

1. Uhrich, K. E.; Cannizzaro, S. M.; Langer, R. S.; Shakesheff, K. M. *Chem. Rev*. **1999**, *99*, 3181.
2. Mandal, T. K. *Eur. J. Pharm. Biopharm.* **2000**, *50*, 337.
3. Peppas, N. A.; Scott, J. E. *J. Control. Release* **1992**, *18*, 95.
4. Luo, S.; Walt, D. R. *Anal. Chem*. **1989**, *61*, 174.
5. Barnard, S. M.; Walt, D. R. *Science* **1991**, *251*, 927.
6. Hassan, C. M.; Stewart, J. E.; Peppas, N. A. *Eur. J. Pharm. Biopharm.* **2000**, *49*, 161.
7. Agayn, V.; Walt, D. R. *Immunomethods* **1993**, *3*, 112.
8. Milanovich, F. P.; Brown, S. B.; Colston Jr., B. W.; Daley, P. F.; Langry, K. C. *Talanta* **1994**, *41*, 2189.
9. Peppas, N. A.; Stauffer, S. R. *J. Control. Release* **1991**, *16*, 305.
10. Ricciardi, R.; Auriemma, F.; Gaillet, C.; De Rosa, C.; Laupretre, F. *Macromolecules* **2004**, *37*, 9510.
11. Hassan, C. M.; Peppas, N. A. *Macromolecules* **2000**, *33*, 2472.
12. Ricciardi, R.; Mangiapia, G.; Lo Celso, F.; Paduano, L.; Triolo, R.; Auriemma, F.; De Rosa, C.; Laupretre, F. *Chem. Mater*. **2005**, *17*, 1183.
13. Willcox, P. J.; Howie, Jr., D. W.; Schmidt-Rohr, K.; Hoagland, D. A.; Gido, S. P.; Pudjijanto, S.; Kleiner, L. W.; Venkatraman, S. *J. Polym. Sci. Pol. Phys.* **1999**, *37*, 3438.
14. Yokoyama, F.; Masada, I.; Shimamura, K.; Ikawa, T.; Monobe, K. *Coll. Polym. Sci*. **1986**, *264*, 595.

15. Ricciardi, R.; Auriemma, F.; De Rosa, C. *Macromol. Symp*. **2005**, *222*, 49.

16. O'Neil, M. J.; Smith, A.; Heckelman, P. E., Eds. *The Merck Index*, 13th Ed., Merck and Co., Whitehouse Station, NJ, 2001, p. 1362.

17. The Molar absorptivity of each reagent was calculated from the slope of a calibration plot of the reagent in THF.

18. Hine, J. *J. Am. Chem. Soc*. **1950**, *72*, 2438.

19. Polystyrene monoliths were prepared by heating polystyrene (7.6 g, MW 235,000) beads in THF (6.0 mL) at 200 °C for 5 hours. 2,2′-dipyridyl, 4,4′-dipyridyl (0.64 g), or *n*-Bu_4NOH (4.95 g) was added to the molten polystyrene and mixed so that a homogeneous mixture resulted. At this temperature, sublimation (and thus loss of 2,2′-dipyridyl and 4,4′-dipyridyl) was observed. Upon cooling the molten polystyrene/reagent mixture, a monolith was obtained. Controlled release studies were conducted by immersing a reagent loaded polystyrene monolith into a mixture of butyl ether (50% v/v%) and hexanes (50% v/v%) contained in a sealed vessel at 25 °C. Samples were removed from the sealed vessel periodically and the UV-vis spectrum of each was collected in order to monitor the diffusion of reagents from the polystyrene monoliths. Examination of the spectra showed that the reagents were not released from the polystyrene monoliths. Polystyrene monoliths were therefore not further investigated for the replenishment of reagents in the current studies.

APPENDIX

Appendix A

Alternative Calculation of Absorbance in Part 2

If the diffusing reagent itself has absorbance at the wavelength of observation, and this absorbance is *not* corrected as a part of reference during the acquisition of spectra, the absorbance by *free* diffusing reagent (A_r) in the region $0 \le x \le u(t)$ needs to be considered. The concentration of the diffusing reagent $C(x)$ linearly decreases in this region as shown in Equation 2.7. Thus, for *both halves* of the plane sheet,

$$A_r = 2\varepsilon_r \int_0^{u(t)} C(x)\,dx = 2\varepsilon_r \int_0^{u(t)} C_0\left(1 - \frac{x}{u(t)}\right)dx = \varepsilon_r C_0 u(t) = \varepsilon_r C_0^{3/2}\left(\frac{2Dt}{L_0}\right)^{1/2} \qquad \text{(Eq. A.1)}$$

The total absorbance A_t from both the product and the free diffusing reagent is thus:[11]

$$A_t = A_p + A_r = (2L_0D)^{1/2}\left[2\varepsilon_p C_0^{1/2} + \varepsilon_r\left(\frac{C_0^{3/2}}{L_0}\right)\right]t^{1/2} \qquad \text{(Eq. A.2)}$$

$$K' = (2L_0D)^{1/2}\left[2\varepsilon_p C_0^{1/2} + \varepsilon_r\left(\frac{C_0^{3/2}}{L_0}\right)\right] \quad (s^{-1/2}) \qquad \text{(Eq. A.3)}$$

Equation A.2 suggests that, if the total absorbance (A_t) is monitored with the time (t), the slopes (K') of the A_t vs. $t^{1/2}$ plots with different concentrations of the reagent (C_0) in the external solution are a linear function of $2\varepsilon_p C_0^{1/2} + \varepsilon_r(C_0^{3/2}/L_0)$. The K' vs. $2\varepsilon_p C_0^{1/2} + \varepsilon_r(C_0^{3/2}/L_0)$ plot (Equation A.3) could then be used as the calibration plot to determine the concentration of the reagent.

Equations 2.15 and 2.16 are in fact a special case of the scenario in Equations A.2 and A.3. When the *free* diffusing reagent itself has no absorbance, $\varepsilon_r = 0$, and Equations A.2 and A.3 become Equations 2.15 and 2.16.

Appendix B

Estimation of Errors for Chromium Determination in Part 3

B.1. Determination of Total Chromium by Atomic Absorption

Analysis of total chromium (III and VI) dissolved in aqueous solution was performed by atomic absorption (AA) spectroscopy. In such an analysis, a series of standard solutions containing a known concentration of Cr(VI) were analyzed to give a calibration plot, an example of which is shown in Figure B.1. In a calibration plot, the measured absorption intensity is plotted on the *y* axis as a function of the known concentration, *x*, for the series of the standards.

In a typical analysis calibration standards were prepared by pipetting known volumes of a Cr(VI) atomic absorption standard solution (Aldrich, 1017 ppm Cr) into separate volumetric flasks. Necessary sample matrix components were also added to the flask before diluting to the mark with deionized water.

The calibration curve was found to approximate a straight line, and the method of the linear least squares fitting was used by the software in the Perkin-Elmer 5100 atomic absorption spectrometer to give the following equation:[1]

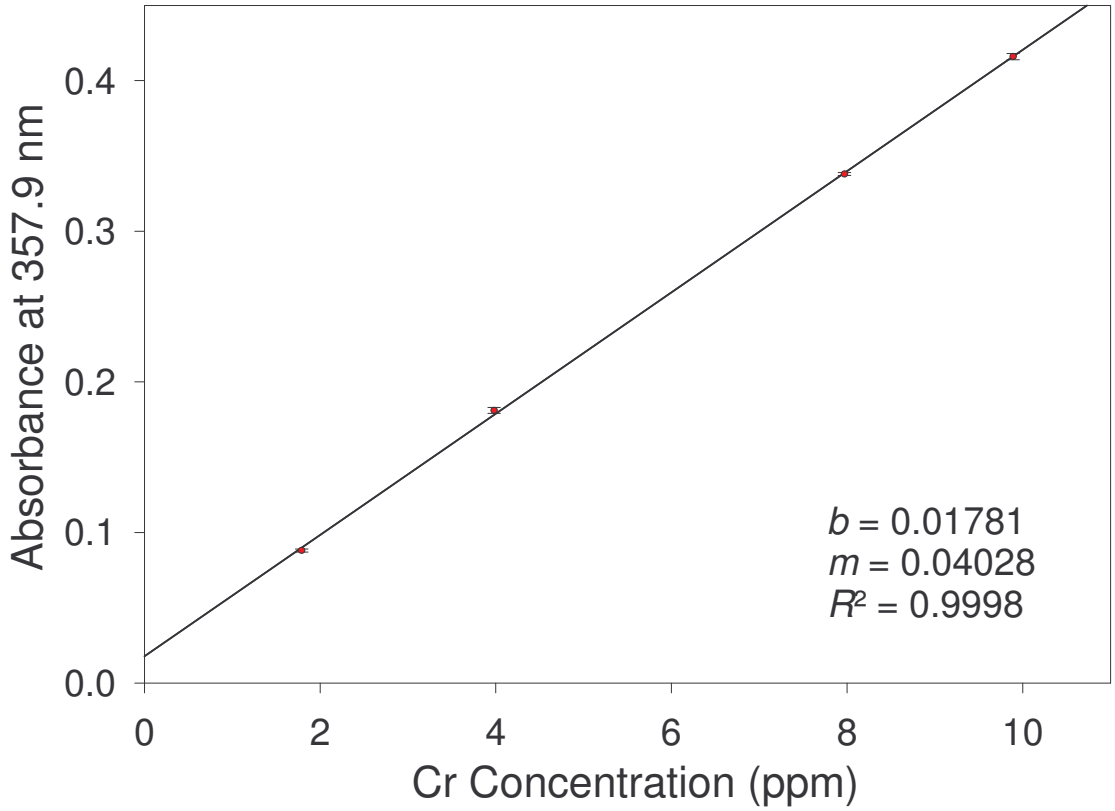

Figure B.1. Calibration plot from the atomic absorption analysis of Cr standard solutions. The blank was *not* used as a point in establishing the calibration plot.[1]

$$y = mx + b \qquad \text{(Eq. B.1)}$$

where the slope of the line, *m,* is equal to 0.04028; and the intercept, *b,* is equal to 0.01781 for the data in Table B.1. The errors in the calibration plot yielded 3.00% error in the calculated Cr concentration. This error is treated as the random error ($Error_{ran}$) in the AA measurement.

Repeated measurements of a single sample with a mean concentration value of 3.994 ppm showed a standard deviation of 0.018 ppm, thus giving 0.45% relative standard deviation for the measurement. This is treated as the systematic error ($Error_{sys}$) associated with the instrument.

The total error associated with the AA measurements ($Error_{AA}$) was thus calculated by the following equation:

$$Error_{AA} = (Error_{sys}^{2} + Error_{ran}^{2})^{1/2} \qquad \text{(Eq. B.2)}$$

The value of 3.03% calculated from Equation B.2 was used as the error associated atomic absorption.

B.2. Determination of Cr(VI) by the Diphenylcarbazide Method and UV-Vis Spectroscopy

Diphenylcarbazide has been used extensively for determination of Cr(VI) in various samples.[2] In Part 3 of this dissertation, diphenylcarbazide was used

Table B.1. Standard chromium concentrations for calibration and measured absorption intensities by AA

Standard Concentration (ppm)	Absorption Intensity
1.79	0.088 ± 0.001
3.98	0.181 ± 0.002
7.97	0.338 ± 0.001
9.89	0.416 ± 0.002

for determination of Cr(VI) in AOP-treated samples. The following method describes the procedure used for preparation of standards and samples for Cr(VI) analysis.

In a 25-mL volumetric flask, concentrated H_2SO_4 (8.75 mL) was diluted with deionized water. 1,5-diphenylcarbazide (0.0263 g) was weighed into a separate 100-mL volumetric flask. Acetone (5.0 mL) and 2.4 mL of the previously prepared H_2SO_4 solution were then added to the flask containing the 1,5-diphenylcarbazide and diluted with deionized water.

Standards and samples were prepared by adding 2.5 mL of the previously prepared 1,5-diphenylcarbazide solution and the proper amount of Cr(VI)-containing solution to a 25-mL volumetric flask. Visible spectra were collected on an Ocean Optics S2000 miniature fiber optic spectrophotometer equipped with a tungsten halogen source lamp. The spectrophotometer was interfaced to a PC for data collection using Ocean Optics OOIBase32 operating software. Optimum results were obtained when spectra were collected approximately 15 min after sample preparation. Blank samples containing only 1,5-diphenylcarbazide and water were used as a reference for all UV-vis measurements. Standard curves in the range of 0.203-0.367 ppm Cr(VI) were prepared routinely using the above method.

Calibration plots may be obtained for standards by plotting the absorbance at 544 nm vs. Cr(VI) concentration. The molar absorptivity for these solutions was found to be 3.78×10^4 $M^{-1}cm^{-1}$ at 544 nm. Repeated measurements of such a solution containing 0.300 ppm Cr(VI) yielded absorbance = 0.239 ± 0.001.

The relative standard deviation of 0.42% was used as error in UV-vis measurements ($Error_{UV\text{-}vis}$).

B.3. Error in the Calculation of Cr(VI)/Total Cr

Cr(VI) and total Cr concentrations in Part 3 of this dissertation were obtained from AA and UV-vis measurements, respectively. The error in the calculation of Cr(VI)/total Cr was calculated from the errors in both AA and UV-vis measurements by the following equation:

$$Error = (Error_{AA}^{2} + Error_{UV\text{-}vis}^{2})^{1/2} \qquad \text{(Eq. B.3)}$$

Using the errors in AA and UV-vis measurements in Parts B.1 and B.2, the error in the Cr(VI)/total Cr calculation was determined to be 3.06%.

References

1. AA WinLab software, the linear least-square fitting calibration program in the upgraded Perkin-Elmer 5100 atomic absorption spectrometer, was used in the calculations of total Cr concentrations. In this software, the blank at (0,0) is used as a data point in establishing the calibration plot. This procedure is different from that in Figure B.1 and Table B.1

2. (a) Allen, T. L. *Anal. Chem*. **1958**, *30*, 447. (b) Urone, P. F. *Anal. Chem*. **1955**, *27*, 1354. (c) Dedkova, V. P.; Shvoeva, O. P.; Savvin, S. B. *J. Anal. Chem.* **2001**, *56*, 758.

Appendix C

Estimation of Errors in Palladium Determination in Part 4

C.1. Determination of Total Palladium by Atomic Absorption

Analysis of total palladium (0 and II) dissolved in aqueous solution was performed by atomic absorption (AA) spectroscopy. In such an analysis, a series of standard solutions containing a known concentration of Pd(II) were analyzed to give a calibration plot, an example of which is shown in Figure C.1. In a calibration plot, the measured absorption intensity is plotted on the *y* axis as a function of the known concentration, *x*, for the series of the standards.

In a typical analysis calibration standards were prepared by pipetting known volumes of a Pd(II) atomic absorption standard solution (Acros, 1000.6 ppm Pd) into separate volumetric flasks. Necessary sample matrix components were also added to the flask before diluting to the mark with deionized water.

C.2. Determination of $Pd(H_2O)_n^{2+}$ by the N,N-Dimethyl-4-Nitrosoaniline Method and UV-Vis Spectroscopy

N,N-Dimethyl-4-nitrosoaniline has been used in the determination of $Pd(H_2O)_n^{2+}$ ions.[1] The calibration curve was found to approximate a straight

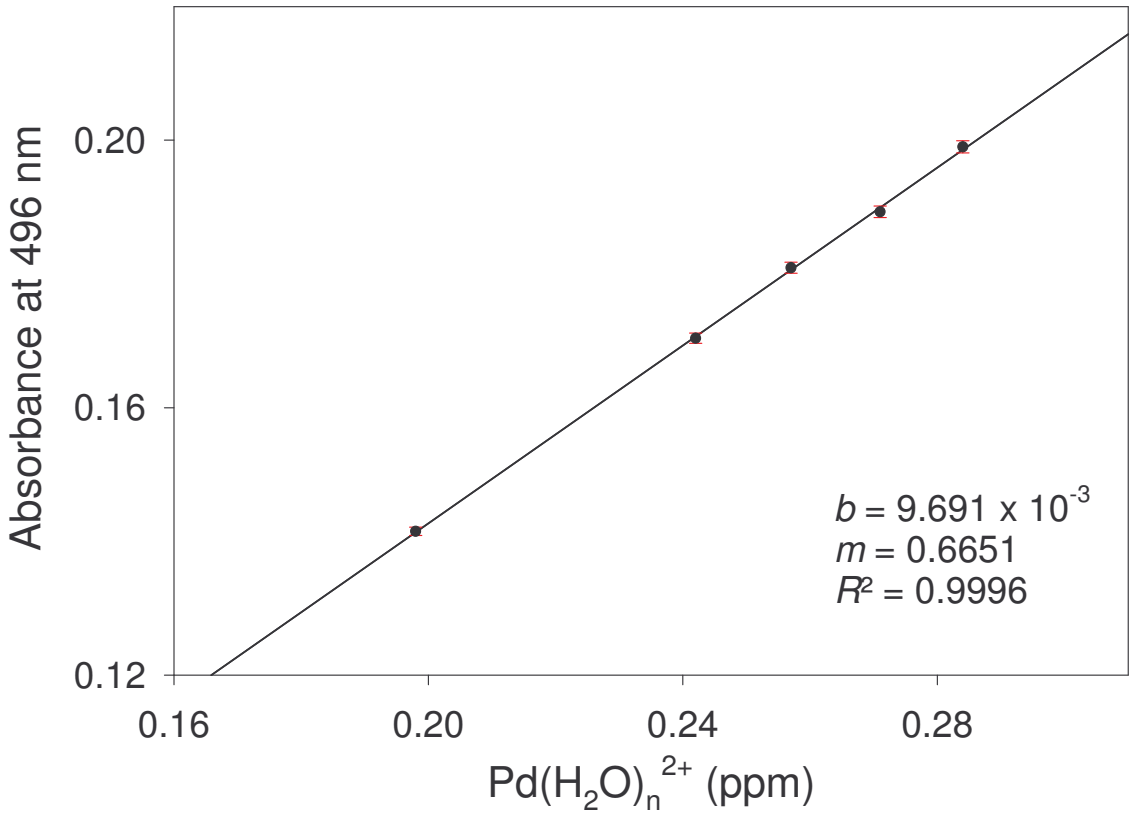

Figure C.1. Calibration plot from the analysis of $Pd(H_2O)_n^{2+}$ standard solutions.

line, and the method of the linear least squares fitting (Equation C.1) was used to give the following equation for the data in Table C.1:

$$y = mx + b = 0.6651\ x + 0.009691 \qquad \text{(Eq. C.1)}$$

The errors in the calibration plot yielded 0.425% error in the calculated $Pd(H_2O)_n^{2+}$ concentration of 0.2589 ppm. This error is treated as the random error ($Error_{ran}$) in the N,N-dimethyl-4-nitrosoaniline method.

Repeated measurements of a single sample with a mean absorbance of 0.06147 showed a standard deviation of 0.000197 on the Hewlett-Packard UV-Vis 8452 spectrometer. The relative standard deviation of 0.320% is treated as the systematic error ($Error_{sys}$) associated with the instrument.

The total error associated with the determination of $Pd(H_2O)_n^{2+}$ concentration (*Error*) was thus calculated by the following equation:

$$Error = (Error_{sys}^{\ 2} + Error_{ran}^{\ 2})^{\ 1/2} \qquad \text{(Eq. C.2)}$$

The value of 0.532% calculated using Equation C.2 was used as the error in the determination of $Pd(H_2O)_n^{2+}$ concentration by the N,N-dimethyl-4-nitrosoaniline method and UV-visible spectroscopy.

Table C.1. Standard $Pd(H_2O)_n^{2+}$ concentrations for calibration and measured absorption intensities by the N,N-dimethyl-4-nitrosoaniline method.

Standard Concentration (ppm)	Absorption Intensity
0.198	0.1415 ± 0.0008
0.242	0.1704 ± 0.0009
0.257	0.1809 ± 0.0009
0.271	0.1893 ± 0.001
0.284	0.1990 ± 0.001

Reference

1. Sarkar, P.; Paria, P. K.; Majumdar, S. K. *J. Indian Chem. Soc*. **1988**, *65*, 117.

Appendix D

Estimation of Errors in Halocarbon Measurements by the Hewlett-Packard UV-Vis 8452 Spectrometer in Part 5

Analysis of $HCCl_3$ and CCl_4 by the modified Fujiwara reactions were performed by UV-vis spectroscopy. In such an analysis, a series of standard solutions containing a known concentration of the analyte species ($HCCl_3$ or CCl_4) were analyzed to give a calibration plot, examples of which are shown in Figures 5.5-5.9. In a calibration plot, the measured absorption intensity is plotted on the *y* axis as a function of the known concentration, *x*, for the series of the standards.

In a typical analysis, calibration standards were prepared by pipetting known volumes of an $HCCl_3$ or CCl_4 standard solution into separate volumetric flasks. Necessary reagents were also added to the flask before diluting to the mark with THF.

An example is given here for the calibration plot in Figure 5.5. The data for this plot are given Table D.1. The calibration curve was found to approximate a straight line, and the method of the linear least squares fitting was used by Sigmaplot software to give the following equation:

$$y = 0.01396\ x - 4.463 \times 10^{-3} \qquad \text{(Eq. D.1)}$$

Table D.1. Standard $HCCl_3$ concentrations for calibration and measured absorption intensities. Data are from the calibration plot in Figure 5.5.

Standard Concentration (ppm)	Absorption Intensity
0.23	0.0022583 ± 0.0000120
0.46	0.0063477 ± 0.0000338
0.93	0.0111 ± 0.0000591
1.85	0.0171 ± 0.0000909
2.32	0.0234 ± 0.000124
4.64	0.0565 ± 0.000301
6.95	0.0970 ± 0.000516
9.27	0.1194 ± 0.000635
13.91	0.1915 ± 0.00102
18.54	0.2558 ± 0.00136

The errors in the calibration plot yielded 1.14% error in the calculated HHC concentration. This error is treated as the random error ($Error_{ran}$) in the UV-vis measurement.

Appendix C.2 gives the systematic error ($Error_{sys}$) of 0.320% for measurements by the Hewlett-Packard 8452 UV-vis spectrometer. This error was used here for the estimation of the systematic error.

The total error associated with the UV-vis measurements (*Error*) in Part 5 was thus calculated by the following equation:

$$Error = (Error_{sys}^{2} + Error_{ran}^{2})^{1/2} \qquad \text{(Eq. D.2)}$$

The value of 1.18% calculated from Equation D.2 was used as the error associated UV-vis measurements. Similar error analyses for the calibration plots in Figures 5.6-5.8 give the values of *m*, *b*, $Error_{ran}$ and *Error*. These values and those for Figure 5.5 are listed in Table D.2.

The total errors were used in estimating the errors in the detection limits in Table 5.1.

Table D.2. Error analyses for Figures 5.5-5.9

	m	***b***	$Error_{ran}$	***Error***
Figure 5.5	0.01396	-4.463×10^{-3}	1.14%	1.18%
Figure 5.6	0.03367	-5.953×10^{-3}	0.820%	0.880%
Figure 5.7	0.03337	−0.04489	2.30%	2.32%
Figure 5.8	2.058×10^{-3}	5.223×10^{-3}	3.31%	3.33%
Figure 5.9	8.158×10^{-3}	0.09024	3.39%	3.41%

Appendix E

Estimation of Errors and Determination of the Percentage of Reagents Released From Monoliths during Controlled Release Studies in Part 6

E.1. Estimation of Errors in the Determination of 2,2′-Dipyridyl, 4,4′-Dipyridyl and *n*-Bu_4NOH

Analysis of 2,2′-dipyridyl, 4,4′-dipyridyl and *n*-Bu_4NOH was performed by UV-vis spectroscopy. In a typical analysis, calibration standards were prepared by pipetting known volumes of a 2,2′-dipyridyl, 4,4′-dipyridyl and *n*-Bu_4NOH standard THF solution into separate volumetric flasks. Necessary reagents were also added to the flask before diluting to the mark with THF. A series of standard THF solutions containing a known concentration of the analyte species were analyzed to give a calibration plot, yielding the molar absorptivities (ε) of $(1.22 \pm 0.05) \times 10^4$, $(1.18 \pm 0.05) \times 10^4$, $(4.75 \pm 0.19) \times 10^3$ M^{-1} cm^{-1} for 2,2′-dipyridyl, 4,4′-dipyridyl and *n*-Bu_4NOH, respectively.

E.2. Determination of the Percentage of Reagents Released From Monoliths during Controlled Release Studies

In the controlled-release studies in Part 6 of this dissertation, the percentage of reagents diffused from a reagent-loaded monolith into solution was studied by the process discussed below. An example is given for the release of 2,2′-dipyridyl from a PVA monolith in Part 6.3.4.1 of this dissertation.

2,2′-dipyridyl (0.2525 g) was uniformly loaded into a PVA monolith to give a total mass of 13.777 g. This monolith was then cut into two cylindrically-shaped pieces, and one piece of 8.191 g was used in control-release studies. The mass of 2,2′-dipyridyl in this piece was 0.1501 g (or 59.45% of 0.2525 g)

This piece of monolith was then immersed in 1000 mL of THF for control-release studies. In 332 hours (Figure 6.4), the concentration of 2,2′-dipyridyl diffused into solution reached a maximum of approximately 0.88 mM. The amount of 2,2′-dipyridyl released from this PVA monolith into the 1000-mL solution is thus 0.14 g, and the percentage of the release is (93 ± 4)%.

Similar studies were performed for the release of 4,4′-dipyridyl and *n*-Bu_4NOH. In the controlled-release studies of 4,4′-dipyridyl (0.817 g in a monolith of 33.51 g) in Part 6.3.4.2, the volume of THF used was 100 mL, and the concentration of 4,4′-dipyridyl reached a maximum of 3.52 mM (Figure 6.6). The the percentage of the release is (6.7 ± 0.3)%. In the controlled-release studies of *n*-Bu_4NOH (0.465 g in a monolith of 12.48 g) in Part 6.3.4.3, the volume of THF

used was 100 mL, and the concentration of *n*-Bu_4NOH reached a maximum of 20 mM (Figure 6.8). The percentage of the release is (73 ± 3)%.

VITA

David Lynn Rodman was born in November, 1977, in Huntsville, Alabama. He attended Huntsville public schools through elementary and middle school, and completed high school at Athens Bible School in Athens, Alabama, in 1996. In the following fall, he began his undergraduate studies at Calhoun Community College, and then transferred to Athens State University, where he earned the outstanding chemistry major award and graduated in 2000 with honors.

Lynn began his graduate studies at the University of Tennessee, Knoxville, in the Fall of 2000. He soon joined Dr. Ziling (Ben) Xue's research group in the chemistry department where he studied sol-gel materials, sensor development, and various other methods related to chemical analysis. Lynn's research resulted in the publication of three papers in various scientific journals by the time he received his Ph.D in the Fall of 2005. During his tenure at UTK, he also presented his research at meetings including the American Chemical Society national meeting, the Pittsburgh Conference, the Organosilicon Symposium, as well as several Measurement and Control Engineering Center meetings. During his graduate studies, Lynn was also involved in the Association of Chemistry Graduate Students (ACGS), where he served on the departmental safety committee as a graduate student representative.

Lynn's next position will be working in the analytical methods development group with Vintage Pharmaceuticals in Huntsville, Al.